


Summer 2008

# Nanoengineered templates for controlled delivery of bioactive compounds

Nalinkanth Ghone Veerabdran  
*Louisiana Tech University*

Follow this and additional works at: <https://digitalcommons.latech.edu/dissertations>

 Part of the [Biomedical Engineering and Bioengineering Commons](#), and the [Pharmacology Commons](#)

---

## Recommended Citation

Veerabdran, Nalinkanth Ghone, "" (2008). *Dissertation*. 463.  
<https://digitalcommons.latech.edu/dissertations/463>

This Dissertation is brought to you for free and open access by the Graduate School at Louisiana Tech Digital Commons. It has been accepted for inclusion in Doctoral Dissertations by an authorized administrator of Louisiana Tech Digital Commons. For more information, please contact [digitalcommons@latech.edu](mailto:digitalcommons@latech.edu).

**NANOENGINEERED TEMPLATES FOR CONTROLLED DELIVERY OF  
BIOACTIVE COMPOUNDS**

by

Nalinkanth Ghone Veerabadran, B.Tech

A Dissertation Presented in Partial Fulfillment  
of the Requirements for the Degree  
Doctor of Philosophy

COLLEGE OF ENGINEERING AND SCIENCE  
LOUISIANA TECH UNIVERSITY

August 2008

UMI Number: 3318926

## INFORMATION TO USERS

The quality of this reproduction is dependent upon the quality of the copy submitted. Broken or indistinct print, colored or poor quality illustrations and photographs, print bleed-through, substandard margins, and improper alignment can adversely affect reproduction.

In the unlikely event that the author did not send a complete manuscript and there are missing pages, these will be noted. Also, if unauthorized copyright material had to be removed, a note will indicate the deletion.

**UMI**<sup>®</sup>

---

UMI Microform 3318926

Copyright 2008 by ProQuest LLC.

All rights reserved. This microform edition is protected against unauthorized copying under Title 17, United States Code.

ProQuest LLC  
789 E. Eisenhower Parkway  
PO Box 1346  
Ann Arbor, MI 48106-1346

LOUISIANA TECH UNIVERSITY

THE GRADUATE SCHOOL

June 30th , 2008

Date

We hereby recommend that the dissertation prepared under our supervision  
by Nalinkanth Ghone Veerabadran

entitled "NANOENGINEERED TEMPLATES FOR CONTROLLED DELIVERY OF  
BIOACTIVE COMPOUNDS"

be accepted in partial fulfillment of the requirements for the Degree of  
Doctor of Philosophy in Biomedical Engineering

Yuri Luov  
Supervisor of Dissertation Research  
[Signature]  
Head of Department  
Biomedical Engineering  
Department

Recommendation concurred in:

David Mills  
[Signature]  
[Signature]  
Tuan feng

Advisory Committee

Approved:  
[Signature]  
Director of Graduate Studies

Stan Napp  
Dean of the College

Approved:  
[Signature]  
Dean of the Graduate School

## **ABSTRACT**

The significance of any drugs, therapeutic proteins, or any bioactive compounds, is based not only on their effects on diseases but also on how specifically, how readily, how controllable and how prolonged their effects on the disease without having any side effects. Thus the techniques involved in the drug encapsulation and its controlled release for a longer duration of time form one of the important processes of drug reformulation. In recent years nanoparticles have created overwhelming attention for delivering drugs by nanoencapsulation. The smaller size of nanoparticles has longer circulation time and higher cellular uptake when compared with larger size of microparticles. Thus, the field of nanotechnology through its subsections of nanomedicine and biomedical nanotechnology is revolutionizing the pharmaceutical industries. The purpose of this research work is to nanoengineer bioresponsive materials for its application as a template for making submicron or nanosized drug delivery systems.

The first half of this work deals with alginate template, a semi-synthetic polymer. Alginate has been reported as suitable for encapsulation of many bioactive agents like cells, enzymes, and drugs, owing to its relatively aqueous environment within the alginate matrix, the mild room condition encapsulation process, and high gel porosity. Recently biotechnological innovations have introduced some new forms of drugs with therapeutic proteins and oligonucleotides. Hence, submicron or nanoemulsions with narrow particle size ranges are becoming favored over larger particulate and/or

polydisperse systems. This work deals in detail with the optimization of the size of calcium alginate nanoparticle preparation by the emulsification technique. By the optimized emulsion method calcium alginate nanoparticles of 300 nm in diameter can be prepared. These nanoparticles were later used for encapsulation and release of curcumin. Earlier, the smallest alginate particle produced had a minimum size of 1-5  $\mu\text{m}$ ; hence, this work remains as a frontrunner in the preparation of calcium alginate nanoparticles.

The second half of this work deals with a natural nanotubular template called halloysite. Halloysite is tubular alumina silicate clay of 15-200 nm inner lumen diameter and 0.5-5 microns long. It was used for loading poorly soluble drugs and sustaining their release. Loading was optimized by varying pH and alcohol / water ratio in the solvent with a maximum drug loading of 12 % by volume. Near linear release of dexamethasone, furosemide, and nifedipine was demonstrated for 5-10 hours. The presence of silicates on halloysite outer surface provides a negatively charged exterior, and makes it possible to do Layer-by-Layer (LbL) assembly of positively charged polyelectrolytes and nanoparticles on halloysite. The LbL assembly was later extended to dexamethasone drug-loaded halloysite for its controlled release. A study of the effect of number of assembled layers and the effect of molecular weight of the assembled polymers on the release profile of the drug revealed that a high molecular weight of the assembled polymers and an optimum number of layers gave a very slow sustained release. Encapsulation of the drugs inside the lumen of the halloysite coupled with LbL assembly of clay-drug composite provides a novel formulation for controlled release of drugs.

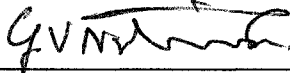
Biocompatibility is a major problem for many materials to be used as a drug constituent. The cytotoxicity studies for halloysite were also done in this work to ensure the valid application of halloysite in drug reformulations.

Halloysite clay was also demonstrated as a nanoreactor for synthesizing silver nanoparticles. Synthesis was carried out by reducing the silver acetate which was loaded inside the halloysite. This in situ synthesis offers a novel way of fabricating surface modified clay materials, nano-rod metals, core-shell type ceramic nanocomposites, and potential application in antimicrobial coatings and wound healing.

## APPROVAL FOR SCHOLARLY DISSEMINATION

The author grants to the Prescott Memorial Library of Louisiana Tech University the right to reproduce, by appropriate methods, upon request, any or all portions of this Dissertation. It is understood that the "proper request" consists of the agreement, on the part of the requesting party, that said reproduction is for his personal use and that subsequent reproduction will not occur without written approval of the author of this Dissertation. Further, any portion of the Dissertation used in books, papers, and other works must be appropriately referenced to this Dissertation.

Finally, the author of this Dissertation reserves the right to publish freely, in the literature, at any time, any or all portions of this Dissertation.

Author 

Date 30<sup>th</sup> June 2008



## **DEDICATION**

**Dedicated to my parents G.Durga & V.Veerabadran,  
to my brother G.V.Jaikanth and  
sister G.V.Jayashree.**

## TABLE OF CONTENTS

ABSTRACT .....	iii
DEDICATION .....	vii
LIST OF TABLES .....	xiii
LIST OF FIGURES .....	xiv
ACKNOWLEDGMENTS .....	xix
CHAPTER 1 .....	1
INTRODUCTION .....	1
Importance of Template Size .....	2
Importance of Template Shape .....	3
Nature and Availability of Template .....	3
Research Goals .....	4
Dissertation Overview .....	4
CHAPTER 2 .....	6
BACKGROUND AND THEORY .....	6
Spherical Alginate Particle .....	6
Chemical Composition and Structure .....	6
Procedure for Preparing Calcium Alginate Particles .....	7
Applications .....	10
Nanotubular Clay Particles- Halloysite .....	11
Chemical Composition and Structure .....	11

Morphology .....	14
Physical and Chemical Properties .....	16
Capillary Force .....	17
Applications .....	18
Preliminary Work .....	22
Layer-by-Layer Assembly .....	25
Preparation of LbL Nanoshells .....	27
Nanoshells Monitoring .....	31
CHAPTER 3 .....	35
OPTIMIZATION OF ALGINATE MICRO / NANO PARTICLE PREPARATION AND ITS USE AS SPHERICAL TEMPLATE FOR ENCAPSULATION AND RELEASE OF CURCUMIN.....	35
Introduction.....	35
Materials and Methods.....	36
Alginic Acid.....	36
Surfactants .....	37
Organic Solvents.....	37
Equipment.....	37
General Procedure to Prepare Calcium Alginate Nanoparticles by Emulsification Technique .....	37
Characterization of Calcium Alginate Nanoparticles .....	38
Encapsulation of Curcumin .....	39
Release Kinetics Study of Curcumin In Vitro .....	39
Results and Discussion .....	40
Optimization of the Calcium Alginate Nanoparticle Preparation Procedure .....	41

Influence of Oil Phase Composition, Alginic Acid Concentration and Ratio of Alginic Acid and CaCl <sub>2</sub> used on Nanoparticles Size .....	42
Influence of Surfactant and Gelling Agent Nature on Nanoparticle Size .....	45
Ca-AOT Preparation Procedure.....	45
Modification of Nanoparticle Washing and Separation Procedure .....	46
SPAN 85 concentration in Isooctane Extracts and Ethanol Supernatants.....	47
Influence of Modified Separation Parameters on Nanoparticle Diameter.....	48
Influence of Solvent on Calcium Alginate Nanoparticle SEM Imaging .....	50
Preparation of Calcium Alginate Nanoparticles Using Nonaqueous Solution of CaCl <sub>2</sub> .....	52
Influence of Viscosity of Alginic Acid on Calcium Alginate Nanoparticles .....	53
Chitosan Coating onto Calcium Alginate Nanoparticles.....	55
Encapsulation and Release of Curcumin .....	57
Conclusion .....	60
CHAPTER 4 .....	62
ENCAPSULATION AND SUSTAINED RELEASE OF POORLY SOLUBLE DRUGS USING NATURAL CLAY NANOTUBULAR TEMPLATE HALLOYSITE.....	62
Introduction.....	62
Materials and Methods.....	64
Surface Characterization.....	64
Drug Loading.....	64
In Vitro Drug Release Kinetics.....	64
Results and Discussion .....	65
Conclusion .....	73

CHAPTER 5 .....	74
TUNABLE CONTROLLED RELEASE OF DEXAMETHASONE USING LAYER-BY-LAYER FORMULATED HALLOYSITE .....	74
Introduction.....	74
Materials and Methods.....	76
Layer-by-Layer Assembly on Halloysite.....	76
Characterization of Assembled Layers .....	77
Dexamethasone Loading .....	77
Encapsulation of Drug-Loaded Halloysite .....	78
In Vitro Dexamethasone Release Kinetics .....	78
Results and Discussion .....	78
Conclusion .....	90
CHAPTER 6 .....	91
HALLOYSITE - IN VITRO CYTOTOXICITY TESTING .....	91
Introduction.....	91
Experiments .....	92
Materials .....	92
Layer-by-Layer Assembly on Halloysite.....	92
Characterization of Assembled Layers .....	93
Cell Culture.....	93
Cytotoxicity Assay.....	93
Results and Discussion .....	94
Conclusion .....	97

CHAPTER 7 .....	98
TEMPLATE SYNTHESIS OF SILVER / SILVER OXIDE NANOPARTICLES USING HALLOYSITE AS NANOREACTOR.....	98
Introduction.....	98
Experiments .....	99
Materials .....	99
Silver/Silver Oxide Synthesis.....	99
Method 1 .....	99
Method 2.....	100
Method 3.....	100
Porosity Test.....	100
Results and Discussion .....	100
Conclusion .....	104
CHAPTER 8 .....	106
CONCLUSIONS AND FUTURE WORK.....	106
Conclusions.....	106
Future Work.....	107
REFERENCES .....	109
VITA .....	120
Peer-Reviewed Journals.....	121
Conference Proceedings .....	121
Conference Talks .....	122
Conference Posters .....	122

## LIST OF TABLES

Table 2.1: Chemical analysis of New Zealand halloysite (Source: Imery's Tableware New Zealand Ltd, Halloysite MP # 47/04).....	12
Table 3.1: Conditions and results of optimization of calcium alginate nanoparticles preparation via emulsification technique.....	43
Table 3.2: Influence of surfactant and gelling agent nature on suspension stability and nanoparticle diameter. ....	45
Table 3.3: Concentration of SPAN85 in supernatants (isooctane extracts and ethanol supernatants). ....	48
Table 3.4: Calcium alginate nanoparticle size for samples prepared according to modified separation procedure.....	49
Table 3.5: Diameter for calcium alginate nanoparticles prepared from alginic acid of different viscosity by emulsification technique.....	54

## LIST OF FIGURES

Figure 2.1: Alginic acid structure. M- mannuronic acid block, G – guluronic acid block [15].	7
Figure 2.2: CLSM (A-fluorescence mode, B-transmission mode) images of calcium alginate microparticles prepared via emulsion technique. For fluorescence image, PAH-RBITC was coated at pH 6.5.	9
Figure 2.3: SEM images of calcium alginate microparticles prepared via emulsification technique. Images were taken after sputter coating the dried sample with 2 nm thickness of Iridium.	10
Figure 2.4: Schematic representation of halloysite-(7A) nanotubes [123].	14
Figure 2.5: Structure of kaolinite layer [57].	14
Figure 2.6: TEM images of dried halloysite from different source a. China, b. New Zealand, and c. USA (Utah).	15
Figure 2.7: Particle size distribution of halloysite from New Zealand (Source: Imery's Tableware New Zealand Ltd, Halloysite MP # 47/04).	15
Figure 2.8: SEM images of halloysite nanotubes before A) and after B) loading with CaCO <sub>3</sub> [65].	20
Figure 2.9: SEM image thin film, produced by LbL deposition of halloysite, Polyethyleneimine and Polystyrenesulfonate. A) Cross – section view, B) top view [66].	20
Figure 2.10: Dexamethasone release comparison in water from halloysite of different source: loading done from drug saturated water solvent.	23
Figure 2.11: TEM picture of Unloaded Halloysite (A) and DNA oligomer loaded halloysite (B).	24
Figure 2.12: DNA loading variation with respect to pH: loading using water as solvent.	25



Figure 2.13: Scheme of electrostatic layer-by-layer self-assembly on 2-D substrates with (top) polycations and polyanions, and (bottom) polycations and negatively charged nanoparticles. ....	29
Figure 2.14: Scheme of electrostatic layer-by-layer self-assembly on 3-D microtemplates, or cores, followed by core dissolution. ....	29
Figure 2.15: Frequency shift and film thickness of each assembled layer for (PSS/PAH) <sub>2</sub> (TA/PAH) <sub>3</sub> adsorption on QCM electrodes. The first two precursor layers are PSS/PAH, and the next three layers are TA/PAH. The tannic acid and poly(allylamine hydrochloride) has an average thickness of $1.57 \pm 0.11$ nm and $1.69 \pm 0.35$ nm, respectively [109]. ....	32
Figure 2.16: Surface charge alternation of polymers poly -L-lysine (PLL) and carboxy methyl cellulose (CMC) coated on CD 40 DNA microspheres (Obtained from EPIC-Therapeutics, a subsidiary of BAXTER Inc.) at pH 6.5. ....	33
Figure 2.17: CLSM images of poly-L-lysine coated CD40 DNA microspheres (Obtained from EPIC-Therapeutics, a subsidiary of BAXTER Inc.). For visualization poly-L-lysine was tagged with Rhodamine-iso-thio-cyanate (RITC).....	34
Figure 3.1: CLSM images of calcium alginate nanoparticles, prepared by general emulsification method. For fluorescence mode imaging (B, left) PAH-RBITC was coated at pH 6.5. ....	40
Figure 3.2: SEM images of calcium alginate nanoparticles, prepared by general emulsification method. Images were taken after sputter coating the dried sample with 2 nm thickness of Iridium.....	41
Figure 3.3: SEM images of nanoparticles obtained from experiment S-2 (Table 3.4). Images were taken after sputter coating the dried sample with 2 nm thickness of Iridium. ....	50
Figure 3.4: SEM images of nanoparticles obtained from experiment S-4 (Table 3.4) after washing with ethanol and before washing with water. Images were taken after sputter coating the dried sample with 2 nm thickness of Iridium.....	51
Figure 3.5: SEM images of nanoparticles obtained from experiment S-4 (Table 3.4) after washing with ethanol and water. Images were taken after sputter coating the dried sample with 2 nm thickness of Iridium.....	51
Figure 3.6: SEM images of nanoparticles obtained from Sample 8 (Table 3.1). Images were taken after sputter coating the dried sample with 2 nm thickness of Iridium. ....	52

Figure 3.7: SEM images of calcium alginate nanoparticles prepared using alginic acid of high viscosity (upper row) and low viscosity (middle row) and using polygalacturonic acid (lower row). Images were taken after sputter coating the dried sample with 2 nm thickness of Iridium.....	55
Figure 3.8: SEM images of calcium alginate nanoparticles before (A,B) and after (C,D) coating with one layer of chitosan. Images were taken after sputter coating the dried sample with 2 nm thickness of Iridium.....	57
Figure 3.9: CLSM images of Curcumin loaded chitosan-alginate particles. Fluorescence was due to innate nature of curcumin. ....	58
Figure 3.10 SEM images of Curcumin loaded chitosan-alginate particles. Images were taken after sputter coating the dried sample with 2 nm thickness of Iridium. ....	59
Figure 3.11: In vitro release kinetics of Curcumin in deionized water at pH 6.5.....	59
Figure 4.1: Chemical formulae of the drugs used: a-Dexamethasone (MW 392.5), b-Furosemide (MW 330.8), and c-Nifedipine (MW 346.3). ....	63
Figure 4.2: Zeta Potential results of halloysite, silica, and alumina. ....	66
Figure 4.3: Profiles of the drugs from halloysite nanotubules in water at pH 7.4: a- loading from 10 % alcohol; b- loading from 50 % ethanol / aqueous solvent. ....	68
Figure 4.4: Amount of Dexamethasone loading depending on pH (a), and its initial release in water at pH 7.4 (b).....	72
Figure 5.1: Schematic illustration of layer-by-layer assembly of polymer / nanoparticle coating on halloysite and halloysite loaded with drug.....	79
Figure 5.2: Zeta potential readings of four bilayer coating of PAH(MW 70000)/PSS(MW 70000) and PEI(MW 2000)/PAA(MW 5100) on halloysite at pH 6.5.....	80
Figure 5.3: Zeta potential readings of layer-by-layer coated polymers (with PEI(MW 2000)/PAA(MW 5100)) along with silica nanoparticles (7nm and 22nm in diameter) on halloysite at pH 6.5.....	81
Figure 5.4: Film thickness monitoring by Quartz crystal microbalance studies for polymer (PEI(MW 2000)/PAA(MW 5100)) and nanoparticle (silica nanoparticles 7nm and 22nm in diameter) assembly.....	82
Figure 5.5: Transmission electron microscopy image of Si nanoparticle with diameter of 7nm assembly on halloysite.....	82

Figure 5.6: Transmission electron microscopy image of Si nanoparticle with diameter of 22nm assembly on halloysite.....	83
Figure 5.7: Mercury porosimeter results of dexamethasone loaded halloysite in comparison with unloaded halloysite. ....	85
Figure 5.8: Zeta potential readings of LbL coating of (PEI(MW 2000)/PAA(MW 5100)) halloysite loaded with dexamethasone drug. ....	86
Figure 5.9: Effect of number of bilayers on the release profile of dexamethasone drug in deionised water at pH 6.5 from LbL (PEI/PAA) coated halloysite loaded with dexamethasone. ....	86
Figure 5.10: Zeta potential readings of layer-by-layer coated halloysite loaded with Dexamethasone drug. ....	87
Figure 5.11: Molecular weight effect of the coated polymers on the release profile of dexamethasone drug in deionised water at pH 6.5 from LbL coated halloysite loaded with dexamethasone. ....	87
Figure 5.12: Zeta potential readings of layer-by-layer coating of very high molecular weight natural polymers (Chitosan and Gelatin B) on halloysite loaded with dexamethasone drug.....	89
Figure 5.13: Molecular weight effect of the coated polymers on the release profile of dexamethasone drug from LbL coated halloysite loaded with dexamethasone.....	89
Figure 6.1: LbL coating of halloysite with natural polymers (poly-L-lysine and protamine sulphate) after coating two bilayers of PEI(MW 2000)/PAA(MW 5100) as precursors at pH 6.5. ....	94
Figure 6.2: Viability of 3T3 cells after 24 hr (A) and after 48 hr (B) as determined by celltiter-96 reagent. The legend stands for 1. Raw halloysite, 2. poly-L-lysine coated halloysite, 3. Protamine sulphate coated halloysite, 4. Sodium chloride (negative control).....	95
Figure 6.3: Viability of MCF-7 cells after 24 hr (A) and after 48 hr (B) as determined by celltiter-96 reagent. The legend stands for 1. Raw halloysite, 2. poly-L-lysine coated halloysite, 3. Protamine sulphate coated halloysite, 4. Sodium chloride (negative control). ....	96
Figure 7.1: SEM images of unloaded empty halloysite. Images were taken after sputter coating the dried sample with 2 nm thickness of Iridium.....	101
Figure 7.2: SEM images of silver nanoparticles prepared by reducing silver acetate by heat. Images were taken after sputter coating the dried sample with 2 nm thickness of Iridium. ....	102

- Figure 7.3: SEM images of silver nanoparticles prepared by reducing silver acetate by hydrogen gas. Images were taken after sputter coating the dried sample with 2 nm thickness of Iridium..... 102
- Figure 7.4: SEM images of silver nanoparticles prepared by reducing silver acetate by normal light in the presence of lysozyme. Images were taken after sputter coating the dried sample with 2 nm thickness of Iridium. .... 103
- Figure 7.5: Porosimeter results of halloysite loaded with silver prepared by reducing silver acetate by normal light in the presence of lysozyme. .... 104

## ACKNOWLEDGMENTS

I would like to extend my hearty gratitude to my advisor and mentor, Dr. Yuri Lvov, who has supported me throughout my doctoral research. Also, I would like to thank Dr. David K. Mills and his student Dr. Skylar S. Stewart-Clark for supporting and guiding me in interesting collaborative work on stem cell encapsulation. I am grateful to Dr. Sidney P. Sit and his student Ms. Stephanie Tully for the help rendered with porosimeter tests. My advisory committee members Dr. Mark DeCoster, Dr. Juan Feng, and my program chair Dr. Steven A. Jones have given great guidance, and I thank them for helping me to perform the deliverables as a graduate student. I would like to thank our collaborators Dr. Matthew Eby and Dr. Glenn Johnson, Air Force Research Laboratory /MLQL, Tyndall, FL, for their valuable discussion on synthesis of lysozyme catalyzed silver nanoparticles. My work on alginate templates would never be possible without the support of Epic Therapeutics Inc (BAXTER Healthcare Corp.) and the people there – Julia Rashba-Step, Ramin Darvari, Kimberly Gillis, and Michael Gallo. I am indebted to Dr. Dmitriy Mongayt of Northeastern University, Boston, MA, for his help in studying the cytotoxicity of halloysite. I would also like to acknowledge Dr. Yuri Voziyanov and Dr. Michael J. McShane (currently at Texas A & M University) for letting me to use their labs when the need arose.

Special thanks needs to be given to three of the post-doctoral research associates in our group, Dr. Tatsiana Shutava, Dr. Zonghuan Lu, and Dr. Grigor Bantchev for their invaluable experience and help in guiding my research.

I cannot forget my fellow lab mates, those who have already graduated and those still pursuing their degrees, for their advice and assistance in the laboratory. Additionally, the IfM faculty and staff have always been there when I needed their assistance, I acknowledge not only their commendable technical help but also in other ways which made my work at IfM a pleasant memorable one.

I would also like to acknowledge Dr. Malcolm D. Prouty for helping me in proof reading my numerous technical documents.

This work would not be possible without financial support provided by research grants from organizations such as the National Science Foundation, the Louisiana Board of Regents, Oak Ridge Institute of Science and Education and others.

Finally, I would like to thank my family and friends for their unyielding support and patience while I have been studying for my doctoral degree.

# CHAPTER 1

## INTRODUCTION

In the past few decades much research has been done in the field of Nanotechnology, a science to create nanodevices and nanostructures. This drive has been mainly inspired from our mother nature, as she stood as a perfect prototype for the Nanoindustry operating in 'bottom up' process for these many years. The fabrication of materials by building from the atomic scale is very attractive for delivering increased functionality, but practical difficulties lie in such precise construction. However, by using some of the nanomaterials (natural or synthetic) the fabrication process has become simpler but still remains challenging based on technological limitations. In the field of drug delivery, one of the most promising biomedical applications of nanotechnology, the use of nanomaterials as nanocarriers for improving the delivery methods, has shown advantageous technically and viable economically. These nanocarriers, formed by the process of nanoencapsulation are of two types, named as nanospheres and nanocapsules. Nanospheres have a matrix type structure in which the active ingredient may be absorbed on the sphere's surface or encapsulated within the particle [1]. On the other hand nanocapsules have the active ingredient confined within a liquid core enclosed by a membrane made by polymer [1, 2]. This work makes an effort to nanoengineer some bioresponsive materials as template for making submicron or nanosized drug delivery systems through the study of surface chemistry at micro and nanoscale.

### **Importance of Template Size**

A wide range of particle sizes (0.5 – 3400  $\mu\text{m}$ ) was used for drug delivery based upon the method employed and the nature of formulation [3]. However, currently due to biotechnological revolution and nanotechnological innovations the advent of proteins, oligonucleotides, DNA, polymers, micelles, micro emulsions, colloidal suspensions etc. as therapeutic agents have reduced that particle size lower limit to 1 nm.

It appears that nanospheres would be most appropriate for proteins and nucleic acid based therapeutics where it is crucial that the therapeutic carrier must enter cells and escape endosomal and lysosomal attack and deliver their cargo by transport through cytosol [4]. Poly (DLlactide-co-glycolide) nanospheres that escaped endolysosomal attack within 10 minutes of uptake as a result of reversal of their surface charge in the acidic endo-lysosomal compartment is one such rationally designed drug delivery system [5]. Also, one should note that smaller sized nanoparticles showed twenty-seven-fold higher transfection than larger nanoparticles in cell lines when other parameters like surface charge, cellular uptake and release profile were the same between them [6].

Because most of the drug delivery systems are spherical, it has been shown that a maximum circulation time of 48 hrs has been achieved for spherical particles (100 – 200 nm in diameter) in blood stream, and particles greater than 200 nm in diameter are cleared much faster than that [7-9]. Moreover, small particles with narrow size distributions have more predictable pharmacokinetics and pharmacodynamics. Hence, size does matter in determining templates for drug delivery systems.



### **Importance of Template Shape**

Many of common drug delivery systems based on liposomes or polymer micelles are spherical in shape. Hence the interaction of spherical particles with cells and within animals has been studied extensively, but the effect of shape has received very little attention. Water soluble carbon nanotubes are known to be cleared within hours from the body on intravenous injection. Recently, Discher et al. [10] filomicelles (filamentous polymeric micelles) between 22-60 nm across and 2-8  $\mu\text{m}$  long remain in the blood longer than their spherical counterparts. Hence, based upon the circulation time the shape of the template is also important in determination of proper template for drug delivery.

### **Nature and Availability of Template**

These parameters determine the economical aspects of the drug delivery systems. If it is a natural material and available in huge quantities then the cost involved for making drug delivery systems will be much less. But some of disadvantages of naturally available material are variation in the properties and size range with respect to its source.

If it is synthetic or artificial then it will be available in low quantities, and the cost involved for making drug delivery systems will be very high in comparison to naturally available templates. But the advantage is the control over the size range and the properties of the template.

Hence, a tradeoff has to be made between source and availability in determining the usage of templates for designing drug delivery systems.

## **Research Goals**

In this research work, two bioactive materials were considered as a prospective template for designing drug delivery systems. The first is the semisynthetic, spherical alginate particle and the second one is a natural nanotubular clay template, known as halloysite. This work was developed on a step by step basis based upon following some of goals, which are as follows:

- Preparing alginate spherical nanoparticles;
- Utilizing spherical alginate nanoparticles for loading and release of drug;
- Studying the application of halloysite in detail for nanoencapsulation and controlled release of drugs;

## **Dissertation Overview**

This dissertation has been organized into several individual chapters, and some redundancy has been maintained to make those chapters a more comprehensible and contiguous piece of work. Chapter 2 gives a brief overview of the background needed for this dissertation. It covers the properties and earlier applications of alginic acid, used for making alginate particles and halloysite. Further, it gives a brief overview of introductory methods used to encapsulate and release macromolecules. Moreover, various characterization methods for the encapsulation and release of the macromolecules are explained.

Chapter 3 describes the process of making alginate nanoparticles by emulsification technique and optimization of that process. These prepared alginate particles were used to study the loading and release of curcumin. Chapter 4 discusses the

use of halloysite for encapsulation and controlled release of poorly soluble drugs, namely dexamethasone, furosemide and nifedipine by simple mechanical means.

Chapter 5 describes the application of Layer-by-Layer assembly for tunable controlled release of dexamethasone. It is shown that an optimum three bilayers of very high molecular weight natural polymers gave best controlled release. Chapter 6 proves the biocompatibility of halloysite by in vitro cytotoxicity studies with 3T3 and MCF7 cells.

Chapter 7 extends the application of halloysite as a nanoreactor for template synthesis of silver/silver oxide nanoparticles. Chapter 8 concludes the dissertation by giving an overview of the encapsulation and release techniques used. Future works that can be added to these encapsulation experiments are also given.

## CHAPTER 2

### BACKGROUND AND THEORY

In this chapter the literature concerning two bioactive materials of our interest spherical alginate particles and nanotubular halloysite clay was reviewed. Also the literature concerning LbL technique used to nanoengineer these biomaterials is reviewed. Relevant instrumentation and theory used are presented for more clarity to understand the references of the same in the following sections.

#### **Spherical Alginate Particle**

Biocompatible biodegradable materials have received much attention as drug delivery vehicles for controlled release preparation [11, 12] and scaffolds for tissue engineering [13, 14]. Among them, alginic acid has been extensively investigated [13-39].

#### **Chemical Composition and Structure**

Alginates are a family of unbranched polysaccharides consisting of 1 - 4 linked,  $\alpha$ -D mannuronic acid (M) and R-L-guluronic acid (G) residues (Figure 2.1). They are a principal component of the cell walls of several brown algae. Depending upon their source, they can have different chemical (e.g., complexation) or physicochemical (e.g., biopolymer rigidity) natures due primarily to the relative proportions and sequences of

the M and G residues. Gelation occurs by cross-linking of the sodium alginate with calcium ions [13-16]. Gluronic-rich alginates are characterized by a higher affinity for divalent metals because of a “zig-zag” structure that can easily accommodate divalent cations, i.e., the “egg-box model” [16]. Other dimetal and trimetal cations can be used to cross linked alginate [17-19], as well as different polycation such as chitosan [20-25] or poly-L-lysine [26]. In some cases other techniques, for example thermal gelation of secondary component (Pluronic), can be used [27].

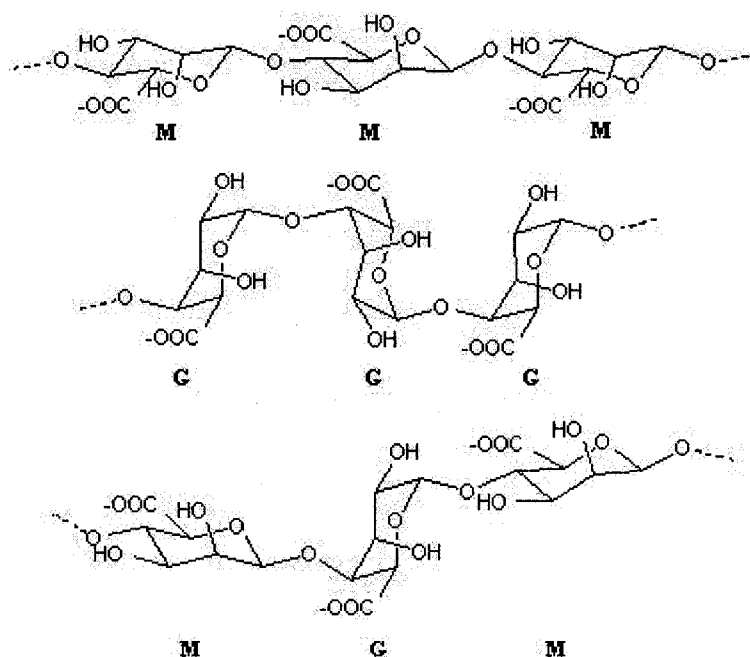


Figure 2.1: Alginic acid structure. M- mannuronic acid block, G – guluronic acid block [15].

### **Procedure for Preparing Calcium Alginate Particles**

Three main experimental techniques are useful for preparation of calcium alginate beds and particles. The most developed technique is emulsification with external addition of soluble gelation agent, which is  $\text{CaCl}_2$  in most cases, also sometimes referred to as

emulsification/external gelation [16, 26, 28-37]. The emulsification/internal gelation involves insoluble, usually calcium, salts with slow pH lowering to release the cation and form calcium alginate matrix [37-39]. One more method, complex coacervation, usually involves precipitation of alginic acid from aqueous solution by polycationic chitosan [20-25]. Mixed approaches are also used [26]. The general procedure for preparing calcium alginate micro particles is as follows.

Typically, 37.5g isooctane were stirred for 1 min at 2000 rpm, 1.06 g SPAN 85 were added and stirred for another 1 min. Then 25 g 3 % degassed alginate solution were added and stirred for 4 min. The mixture was moved to ultrasonication system, the batch was iced and ultrasonicated at 48% power for 2 min, and then it was moved back to the stirring system and 0.56 g TWEEN 85 in 2.50 g isooctane were added. The stirring was continued for 5 min at 2000 rpm. Then 10g of 10% CaCl<sub>2</sub> (pH 9) preliminary filtered through 0.20 µm syringe filter were added and stirred for 5 min at 2000 rpm and then at 1000 rpm for 15-20 min. To separate microparticles, 500 ml DI water was placed into a separation funnel, and the mixture was poured in and intensively but briefly shaken. Then after 30 min, when organic and aqueous layer were well distinguishable, microparticles were collected from the middle surfactant layer and centrifuged at 5000 rpm for 10 min. The supernatant was removed; the microparticles were washed with ethanol three times and finally dispersed in DI water.

The microparticles obtained by following the general procedure have an average diameter of 1454.4 nm and polydispersity of 0.041. The surface charge of the microparticles is negative with the average value of  $-28.29 \pm 2.35$  mV.

CLSM and SEM images of prepared calcium alginate microparticles are presented in Figure 2.2 and Figure 2.3 respectively. The diameter of nanoparticles varies from 2.5 to 0.5 micrometers. For confocal microscopy imaging, polyallylamine hydrochloride (PAH) labeled with a fluorescent dye RBITC was added to the suspension of calcium alginate microparticles. Positively charged polyelectrolyte PAH- RBITC forms a complex with negatively charged surface of calcium alginate microparticles and helps to visualize the particles.

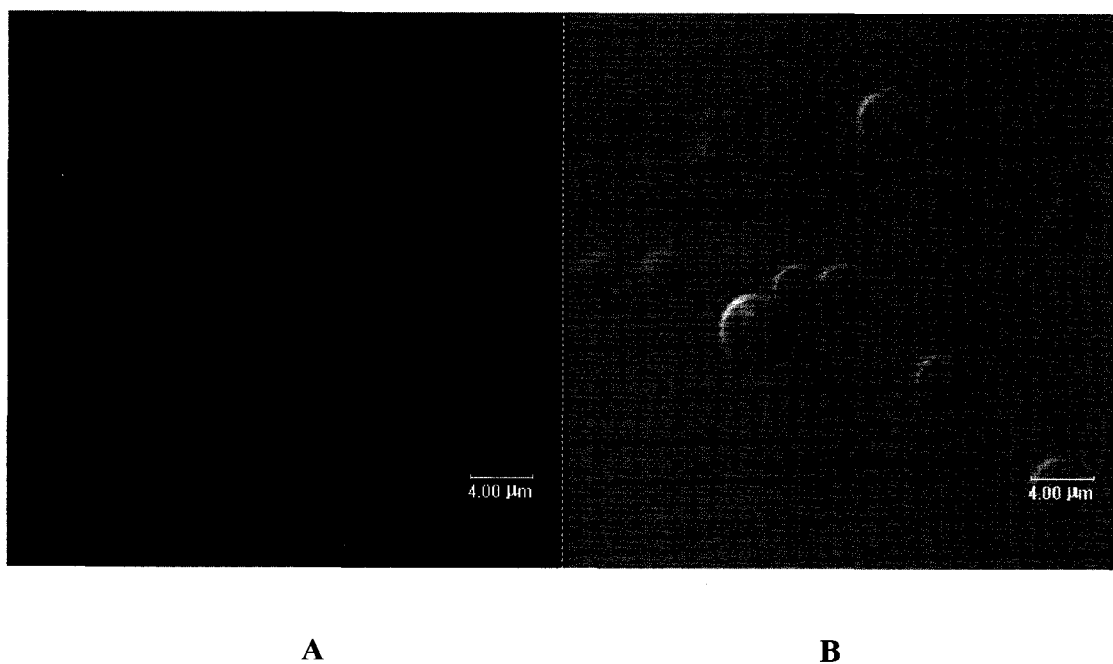


Figure 2.2: CLSM (A-fluorescence mode, B-transmission mode) images of calcium alginate microparticles prepared via emulsion technique. For fluorescence image, PAH-RBITC was coated at pH 6.5.

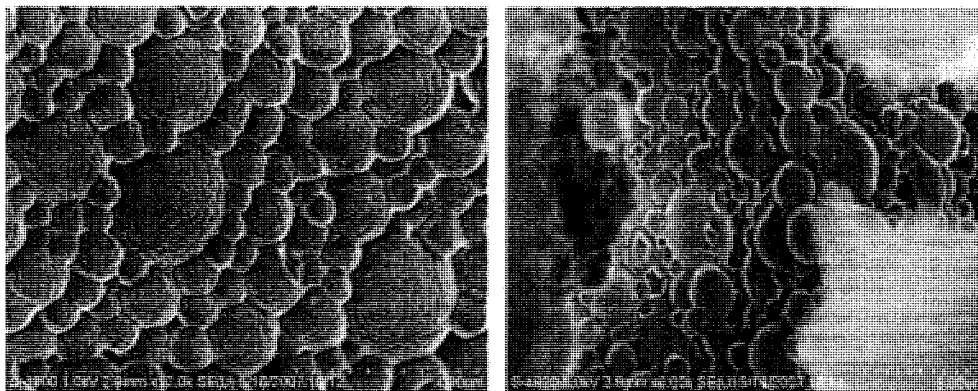


Figure 2.3: SEM images of calcium alginate microparticles prepared via emulsification technique. Images were taken after sputter coating the dried sample with 2 nm thickness of Iridium.

### **Applications**

Polysaccharides such as alginates have been used extensively in the food, cosmetics, pharmaceutical and biomedical industries for their gel-forming properties in the presence of multivalent cations. Microencapsulation in calcium alginate microparticles has been widely used for the immobilization of lactic acid bacteria owing to its ease of handling, nontoxic nature, and low cost (27-29). Alginate encapsulation has been reported as suitable for many biological and biologically active components including cells [40], enzymes [33-35], and drugs [29-32, 36].

Several macromolecular drug delivery systems are based on calcium alginate (Ho and Neufeld, 2001 [41]; Guet al., 2004 [42]). Besides release through diffusion out of the calcium alginate gel, swelling and erosion of the drug delivery system has been described as the major source of release of encapsulated macromolecular drugs (Murata et al., 1993 [43]). Correlation between the calcium alginate swelling-erosion rate and drug release rate allowed Kikuchi's team to produce a pulsatile drug delivery system characterized by a controlled lag time before release (Kikuchi et al., 1997 [44]). Chrétien's team has



shown that alginate impregnated in the acryl microspheres controlled the release rate of low molecular weight drugs [45].

Although an exhaustive amount of work has been done on alginate microparticle preparation and its use in drug delivery, only a limited amount of research has been done for alginate particles less than 1 micron. Those nanosizes are found to be extremely important for making protein or nucleic acid based therapeutic delivery systems. Earlier, the smallest alginate particle produced had a minimum size of 1-5  $\mu\text{m}$  [46, 47].

### **Nanotubular Clay Particles- Halloysite**

Halloysite is a two-layered aluminosilicate which has a predominantly hollow tubular structure in the submicron range and is chemically similar to kaolinite [48, 49]. These minerals are formed from kaolinite over millions of years due to the action of weathering and hydrothermal processes [50]. Layers are rolled into nanotubes due to the strain caused by lattice mismatch between adjacent silicone dioxide and aluminum oxide sheets [48, 50, 51].

Halloysite is mined from natural deposits in countries such as USA, Australia, New Zealand, Korea, China, and Turkey. The largest deposit in the United States is at the Dragon Mine in Utah [49, 51, 52, 53, 54].

### **Chemical Composition and Structure**

Halloysite occurs in nature as hydrated mineral that has the ideal chemical formula of  $\text{Al}_2\text{Si}_2\text{O}_5(\text{OH})_4 \cdot 2\text{H}_2\text{O}$ , which is similar to kaolinite except for the presence of an additional water monolayer between the adjacent layers. It is also called halloysite –

(10A) due to its layer thickness close to 10 Å. Heating halloysite – (10A) can easily and irreversibly dehydrate to form halloysite – (7A) [48, 50, 51, 55, 56].

Besides aluminum and silicon oxides and water of hydration, halloysite minerals were observed to contain trace amounts of other metal oxides such as iron, chromium, titanium, etc [50, 51]. Therefore it is difficult to assess the exact chemical composition of the halloysite minerals [51].

Iron oxide is the most common impurity observed in halloysite minerals (up to 12.8 wt %). This high amount of iron oxide may be due to the presence of associated iron oxides in mineral as well as due to the isomorphous substitution of  $\text{Fe}^{+3}$  for  $\text{Al}^{+3}$  in the octahedral alumina sheet [51]. According to Joussein et al.  $\text{Fe}^{+3}$  has never been reported to substitute  $\text{Si}^{+4}$  in the tetrahedral sheet of halloysite [51]. A typical chemical analysis of the halloysite from New Zealand is shown in Table 2.1.

Table 2.1: Chemical analysis of New Zealand halloysite (Source: Imery's Tableware New Zealand Ltd, Halloysite MP # 47/04).

Chemical Analysis	%
Ignition Loss	14.9
$\text{SiO}_2$	45.4
$\text{Al}_2\text{O}_3$	38.2
$\text{Fe}_2\text{O}_3$	0.48
$\text{TiO}_2$	0.12
CaO	<0.02
MgO	<0.09
$\text{K}_2\text{O}$	<0.01
$\text{Na}_2\text{O}$	<0.05
Total	99.62

In Figure 2.4 and Figure 2.5 the schematic structure of halloysite – (7A) nanotubes and kaolinite layer are shown respectively. Halloysite layer, which has a

characteristic 7.2 Å of thickness, is structurally similar to the kaolinite layer [51, 57]. The outside diameters of the tubes vary from 40 to 190 nm, with an average value of 70 nm. The diameters of internal lumen range from 15 to 100 nm and average 40 nm [48]. The lengths of tubules cover wide a range of 1 to 20 μm [49].

Halloysite forms by kaolinite layer rolling due to the action of weathering and hydrothermal processes [50]. In halloysite nanotubes silica layer is relevant to the outer surface of tube, while the alumina layer is relevant to the inner surface [50, 51]. One of the possible reasons for the formation of halloysite tubules is the lattice mismatch between adjacent tetrahedral silica sheets and octahedral alumina sheets that causes the formation of strain in platy layer [48, 50, 51]. In kaolinite minerals that strain is reduced by rotation of alternate silica tetrahedrons blocked in hydrated halloysite minerals due to the presence of interlayer water molecules [51].

Bates et al. showed that halloysite – (7A) nanotubes were collapsed to form laths or ribbons which were due to the intralayer strain produced by dehydration of halloysite – (10A) to halloysite – (7A) [1]. No evidence of hexagonal-shaped flakes was found although splitting and unrolling may lead to the formation of rectangular laths. The tube terminations of uniform character were also not observed [48].

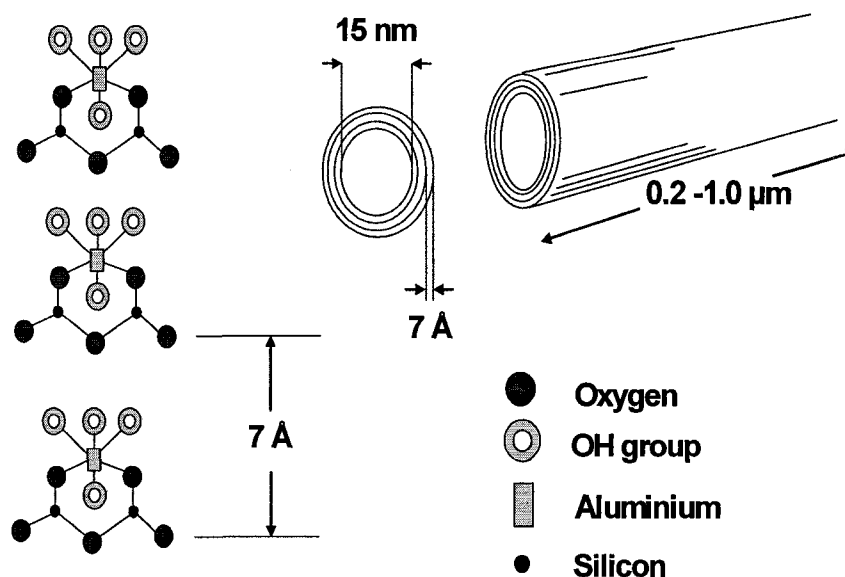


Figure 2.4: Schematic representation of halloysite-(7A) nanotubes [123].

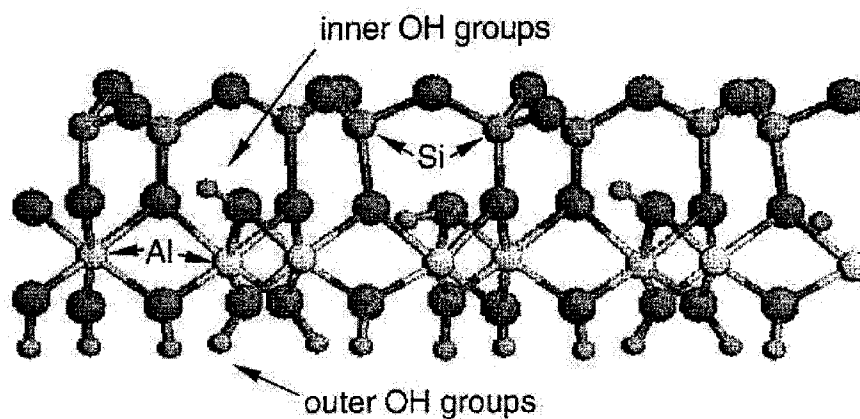


Figure 2.5: Structure of kaolinite layer [57].

## Morphology

The particle morphology of halloysite nanotubes depends on their geological occurrences and crystallization conditions and varies from tubular to platy or tabular in shape. Chemical compositions of different morphologies are also different. Platy halloysite particles always contain relatively large amounts of iron than tubular particles [51]. Figure 2.6 shows the variations in the morphology of the halloysite from different

sources and within one source the size distribution varies a lot. Figure 2.7 shows the size distribution in a halloysite sample of New Zealand.

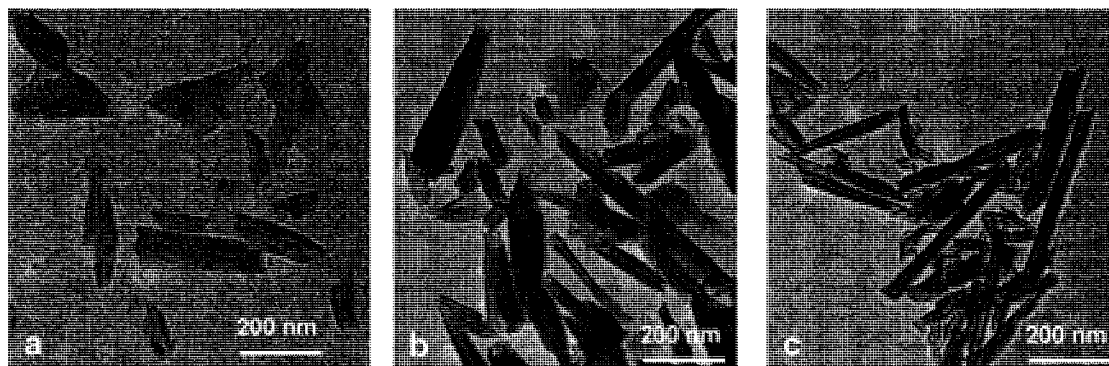


Figure 2.6: TEM images of dried halloysite from different source a. China, b. New Zealand, and c. USA (Utah).

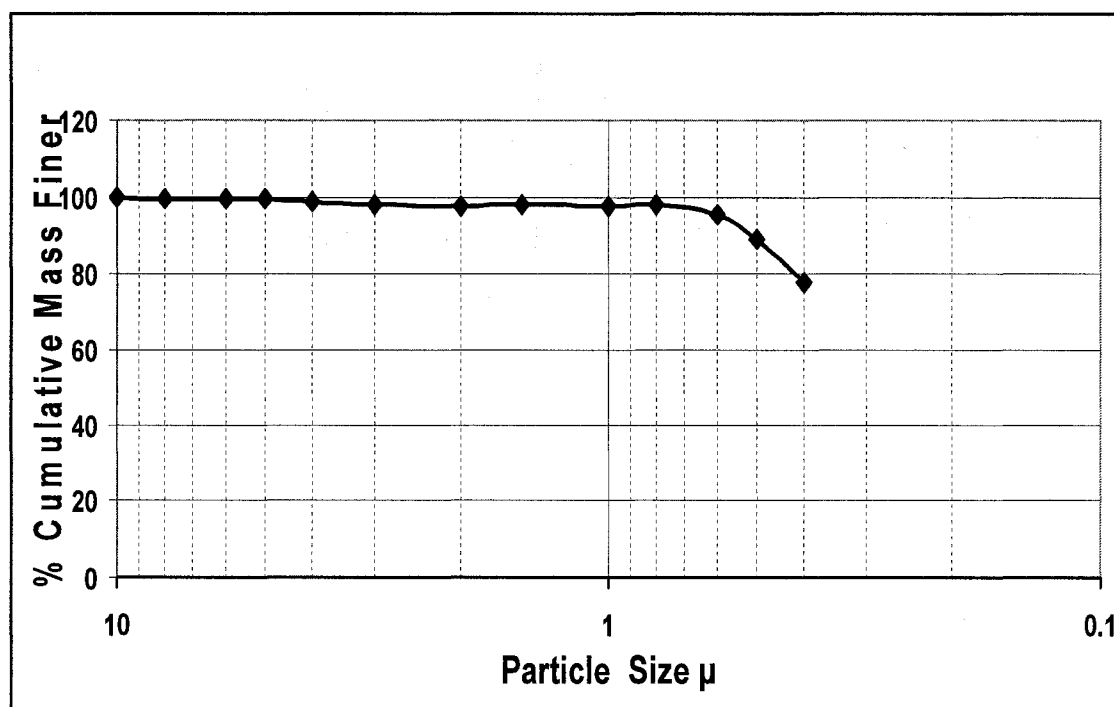


Figure 2.7: Particle size distribution of halloysite from New Zealand (Source: Imery's Tableware New Zealand Ltd, Halloysite MP # 47/04).

## **Physical and Chemical Properties**

Halloysite minerals have relatively high specific surface areas (SSA) which vary from 50 to 140  $\text{m}^2\text{g}^{-1}$  with deposit. They are abundant with narrow cylindrical pores. Therefore they can absorb relatively big class of compounds from inorganic salts (such as the salts of alkaline metals and ammonia) [51, 58] to organic molecules (such as ethanol, glycerol, acetone, dimethylsulphoxide, formaldehyde) [51, 59, 60] as well as polymers and biologically active agents (such as tetracycline hydrochloride, khellin, nicotinamide adenine dinucleotide, and Poly-ethylene Glycol) [49, 55].

Absorption of salts and small organic molecules mainly take place mainly by their intercalation into interlayer space [51, 55, 58], whereas big polymer molecules, proteins and drugs, are bound to its outer and inner faces [49, 55]. Intercalation does not occur with polymers, proteins, and other macromolecules due to their large molecular size [55]. Among all of the organic compounds, only the ones that have small molecular sizes and hydrophilic functional groups such as  $-\text{OH}$  and  $-\text{NH}_2$  were observed to form an intercalation complex with halloysite nanotubes, possibly due to the formation of hydrogen bonds between them and alumina or silica layers [51, 55, 59, 60].

The adsorptive and ion exchange properties of halloysite nanotubes are highly affected by their surface charges which are pH-dependent [50, 51]. Surface charge pH dependence of kaolinite and halloysite were studied by Tari et al. in [50]. Zeta potential curves of both halloysite and kaolinite fall between the curves of  $\text{SiO}_2$  and  $\alpha\text{-Al}_2\text{O}_3$  indicating that both materials contribute to the surface charges of observed minerals. However, halloysite has higher negative surface charge compared with kaolinite showing the predominance of silica properties at the outer surface [50].

## Capillary Force

The capillary force which helps in higher adsorption of several materials is calculated by using the following simple formula, with notes on the dimension in SI units, the height  $h$  of a liquid column (m) is given by [61]:

$$h = (2\gamma \cos\theta) / (\rho gr)$$

where:

- $\gamma$  is the liquid-air surface tension (J/m<sup>2</sup> or N/m)
- $\theta$  is the contact angle
- $\rho$  is the density of liquid (kg/m<sup>3</sup>)
- $g$  is acceleration due to gravity (m/s<sup>2</sup>)
- $r$  is radius of tube (m)

For a water-filled tube in air at sea level,

$\gamma$  is 0.0728 J/m<sup>2</sup> at 20 °C

$\theta$  is 20° (0.35 rad)

$\rho$  is 1000 kg/m<sup>3</sup>

$g$  is 9.8 m/s<sup>2</sup>

therefore, the height of the water column is given by:

$$h = (1.4 \times 10^{-5}) / r$$

For halloysite nanotubes of average inner radius of 7nm the capillary force in terms of height of the water column is  $h \sim 2000$  m (in terms of atmosphere  $h \sim 200$  atm). Hence it is understandable that this much higher capillary force helps halloysite in quick adsorption of several materials.

## **Applications**

Before the discovery of their fine nanotubular structuring, halloysite minerals have widely been used in the production of the porcelain products, and bone china. Establishment of their structure and other exciting physicochemical properties opened a broad range of new applications for these abundantly available materials [51].

Halloysite nanotubes can replace carbon nanotubes or boron nitride nanotubes in a number of nanotechnology applications in which chemistry of the tubes is less important [62]. These nanotubes can be loaded with the big variety of other metal ions (such as  $\text{Fe}^{+2}$ ,  $\text{Fe}^{+3}$ ,  $\text{Ni}^{+2}$ ,  $\text{Cu}^{+2}$ ,  $\text{Bi}^{+3}$ ,  $\text{Ag}^{+1}$ ) by mixing them with concentrated solution of corresponding metal nitrate or chloride and subjecting the obtained mixture into a vacuum jar. The procedure of vacuum pulling can be repeated several times to increase the amount of loaded substance. Loading efficiency of halloysite nanotubes vary from trace amounts to almost 100% depending on the loaded substance. Potential exists to modify loaded compounds inside halloyside nanotube by heating or electron irradiation to produce insulated nanorods and nanowires with specific magnetic and electric properties [62].

Besides inorganic salts, halloysite nanotubes can also be filled with a large range of organic and biologically active agents including lubricants, herbicides, pest repellents, pharmaceuticals, cosmetics, food and personal products, as well as other agents that could benefit from a controlled release [49, 51, 55, 56, 63]. Having chemically different external (silicone dioxide) and internal (aluminium oxide) surface structure, halloysite nanotubes offer scope for chemical control of preferential internal, rather than external loading of desired compounds [62]. Price et al studied the release profiles of



oxytetracycline hydrochloride (water soluble antibiotic), khellin (vasodilator that promotes hair growth) and nicotinamide adenine dinucleotide – NAD (an important coenzyme in many biochemical reactions including fatty acid and nucleic acid biosynthesis) from halloysite nanotubes [49]. Agents were loaded to halloysite from water solution or molten state by using vacuum jar. To reduce the release rate for oxytetracycline hydrochloride, it was loaded to halloysite nanotubes together with compatible polymeric material epoxy Qitol 651. Before loading hydrophobic agent – khellin, water associated with halloysite was removed by heating the clay in ethylene glycol at 100 °C [49].

Due to their porous structure and chemically active external and internal surfaces halloysite particles can be used in the remediation of acid mine drainage, water purification in refining industries, as well as in the separation of liquids and gaseous mixtures [51]. Kutsuna et al. studied catalytic degradation of tetrachloroethene ( $\text{CCl}_2 = \text{CCl}_2$ ) on halloysite and kaolinite under photoillumination. This substance is widely used for cleaning metals and semiconductors and causes groundwater pollution [64].

Schukin et al. studied the possibility of using the inner lumen of halloysite tubes as nanoreactors for biomimetic synthesis of inorganic substances. Authors used the reaction of urease catalysed deposition of  $\text{CaCO}_3$  into halloside nanotubes as a model reaction to demonstrate the possibility of conducting enzymatic biomineralization inside the pores of halloysite particles [65].

Complete loading of halloysite nanotubes was achieved by immersion of urease loaded halloysite particles in a half-molar (0.5M) water solution of urea and calcium chloride for 30 min (Figure 2.8) [65].

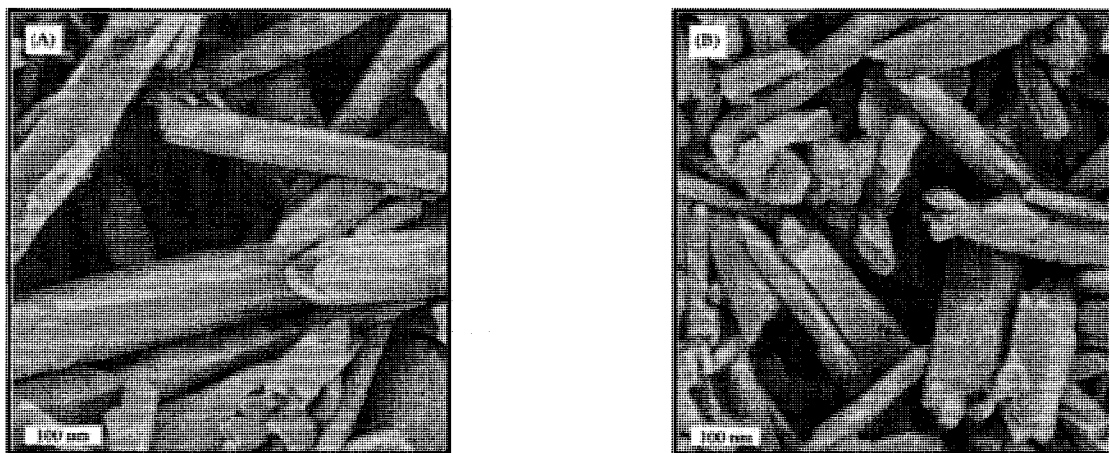


Figure 2.8: SEM images of halloysite nanotubes before A) and after B) loading with  $\text{CaCO}_3$  [65].

Halloysite nanotubes, having negative surface charge, can be used in production of thin films with specific enzymatic properties by using layer-by-layer (LbL) nanoassembly technique. Lvov et al. analyzed the structure of thin films produced by sequential adsorption of Polyethyleneimine (PEI) and halloysite nanotubes (Figure 2.9) [66].

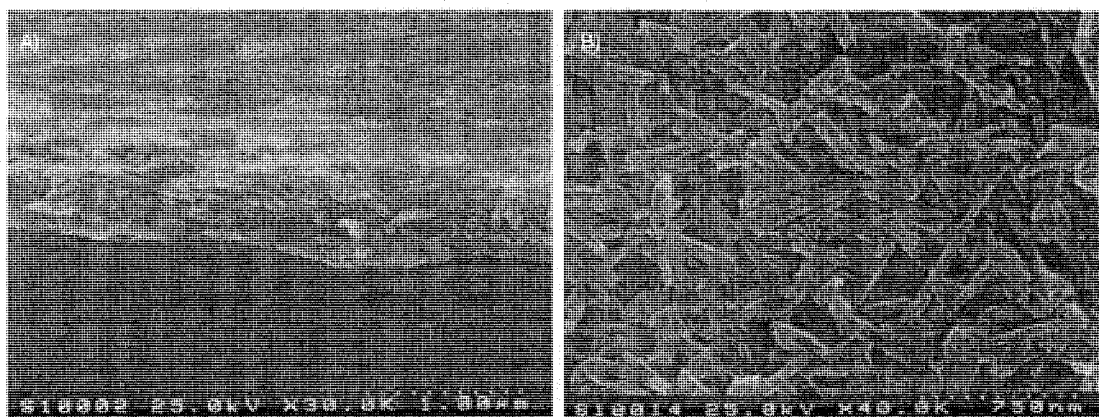


Figure 2.9: SEM image thin film, produced by LbL deposition of halloysite, Polyethyleneimine and Polystyrenesulfonate. A) Cross – section view, B) top view [66].

The assembly of Alcohol dehydrogenase (ADH) - an enzyme that catalyses the oxidation of alcohols to aldehydes in the presence of the cofactor Nicotinamide Adenine Dinucleotide (NAD), and halloysite multilayers - was also achieved. This work promises the production of enzymatic microreactor by the assembly of NAD-loaded halloysite nanotubes and ADH. Slow release of NAD from halloysite nanotubes, deposited together with ADH enzyme into polymer film by LbL technique, can extend the period of enzymes catalytic activity [66].

Lu et al. studied the effect of coating of lignocellulose wood fibers (used for the production of paper) with halloysite and other particles by using LbL nanoassembly. Although coating of wood fibers with halloysite slightly reduced paper brightness and tensile strength, it drastically increased the porosity. High-porous papers produced by LbL nanoparticle coating can be used in pharmaceutical and biomedical applications such as nano drug reservoirs for molecular loading and controlled release [52].

Modification of electrical, physicochemical properties of halloysite particles was achieved by their surface coating with metals and other substances. Such coated particles are ideal for use in electronic fabrication and other high-tech ceramic composite applications [51, 53]. Baral et al. carried out the metallization of halloysite particles by using electroless plating technique to deposit a thin nickel film on the surface of halloysite nanotubes [53]. Before metallization, the surface of halloysite particles was activated by acidic palladium chloride ( $\text{PdCl}_2$ ) solution and acidic stannous chloride ( $\text{SnCl}_2$ ) solution. Activation of the surface can be explained by the formation of small palladium metal particles on the substrate surface. These particles catalyze metal ion reduction on halloysite external surface [53].

Halloysite nanotubes were plated in Niposit468 nickel plating bath. This method was known to deposit up to 99.9% pure ferromagnetic nickel metal on substrate surface. The efficiency of halloysite particle coating was verified by EDX elemental analysis which showed that 95.5 atom% of metallic nickel is present within a 5-10 nm depth of substrate surface. TEM analysis of nickel-coated halloysite particles indicated that the average thickness of nickel film is about 20 nm [53].

### **Preliminary Work**

Some preliminary work was done with halloysite to understand the effect of morphology on loading and release of a poorly soluble drug, dexamethasone. Figure 2.10 shows the effect of the halloysite source on the release profile of dexamethasone drug. The China halloysite has a very slow release because the morphology of these tubes (Figure 2.6 a) are very short and has a lower lumen diameter when compared with the rest, and the New Zealand halloysite has a very fast release, that can be attributed to the presence of longer nanotubes (Figure 2.6 b) and as well as large hollow cones peculiar to halloysite from New Zealand.

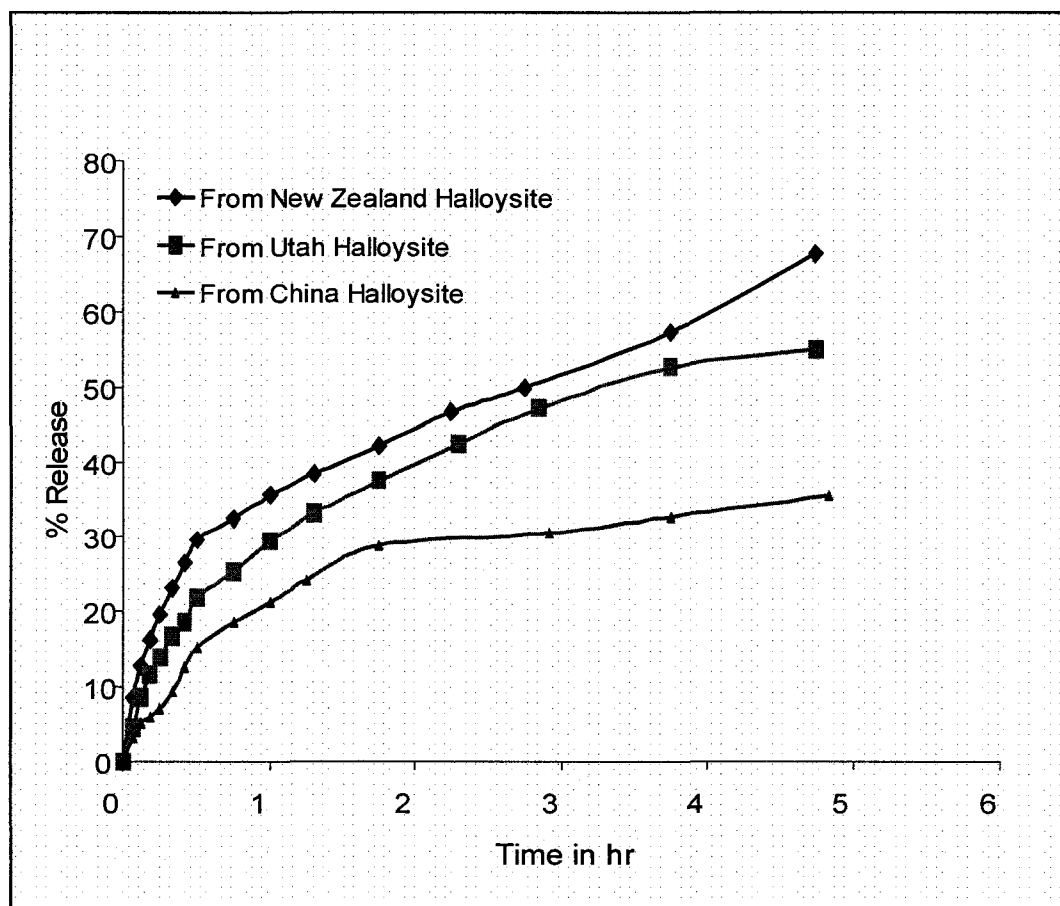


Figure 2.10: Dexamethasone release comparison in water from halloysite of different source: loading done from drug saturated water solvent.

Loading of halloysite with DNA Oligomer was experimented by pulling vacuum in a single step, as the fluorescein tagged DNA Oligomer is highly sensitive to light. The loading is done at three different pH conditions and the amount of DNA loaded is found out by observing the difference in the fluorescence intensity of fresh DNA solution and spent DNA solution (after halloysite adsorption) using fluorescence spectrophotometer. To confirm the presence of DNA inside the lumen a TEM image of loaded halloysite was taken.

It is very difficult to decipher the presence of DNA Oligomer inside the lumen from the TEM image of loaded halloysite (Figure 2.11). However the presence of Uranyl

acetate material inside the lumen, which negatively stains the DNA, confirms the presence of DNA inside the lumen. Further, the amount of loading increases with the decrease in pH (Figure 2.12). We know that halloysite has an inner alumina layer and outer silica layer and, from our characterization, the net negative charge decreases with decrease in pH, suggesting an increase in the positive charge of inside alumina layer. This positive charge aids in more adsorption of negatively charged DNA electrostatically. Hence, this experiment reaffirms that the DNA Oligomer adsorbed is present inside the lumen having alumina layer, acting as a driving force for the loading of DNA.

**A****B**

Figure 2.11: TEM picture of Unloaded Halloysite (A) and DNA oligomer loaded halloysite (B).

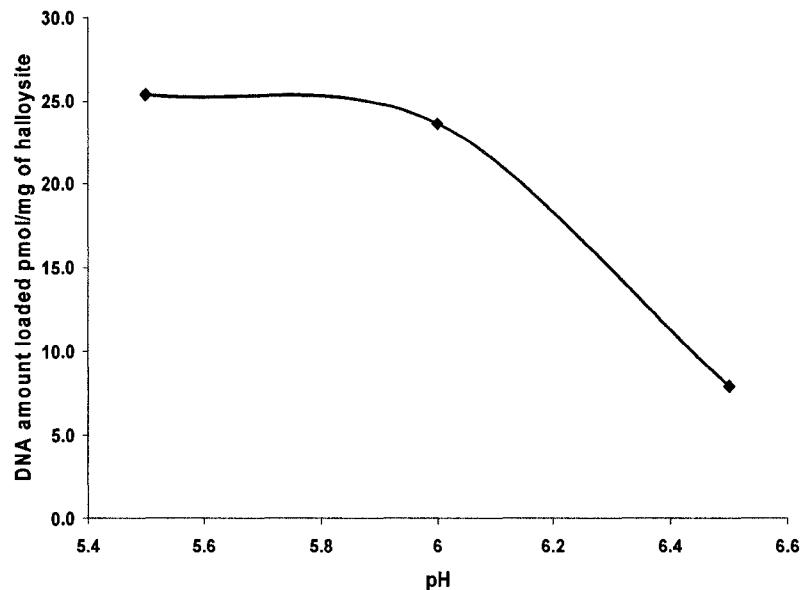


Figure 2.12: DNA loading variation with respect to pH: loading using water as solvent.

Nanotubular structure and variety of specific physicochemical properties make halloysite particles impressive in a broad range of nanotechnology applications including being nanocapsules for biologically active substances, production of thin polymer films by LbL nanoassembly, modification of paper properties, etc. However, the potentials for the applications of these naturally abundant materials have not been totally discovered. There is no doubt that further in-depth research on halloysite will open new technological and biomedical application areas for these exciting nanotubes.

### Layer-by-Layer Assembly

Nanoencapsulation of drugs involves the formation of drug-loaded particles with diameters ranging from 1 to 100 nm [67]. It describe the preparation of nanoscale assemblies, which can be relatively simple nanoemulsions, nanoparticles, polymer conjugates of proteins or drugs, or complex multicomponent systems containing drugs,

proteins, or genes, as well as arrays of targeting ligands and/or signal systems, to enable in vitro or in vivo detection. Currently, only two nanoparticle products, Doxil<sup>®</sup> and Abraxane<sup>®</sup> have been approved by FDA for clinical use in cancer chemotherapy. But many more are being developed and are in phase I, II, or III of the drug development process. These complex nanosized products are formed either by self-assembling or involve covalent conjugation techniques. The bioactive materials used to fabricate such drug delivery packages typically include synthetic or semi-synthetic polymers such as poly-ethylene glycol, and/or natural materials such as lipids, dendrimers, biopolymers, and proteins. Formation of nanoshells is one method of making drug delivery systems.

Among the nanoshells the metallic nanoparticles with a dielectric core having thin metallic coating [68-74] and nanoshells formed by electrostatic Layer-by-Layer (LbL) self-assembly [75] are the most widely studied nanoshells. In this work the materials under consideration for study (Alginate and Halloysite) are not dielectric, hence the background and theory of electrostatic LbL assembly was discussed in detail.

In the last 10-15 years, electrostatic Layer-by-Layer self-assembly has been developed as a pragmatic, versatile, reliable and simple method to form nanoshells by several researchers like Lvov et al. [75-79], Tieke et al. [80]. The Layer-by-Layer (LbL) nanoencapsulation method involves the formation of a nanothick shell around a core of any shape and size. The desirable features of LbL assembly are that the nanoshell is stable, permeable, compatible, and allows the release of the core material through it. Depending upon the usage of core templates, the cores are divided into two types namely “passive” (such as 50 – 300 nm latex or silica), which later will be dissolved to provide space for active ingredient, and “active” (such as drug, protein, and DNA) which itself



acts as functional ingredient. The ease with which we can tailor several varieties of biofunctional materials as cores [82] and as well as shells [75, 76, 78, 79] was one of the key advantage of electrostatic Layer-by-Layer assembly. Of recently, only general aspects of this method have been studied, however still further elaboration and understanding is needed to achieve its complete potential.

### **Preparation of LbL Nanoshells**

The sequential adsorption of oppositely charged colloids was reported in a seminal paper in 1966 by Iler [81]. The technique of LbL self-assembly for thin films by means of alternate adsorption of oppositely charged linear polyions was then further developed in the early 1990s [82-85]. The basis of the method involves resaturation of polyion adsorption, resulting in the reversal of the terminal surface charges of the film after deposition of each layer.

Layer-by-Layer self-assembly can construct an ultrathin film via alternate adsorption of oppositely charged polyions, nanoparticles, and biomolecules. The obtained films have thicknesses in the nanometer range and tunable properties to their environment, such as permeability, solubility, and morphology [77, 86-89]. The development of polyelectrolyte microcapsules is based on LbL assembly on nano or microscale cores, for instance cells, and inorganic or organic particles, including drugs, which have recently gained intensive attention [82, 90-95].

Cores with diameters ranging from nanometers to microns are coated with alternating layers of linear polycations, polyanions, and other materials. After dissolving the cores, hollow microcapsules were gained with ordered walls of desired composition, and thicknesses in the range of 5 – 100 nm. The capsules have tunable permeability for

molecules of different sizes on the basis of open-and-close mechanisms by adjusting the environmental stimuli [96-102]. These capsules offer broad perspectives in encapsulation, transport, and controllable delivery of drugs, minerals, and proteins. Changing the pH value of solutions induces the formation of tiny pores in the nanometer range, allowing macromolecules to pass through the capsule walls [98, 101]; adjusting solution ionic strength or adding organic solvent will also influence permeability [95, 100, 102]. These permeability controls are achieved by changing the charge densities of linear polyelectrolytes, resulting in relaxing the capsule walls. However, the austere conditions of these methods limit their use in the biomedical field for controlled drug delivery applications because they are often inconsistent with physiological conditions occurring within the human body.

The basic scheme of the LbL assembly was shown in Figure 2.13 for 2D substrates and in Figure 2.14 for 3D substrates. A standard approach for film preparation can be obtained elsewhere [82, 84, 103].

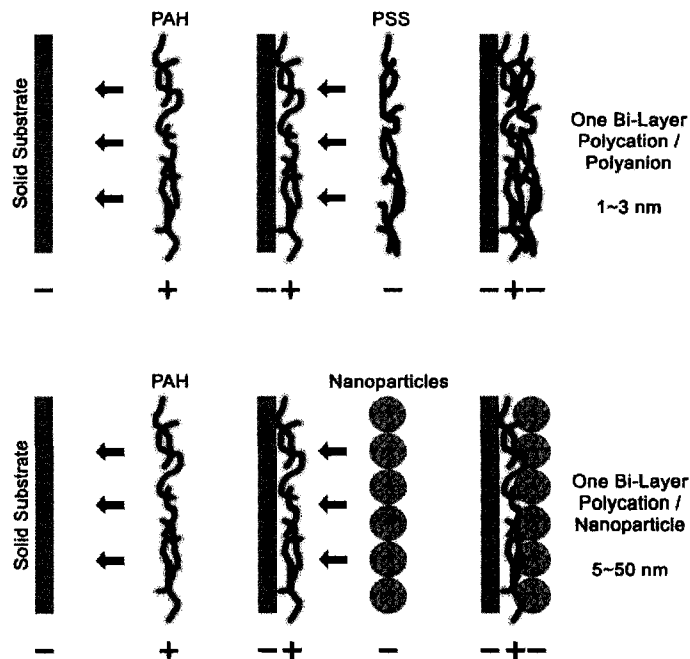


Figure 2.13: Scheme of electrostatic layer-by-layer self-assembly on 2-D substrates with (top) polycations and polyanions, and (bottom) polycations and negatively charged nanoparticles.

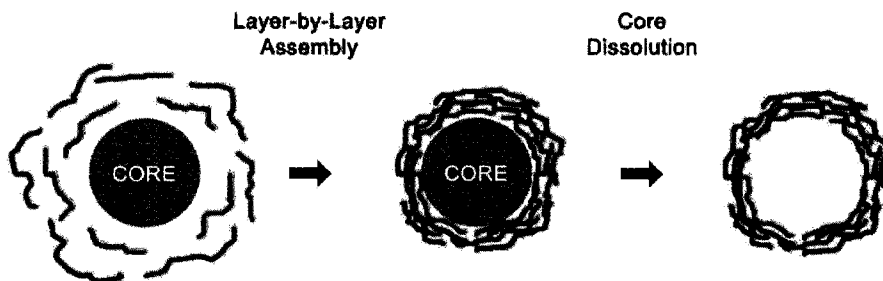


Figure 2.14: Scheme of electrostatic layer-by-layer self-assembly on 3-D microtemplates, or cores, followed by core dissolution.

These methods provide the possibility of designing ultrathin multilayer films with a precision better than one nanometer of defined molecular composition. To date, these methods have been used with more than 50 different charged macromolecules. The polyions predominately used in the assembly are as follows:

- Polycations: chitosan (CH), gelatin A (GA), poly(allylamine hydrochloride) (PAH), poly(dimethyldiallylammonium chloride) (PDDA), polyethylenimine (PEI), poly-L-lysine (PLL), and protamine sulfate C (PS).
- Polyanions: sodium carboxymethyl cellulose (CMC), chondroitin sulfate sodium salt (CS), deoxyribonucleic acid (DNA), dextran sulfate sodium salt (DS), gelatin B (GB), heparin sodium salt (HEP), poly(acrylic acid) (PAA), poly(sodium 4-styrenesulfonate) (PSS), poly(vinyl sulfate) (PVS), sodium alginate (SA), and tannic acid (TA).

These charged materials can be combined with enzymes, antibodies, viruses, and inorganic nanoparticles to produce multifunctional shells in both 2-D and 3-D nanoassembly processes. The architecture of these shells can be designed with nanometer precision to meet different requirements such as thickness, biocompatibility, controlled permeability, targeting, and optical or magnetic properties.

Any charged polyelectrolytes, polymers, nanoparticles, biomolecules, lipids and viruses can be used for LbL assembly process on any charged template of any shape and size. The only determining factor for successful assembly is the reversal of the charge upon deposition of the layers. This is achieved by selecting proper assembly conditions like pH, temperature and concentration of the assembling components [104]. The use of any kind of materials as coating component is often advantageous as proper selection of the materials helps us in achieving the desired mechanical strength, elasticity, electrical and optical characteristics of the shell, and other properties make them unique building blocks for the creation of composite materials. In addition, the incorporation of bioactive

compounds like drugs, therapeutic proteins and nucleic acids in multilayer films may lead to applications in biosensors, pharmacy, and biotechnology [99, 105, 106].

### **Nanoshells Monitoring**

For the time-dependent monitoring of LbL assembly in situ, a quartz crystal microbalance (QCM) is most often used because of its proven suitability [82, 107, 108]. First of all, the kinetics of the adsorption process can be delineated by the QCM technique, indispensable for establishing proper assembly conditions (e.g., saturation adsorption time). Multilayer assembly is generally characterized by means of the quartz crystal microbalance technique in two ways: 1) after drying a sample in a nitrogen stream, the resonance frequency shift is measured and the calculation of the adsorbed mass is done by the Sauerbrey equation; or 2) by monitoring of the resonance frequency during the adsorption process onto one side of the resonator, which is in permanent contact with the polyion solutions. The Sauerbrey equation is given as

$$\Delta f = -\frac{\Delta m f^2}{\rho v}, \quad (2.1)$$

where  $\Delta f$  is the change in frequency,  $\Delta m$  is the change in mass per surface area,  $f$  is the frequency of the resonator (9 MHz),  $\rho$  is the density of the quartz ( $2,650 \text{ kg}\cdot\text{m}^{-3}$ ), and  $v$  is the propagation of sound in quartz ( $3,340 \text{ m}\cdot\text{s}^{-1}$ ). In solution, QCM frequency shifts of about 800 Hz are seen for every adsorption cycle, which is more than that detected for a dried film of PSS/PAH. This difference is ascribed to the strong hydration of the most recently adsorbed layer. The bound water is included in the film, and is removed after drying, meaning that most polyion films swell by 40 – 60 % before drying,

and that only 5 – 10 % of the water remains in polyion films after drying. Figure 2.15 shows the thickness of  $(\text{PSS}/\text{PAH})_2(\text{TA}/\text{PAH})_3$  films adsorbed on QCM resonators.

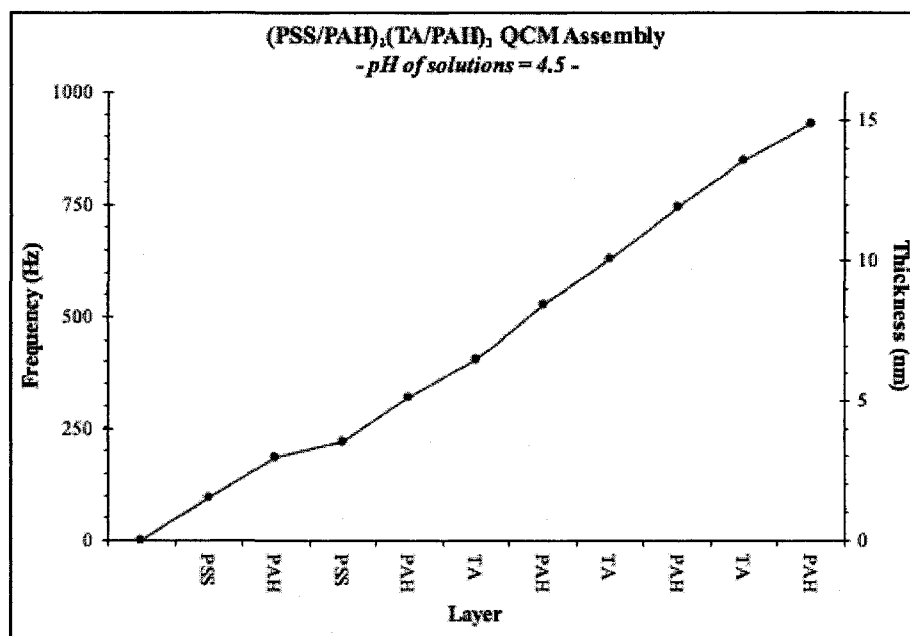


Figure 2.15: Frequency shift and film thickness of each assembled layer for  $(\text{PSS}/\text{PAH})_2(\text{TA}/\text{PAH})_3$  adsorption on QCM electrodes. The first two precursor layers are PSS/PAH, and the next three layers are TA/PAH. The tannic acid and poly(allylamine hydrochloride) has an average thickness of  $1.57 \pm 0.11$  nm and  $1.69 \pm 0.35$  nm, respectively [109].

Another method to check and confirm the assembly process is by observing the reversal of surface charge after each polymer or polyion coating as shown in Figure 2.16. The zeta-potential or surface potential, of the suspended nanoshells is measured after each layer has been applied. In Figure 2.16 negatively charged CD 40 DNA microspheres are used as cores, poly-L-lysine (PLL) as polycation, and carboxy methyl cellulose (CMC) as polyanion. Since the adsorption is carried out at a relatively high concentration of polymers (PLL), a number of charged ionic groups remain exposed at the outer surface even after the charge compensation or nullification by the cores, and thus the surface

charge is effectively reversed and helps in preventing further polymer (PLL) adsorption. The CD 40 microspheres are then washed by centrifugation to remove excess free polymers. The surface is then immersed in a solution of anionic CMC. Again, a layer is adsorbed, but now the original surface charge (negative) is restored, and the surface is ready for further assembly of positively charged polymers. These two steps are repeated alternately until a layer of the desired thickness is obtained. More than two components can be used in one assembly step as long as proper reversal of charges are observed for each subsequent adsorption [75, 82, 110].

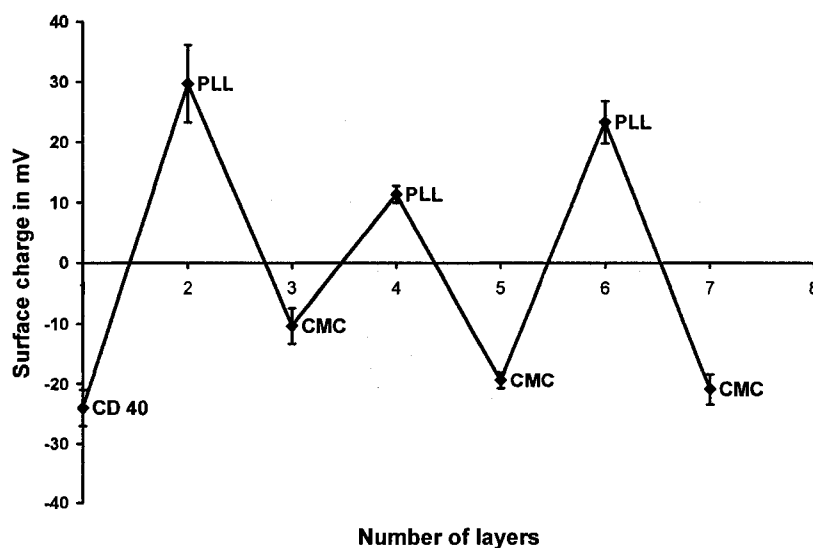


Figure 2.16: Surface charge alternation of polymers poly-L-lysine (PLL) and carboxy methyl cellulose (CMC) coated on CD 40 DNA microspheres (Obtained from EPIC-Therapeutics, a subsidiary of BAXTER Inc.) at pH 6.5.

Visual confirmation of the layers assembled can be obtained by CLSM images. For example, Figure 2.17 shows the CLSM images of poly-L-lysine (PLL) coated microspheres. PLL coating can be observed by red rings due to its tagging by Rhodamine-iso-thio-cyanate and the microspheres in green due to its innate fluorescence.

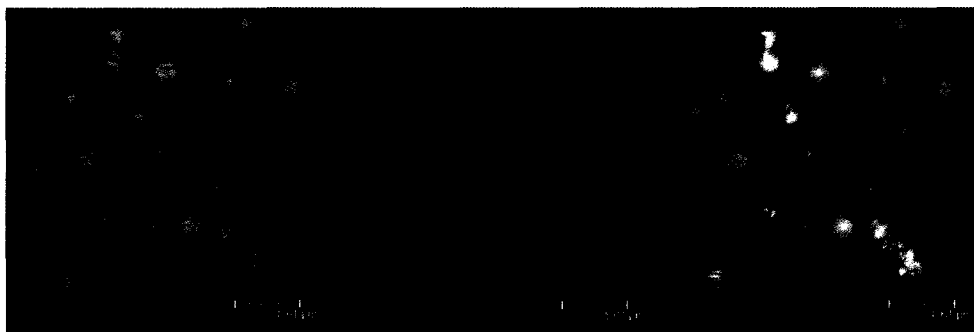


Figure 2.17: CLSM images of poly-L-lysine coated CD40 DNA microspheres (Obtained from EPIC-Therapeutics, a subsidiary of BAXTER Inc.). For visualization poly-L-lysine was tagged with Rhodamine-iso-thio-cyanate (RITC).

The growth steps of 1.1 – 2.0 nm for a bi-layer of polyelectrolytes are typical for alternate linear polyion assembly, and a thickness of one layer often equals to half of this value [111]. These values correspond to a polyion cross-section, and show that in one cycle of excessive adsorption, approximately one-monolayer coverage of the substrate takes place. The nanoparticle/polyion bi-layer thickness is determined by the diameter of the particles. Model fitting of X-ray data gives a surface roughness of the polyion film on the order of 1 nm, while atomic force microscopy and scanning electron microscopy data reveal a surface roughness of 1 – 2 nm [112]. Polyion films are insoluble in water and in many organic solvents, and are stable to 250 – 280 °C [113].

The polycation/polyanion bi-layer thickness depends on the charge density of the polyions. It was shown that more than 10 % of polyion side groups have to be ionized for a stable reproducible multilayer assembly via alternate electrostatic adsorption [114]. High ionization of polyions results in a smaller step of film growth (1 – 2 nm), and lower ionization gives a larger growth step (3 – 6 nm). It can be reached either by adding salt to a polyion solution (as discussed above for strong polyelectrolytes, such as PDPA and PSS), or by varying the pH for weak polyelectrolytes [86].



**CHAPTER 3**

**OPTIMIZATION OF ALGINATE MICRO /  
NANO PARTICLE PREPARATION AND  
ITS USE AS SPHERICAL TEMPLATE  
FOR ENCAPSULATION AND  
RELEASE OF CURCUMIN**

**Introduction**

Alginate encapsulation has been reported as suitable for many biological and biologically active components including cells [40], enzymes [33-35], and drugs [29-32, 36], owing to the relatively inert aqueous environment within the matrix, the mild room-temperature encapsulation process, and high gel porosity allowing high diffusion rates of macromolecules.

Most of the preparation methods have been developed for beads and microparticles of gelled alginic acid with sizes much greater than several microns, sometimes several tens of microns [15-35, 37-39]. At the same time, only a limited amount of research has been done for particles less than 1 micron, and especially, for those with diameter less than 300 nm that, as believed, are more promising for drug delivery applications [24-26, 36].

This work describes the development of a simple reproducible experimental approach to prepare calcium alginate nanoparticles with diameter less than 300 nm via emulsification technique. Emulsification is a well developed method to obtain micro and nanodroplets of target substance in continuous organic phase. Emulsification/external gelation technique is widely used to prepare calcium alginate nanoparticles with a diameter larger than several hundred of nanometers or several microns. Different parameters of preparation procedure were varied to reduce calcium alginate particle size considerably and achieve nanoparticles with diameter less than 300 nm. The following parameters were alternated: oil (organic) phase composition, oil/water phase ratio, hydrophobic/hydrophilic surfactant ratio, different surfactants, varying concentration of alginic acid solution, ratio between gelation agent (CaCl<sub>2</sub>) and alginic acid, another gelling agent, type (source) of alginic acid with varying G/M ratio.

## **Materials and Methods**

### **Alginic Acid**

The following different types of alginic acid were used:

Alginic acid sodium salt of medium viscosity (Sigma, viscosity of 2% solution at 20 0C is 225 mPas).

Alginic acid sodium salt of high viscosity (FMC Biopolymer, Protanal LF 200 S, G/M 65%-75% / 25%-35%, viscosity (1% solution at 20 0C) is 200-400 mPas).

Alginic acid sodium salt of medium viscosity (FMC Biopolymer, Protanal LF 10/60 S, G/M 65%-75% / 25%-35%, viscosity (1% solution at 20 0C) is 20-70 mPas).

Alginic acid sodium salt of medium viscosity (FMC Biopolymer, Protanal LFR 5/60 S, G/M 65%-75% / 25%-35%, viscosity (1% solution at 20 0C) is <10 mPas).

## **Surfactants**

The following different surfactants were used:

SPAN85 (Sigma), SPAN 20 (Sigma), TWEEN 85 (Sigma), and AOT (Bis(2-ethylhexyl) sulfosuccinate sodium salt or Docusate sodium salt, Sigma Aldrich ).

## **Organic Solvents**

The following different organic solvents were used:

isooctane (Sigma), cyclohexane (Sigma Aldrich), hexadecane (Sigma), hexane (Fisher Scientific), ethanol (Sigma), and chloroform (Fisher Scientific C298-500, Lot 011399).

In addition polygalacturonic acid potassium salt (Sigma), chitosan low molecular weight (Aldrich), and calcium chloride (Fluka) were used.

## **Equipment**

A Cole-Parmer ultrasonic processor CPX750 and a Stir-pak laboratory mixer, model 50002-02, equipped with a stirring head, model 50002-40, were used for emulsion preparation.

Eppendorf 5804R centrifuge was used to separate nanoparticles from supernatant, a Branson 1510 Sonicator resuspended nanoparticles after centrifugation.

## **General Procedure to Prepare Calcium Alginate Nanoparticles by Emulsification Technique**

Typically, 37.5g isooctane were stirred for 1 min at 2000 rpm, 1.70 g SPAN 85 were added and stirred for another 1 min. Then 25 g 3 % degassed alginate solution were

added and stirred for 4 min. The mixture was moved to ultrasonication system, the batch was iced and ultrasonicated at 80% power for 20 min, then 0.90 g TWEEN 85 in 2.80 g isooctane were added, and the ultrasonication was continued for 10 min at 2000 rpm. Then 10g of 10% CaCl<sub>2</sub> (pH 9), preliminary filtered through 0.20 µm syringe filter were added and sonicated for 5 min at 2000 rpm and then stirred at 1000 rpm for 15-20 min. To separate microparticles, 500 ml DI water was placed into a separation funnel, the mixture was poured in and intensively but briefly shaken. After 30 min, when organic and aqueous layer were well distinguishable, microparticles were collected from the middle surfactant layer and centrifuged at 5000 rpm for 10 min. The supernatant was removed, the microparticles were washed with ethanol two times and finally dispersed in DI water. The particles were stored at 4°C.

### **Characterization of Calcium Alginate Nanoparticles**

The measurements of nanoparticle hydrodynamic diameter and surface charge measurements were carried out on a ZetaPlus Brookhaven microelectrophoretic instrument in either water or ethanol. For the measurements, 0.1 mL of nanoparticle suspension was redispersed in 2 mL of the solvent of choice.

The morphology of the particles was observed by taking SEM images on Hitachi S-4800 Scanning Electron Microscope. The samples for SEM imaging were typically prepared by applying 2-5 µL of diluted nanoparticles suspension in water or ethanol on the surface of Si template followed by overnight drying. To enhance image quality, the samples surface was spattered with 2 nm layer of iridium.

Confocal laser scanning microscopy (Leica DMI RE2) was also used to visualize the morphology of calcium alginate microparticles. Typically 2-5  $\mu\text{L}$  of microparticles suspension was placed on a glass slide and the images were taken.

### **Encapsulation of Curcumin**

Curcumin-loaded chitosan-alginate microspheres were prepared by complex coacervation-emulsification technique. Briefly, 1 g of 1% chitosan solution in 1 % acetic acid containing curcumin solution in ethanol was added concomitantly with 1 g of 1 % alginate solution into 50 g of light mineral oil ( Hexadecane) containing 0.5 g of Tween 85. The mixture was homogenized (@2000 rpm) for 5 min and additional 10ml of hexadecane added, then sonicated for 5 min (@30 watt power) and then 10gm of 10% Calcium chloride solution is added and further sonicated for 5min. The obtained microspheres were then freeze-dried and kept in a tight, light-resistant container at  $-20^{\circ}\text{C}$  for further studies.

### **Release Kinetics Study of Curcumin In Vitro**

Around 1mg of curcumin-loaded microspheres is taken and dispersed in 2ml of 10mM PBS buffer solution at pH 7.4 and its time-based absorbance is measured in a Glass UV-Vis spectrophotometer (Agilent-8453). The peak is observed at 434 nm. The rate of release was calculated based upon ethanol extraction of curcumin from microspheres. For comparison pure curcumin release in similar fashion is studied in a PBS buffer.

## Results and Discussion

Calcium alginate nanoparticles obtained by the general procedure have an average diameter of 269.4 nm and polydispersity of 0.114. The surface charge of the microparticles is negative with the average value of  $-17.98 \pm 0.66$  mV.

CLSM images of obtained calcium alginate nanoparticles are presented in Figure 3.1. The diameter of nanoparticles is much less than 1.0 micrometer. For confocal microscopy imaging to visualize the nanoparticles, polyallylamine hydrochloride PAH - labeled with a fluorescent dye RBITC, which forms a complex with the negatively charged surface of calcium alginate nanoparticles - was added.

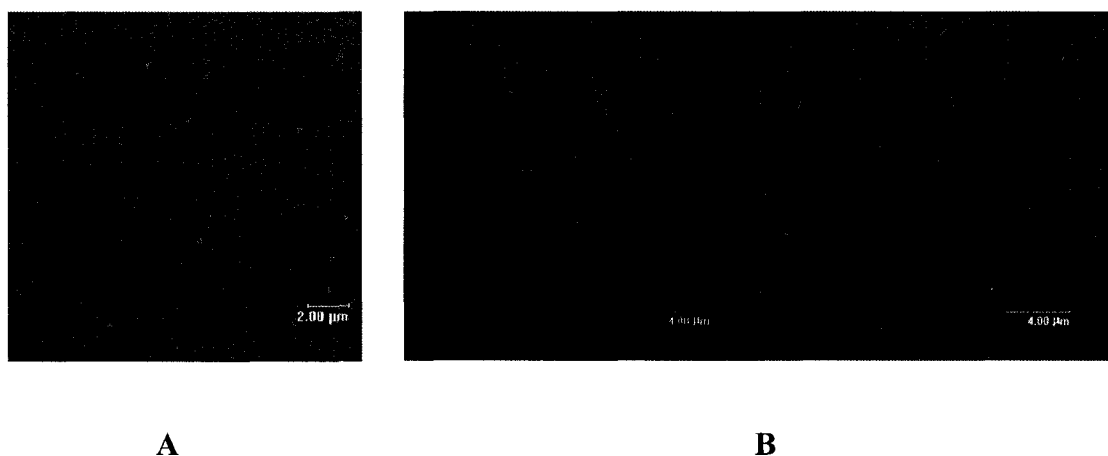


Figure 3.1: CLSM images of calcium alginate nanoparticles, prepared by general emulsification method. For fluorescence mode imaging (B, left) PAH-RBITC was coated at pH 6.5.

SEM images of the same particles are shown in Figure 3.2. The size of bigger particles was around 300 nm, most of the nanoparticles have a diameter of 200 nm, and the small ones are around 100 nm. According to the light-scattering measurements performed on a Brookhaven Zeta-sizer, the hydrodynamic diameter of the particles from the same sample is  $317 \pm 5.95$  nm. The data collected using Zeta-sizer give overestimated

value of nanoparticle size. The real diameter is  $2/3$  of the value obtained by light scattering. This result might be due to the hydrodynamic behavior of the particles in the water solvent (swelling of the particles by absorption of solvent) while measuring the particle size by light scattering.

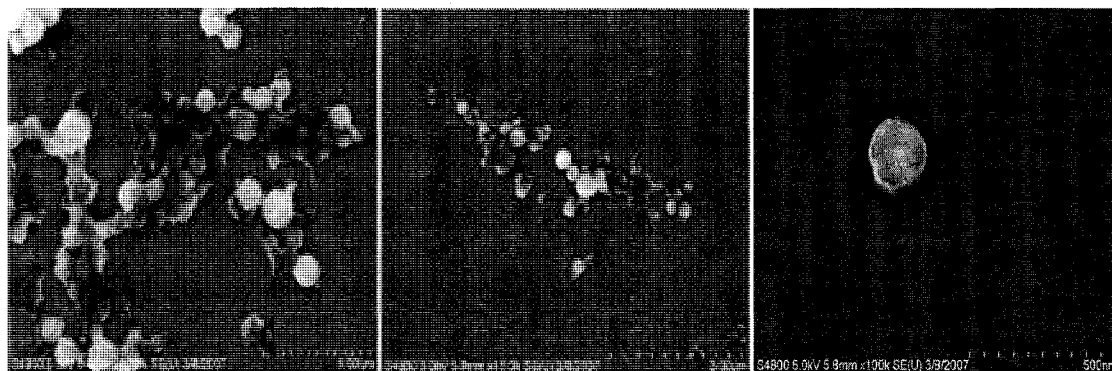


Figure 3.2: SEM images of calcium alginate nanoparticles, prepared by general emulsification method. Images were taken after sputter coating the dried sample with 2 nm thickness of Iridium.

### **Optimization of the Calcium Alginate Nanoparticle Preparation Procedure**

To optimize the procedure of calcium alginate nanoparticle preparation and prepare nanoparticles with diameter smaller than 300 nm, several experiments has been carried out by varying different parameters, such as:

- Oil (organic) phase composition. Hexadecane, hexane, cyclohexane and sometimes chloroform were added to the oil phase, which was isooctane in most cases. The solvent mixtures have different viscosity, surface tension at the oil/water phase border, evaporation temperature, which can affect size of alginate emulsion droplets and in some cases favor the formation of nanoparticles of small sizes;

- ratio between oil and water phase;
- concentration of alginic acid solution;
- ratio between  $\text{CaCl}_2$  and alginic acid;
- ratio of hydrophobic surfactant SPAN85 to hydrophilic surfactant TWEEN 85. It can influence the size of initial alginic acid emulsion micelles.

- other surfactants, such surfactants as SPAN20 and AOT were tried. SPAN20 is hydrophilic surfactant with shorter hydrophobic tail than SPAN85, and its application can probably decrease nanoparticles size. AOT is a well known stabilizer for oil-in-water emulsions.

- another gelling agent. Ca-AOT was tried as a gelling agent. It allows avoiding the step of mixing prepared alginic acid emulsion with new portion of aqueous solution ( $\text{CaCl}_2$ ) and might affect nanoparticle particle size.

**Influence of Oil Phase  
Composition, Alginic Acid  
Concentration and Ratio of  
Alginic Acid and  $\text{CaCl}_2$  used  
on Nanoparticles Size**

Calcium alginate nanoparticles were prepared by following the emulsification procedure given above. The changes introduced in the procedure to optimize sample quality and obtain nanoparticles of smaller size and the results on measurements of nanoparticle hydrodynamic diameter are given in Table 3.1. In several cases, nanoparticles of diameter less than 300 nm were prepared (Indicated in inclined and bold style format). Separate emulsification of alginic acid and calcium chloride followed by mixing of the emulsions under continuous stirring or sonication (see Exp-4 in Table 3.1) gives relatively better results than other tried approaches. The procedure consists of



separate emulsification of 10 ml of 10% CaCl<sub>2</sub> solution in water and 5 g 3% alginate sodium salt in 37.5g (54.2 mL) isooctane containing 1.7 g SPAN 85 each by sonication at 90% power for 30 min. The absence of hydrophilic surfactant TWEEN85 also seems to tend decrease the nanoparticle size.

Table 3.1: Conditions and results of optimization of calcium alginate nanoparticles preparation via emulsification technique.

Conditions different from general procedure	Parameters changed relatively the general procedure	Hydrodynamic diameter, nm	Half width, Nm	Polydispersity
<b>General procedure</b> <b>Exp-1</b>	Different fractions were collected.	376.2±14.1	152.1±19.3	0.19±0.05
		317.0±5.9	105.2±15.5	0.13±0.04
		341.7±12.2	131.8±14.2	0.17±0.04
<b>Exp-2</b> 5 g of 3 % alginate solution	1) oil-to-water ratio decreased 5 times, 2) otherwise the same, Different fractions were collected.	424.0±11.05	146.5±11.9	0.16±0.03
		298.2±11.5	105.8±19.2	0.13±0.05
<b>Exp - 3</b> 5 g 3 % alginate solution No TWEEN	1) oil-to-water ratio increased 5 times 2) Only hydrophobic surfactant SPAN85	238.2±11.0	115.8±6.6	0.25±0.04
		283.4±6.4	150.2±2.6	0.21±0.03
<b>Exp - 4</b> 5 g 3 % alginate solution and 10g 10% CaCl <sub>2</sub> were emulsified in 54.2 ml isooctane each and mixed No TWEEN85	1)separate emulsification of alginate and CaCl <sub>2</sub> followed by mixing 2)Only hydrophobic surfactant SPAN85 3)increased ratio oil-to-water	180.6±4.4	68.8±4.6	0.15±0.02
		164.8±4.5	53.4±5.7	0.12±0.02
<b>Exp - 5</b> 2 g 3 % alginate solution, 1.7 g SPAN 85 and 1.5g TWEEN 85 54 ml isooctane+ 50 ml hexadecane 40 min total sonication time, 1 ml of 10 % CaCl <sub>2</sub> added under sonication	1)increased amount of oil phase, 2)increased ratio hydrophilic/hydrophobic surfactant 3) less volatile solvent 4)longer sonication time 5) decreased amount of CaCl <sub>2</sub>	742.1-801.9 ±21.8-25.3	404.8- 441.8 ±13.9- 23.5	0.30-0.31 ±0.02-0.03
<b>Exp - 6</b> 2 g 3 % alginate, 2.8 g SPAN85 and 1.7 g TWEEN 85, isooctane/	1)increased amount of oil phase 2)increased amounts of both surfactants	342.0-381.0 ±4.4-13.0	140.8- 168.8 ±11.6- 8.9	0.17-0.20 ±0.02-0.03

Conditions different from general procedure	Parameters changed relatively the general procedure	Hydrodynamic diameter, nm	Half width, Nm	Polydispersity
hexadecane (1:1) oil phase 2g 10% CaCl <sub>2</sub> under stirring	3) less volatile solvent 5) decreased amount of CaCl <sub>2</sub>			
<b>Exp - 7</b> Isooctane/hexadecane (1:1), 2.8 g SPAN85 + 1.7 g TWEEN85, 1 g 10% CaCl <sub>2</sub> and 1 g 3 % alginate solution per 50 mL oil phase each	1)increased amount of oil-to-water 2)increased amounts of both surfactants 3) less volatile solvent 4) separate emulsification of both components,5) mixing under stirring	364.7-381.9 ±8.7-24.9	143.1-157.7 ±9.4-16.6	0.16-0.17 ±0.02
<b>Exp - 8</b> 5 g 3 % alginate per 37.5g isooctane +1.7 g SPAN 85,10g 10% CaCl <sub>2</sub> per 37.5g isooctane +1.7 g SPAN 85	1)smaller amount of alginate solution, 2)increased amount of oil-to-water 3)separate emulsification followed by mixing under sonication.	240.9±11.9	112.15±7.25	0.22±0.02
<b>Exp - 9</b> 5 g 3 % alginate, 2.3 g SPAN 20, no TWEEN85, Otherwise as Exp3	1) smaller chain hydrophobic surfactant 2) no TWEEN85	686.7±41.5	172.9±23.4	0.07±0.02
		291.6	-	-
<b>Exp - 10</b> 1 g 3 % alginate solution Otherwise the same as Exp3	1)much smaller amount of alginic acid 2) large ratio CaCl <sub>2</sub> to alginate	612.4± 28.3	371.7±10	0.38±0.03
<b>Exp - 13</b> 25 mL hexane +5 mL chlorophorm, 2.5 mL 1% alginate, 0.9 g SPAN85, 0.45g TWEEN85	1)chlorophorm in oil phase	Not stable emulsion	-	-
<b>Exp - 14</b> 30 mL cyclohexane, 0.9 g SPAN85, 1.0 g TWEEN85, 2 mL 1% alginate+ cyclohexane to 40 mL total volumes, 20 mL of the emulsion above in 5 mL 10% CaCl <sub>2</sub> , Mixing 30 min	1) Low concentration of alginic acid 2) high ratio oil/water, 3) cyclohexane as oil phase	302.5 ±16.8	169.3±9.1	0.31±0.01
		231.4±5.0	111.7±4.4	0.23±0.01

### Influence of Surfactant and Gelling Agent Nature on Nanoparticle Size

**Ca-AOT Preparation Procedure.** Ca-AOT (Docusate calcium salt) was prepared by mixing 3.7 g Na-AOT in 100 ml methanol and 1.0 g CaCl<sub>2</sub> in 100 ml water. Solvent was evaporated to 75 mL and white precipitate was collected, washed with DI water three times to remove NaCl and dried.

From the results shown in Table 3.2 one can see that AOT does not stabilize alginic acid and calcium chloride emulsions to a sufficient degree. Ca-AOT as a gelling agent-surfactant increases nanoparticle size. Both these approaches are considered unsuccessful.

Table 3.2: Influence of surfactant and gelling agent nature on suspension stability and nanoparticle diameter.

Conditions different from general procedure	Parameters changed	Hydrodynamic diameter, nm
<b>Exp – 11</b> 25 mL hexane, 0.75ml 0.1 M Na-AOT, 1.0 mL 3% alginate, 1.39 mL of ~30mM Ca-AOT in 0.1 mL increments under sonication	1)Na-AOT as surfactant 2)Ca-AOT as gelling agent	Not stable
<b>Exp – 12</b> 25 mL hexane +3 mL chloroform, 0.75ml 0.1 M Na-AOT, 0.5 mL 3% alginate, 3 mL of ~30mM Ca-AOT in 0.1 mL increments under sonication	1)Ca-AOT as gelling agent 2)chloroform in the oil phase 3) Na-AOT as surfactant	Not stable
<b>Exp – 15</b> 30 mL cyclohexane, 0.9 mL SPAN85, 1.0 mL TWEEN85 2 mL 1% alginate+ cyclohexane to 40 mL total volumes a) 20 mL of the emulsion above +10 mL Ca-AOT 30 mM, mixing 60 min b) mixture a) 10 mL 10 % CaCl <sub>2</sub> mixing, ultrasonication for 5 min	In a) Ca-AOT as gelation agent	In a) 600  In b) 600

## **Modification of Nanoparticle**

### **Washing and Separation**

### **Procedure**

While working with nanoparticles of small size, a problem in separation was identified. Very small particle size and material softness of Ca-alginate nanoparticles centrifugation from aqueous supernatant does not seem to be a good separation procedure. If centrifugation speed is high, the particles form a pellet on the bottom, which is very difficult to separate. If the centrifugation speed is too slow, a very big loss of the nanoparticles during washing was observed. In addition, if nanoparticle diameter is small and no hydrophilic surfactant is used, the final emulsion containing calcium alginate nanoparticles is very stable. It is difficult to break it and separate the nanoparticles.

To overcome the difficulties, the following modifications were introduced into nanoparticle separation procedure. Ethanol was used to break the emulsion containing SPAN85 and wash the nanoparticles.

1) The mixture obtained after addition of alginic acid emulsion to  $\text{CaCl}_2$ -containing solution or emulsion (see paragraph 3.1 for details) was transferred into a separation funnel to separate isooctane phase containing SPAN85. No extra water was added. 100 mL of ethanol was added to the mixture to break the emulsion and easy separation. After 1 hour needed for phase separation transparent isooctane layer was discharged. SPAN85 was removed from the ethanol/water layer containing nanoparticles by multiple extractions with isooctane. Concentration of SPAN 85 in the isooctane extracts was estimated by UV-vis spectroscopy (an Agilent 8045 spectrometer). Extinction coefficients of SPAN85 ( $\lambda=268$  nm) in isooctane and ethanol found by calibration of A (a.u) vs.  $C_{\text{span85}}$  (mg/ml) are 0.185 and 0.178  $\text{L g}^{-1}\text{cm}^{-1}$ .

Calcium alginate nanoparticles were separated from ethanol/water supernatant by centrifugation at 2000 rpm for 15 min. The nanoparticles were washed either with ethanol only or once with ethanol and then with DI water. Centrifugation speed was increased if necessary but not exceeds 5000rpm. Finally, the nanoparticles were resuspended in water or ethanol and frozen at  $-80^{\circ}\text{C}$ , in case of water.

However, while only ethanol was used to break the emulsion and wash nanoparticles, another problem was discovered, such as the absence of a clearly visible layer of nanoparticles. That is why the changes below were introduced.

2) To separate microparticles, 500 ml DI water was placed into a separation funnel, the mixture was poured in and intensively but briefly shaken. 100ml ethanol and 50 ml of isooctane were added and shaken. After 30 min the top isooctane layer was discarded. 50 ml of isooctane were added to the bottom ethanol mixture containing particles and the above procedure was repeated. Nanoparticles were collected from the middle surfactant layer and centrifuged at 5000 rpm for 10 min. The supernatant was removed; the nanoparticles were washed with ethanol two times and finally dispersed in DI water.

### **SPAN 85 concentration in Isooctane Extracts and Ethanol Supernatants**

Calcium alginate nanoparticles were prepared by separate emulsification of  $\text{CaCl}_2$  and alginic acid in isooctane –SPAN85 oil phase followed by their mixing under constant stirring or sonication. Only ethanol (no water) was used to break the emulsion. SPAN85 was removed from the reaction mixture by multiple extractions with isooctane. The SPAN85 concentration in the supernatant was estimated spectrophotometrically (Table

3.3). Multiple extraction of SPAN85 with isooctane followed by washing nanoparticles with ethanol several times can remove SPAN85 from the samples almost completely.

Table 3.3: Concentration of SPAN85 in supernatants (isooctane extracts and ethanol supernatants).

Experiment	Phase	C(SPAN85), g/l
S-3	isooctane supernatant	20.9
	isooctane 1st extraction	2.9
	isooctane 2nd extraction	1.5
	ethanol supernatant	18.1
S-4	supernatant isooctane	19.7
	1st wash isooctane	8.0
	2 nd wash isooctane	4.2
	supernatant ethanol	7.7
	1 st wash ethanol	1.4
	1 st wash with water	~ 0

### **Influence of Modified Separation Parameters on Nanoparticle Diameter**

Calcium alginate nanoparticles were prepared by separate emulsification of CaCl<sub>2</sub> and alginic acid in isooctane –SPAN85 oil phase followed by their mixing under constant stirring or sonication. Only ethanol (no water) was used to break the emulsion. SPAN85 was removed from the reaction mixture by multiple extractions with isooctane. The hydrodynamic diameter (Table 3.4) of the nanoparticles was measured using a Brookhaven Zeta plus analyzer instrument.

SEM images of for Ca-alginate nanoparticles prepared according to the general procedure presented in Figure 2.3. The size of bigger particles is around 300 nm, most of the nanoparticles have a diameter of 200 nm, and the small are around 100 nm. The SEM images of calcium alginate nanoparticles obtained using the modified separation and washing procedure are presented in Figure 3.3. The sample (S-2) consists of

nanoparticles with diameter less 300 nm, however, some 400 nm diameter nanoparticles are visible. It should be noted that the measured hydrodynamic diameter of nanoparticles in this sample is 439.7 nm.

Table 3.4: Calcium alginate nanoparticle size for samples prepared according to modified separation procedure.

Conditions different from general procedure	Particles separation and washing steps	Hydrodynamic diameter, nm
S-1 General procedure	General procedure	180.6±4.4 (in water)
S-2 5.6 mg of 3 % alginic acid was used.	No water, heavy fraction was collected by centrifugation at 2000 rpm for 10 min.	439.7±10.85 nm (in ethanol), 680.9±8.0 nm (in water), <300 nm (SEM)
S-3.	No water. Nanoparticles were collected at 2000 rpm (10 min ) and remaining in the supernatant at 5000 rpm (15 min)	293.3±7.7 nm in ethanol 242.9±4.2 nm (in ethanol) 201.9±5.9 nm (in ethanol, supernatant)
S-4 double amount of SPAN 85 was used.	No water. Nanoparticles were washed twice with ethanol, once with water and collected at 5000 rpm (15 min ).	244.1±6.2 nm (in alcohol), 334.2±15.0 nm (in water). <250 nm (SEM)

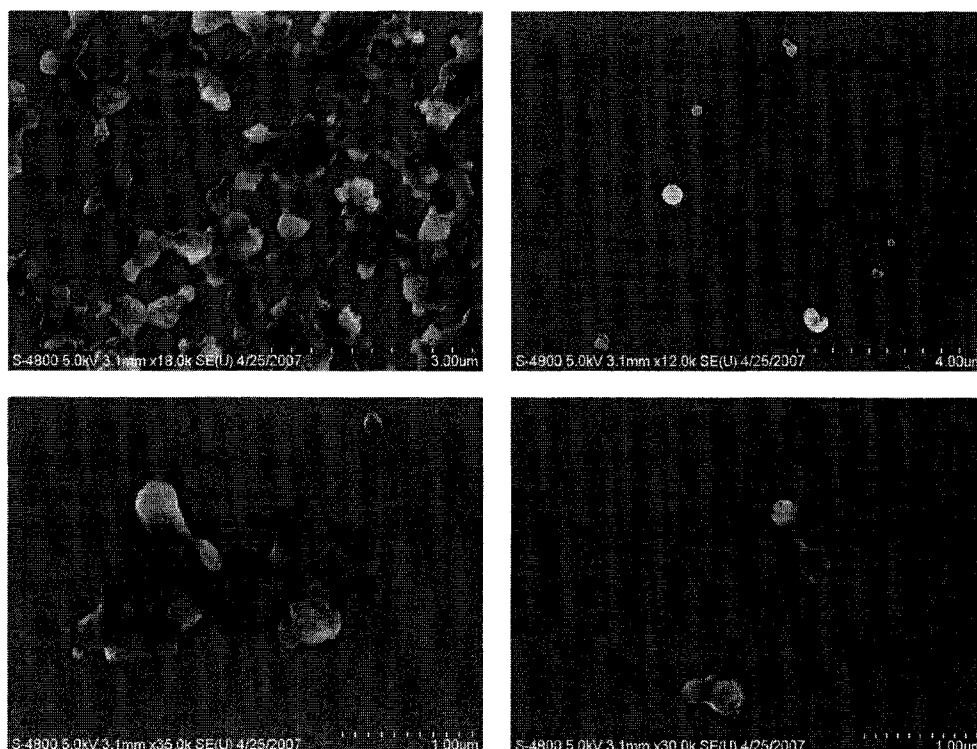


Figure 3.3: SEM images of nanoparticles obtained from experiment S-2 (Table 3.4). Images were taken after sputter coating the dried sample with 2 nm thickness of Iridium.

### **Influence of Solvent on Calcium Alginate Nanoparticle SEM Imaging**

While a drop of calcium alginate suspension (sample S-4) in ethanol was applied to Si surface and dried overnight, particles smaller than 250 nm are clearly visible (Figure 3.4). There are many particles of much smaller sizes (less than 100 nm). For the sample prepared from aqueous solution (Figure 3.5), there is bigger agglomeration but small size particles are still visible. The fact that SEM images in both cases are not resolved completely can be related both with sample preparation conditions and with image recording conditions (small soft organic particles are difficult to visualize). While the samples for SEM were prepared from water, the nanoparticles are probably swollen and it



can affect their alignment during drying causing high agglomeration. The partial dissolution of nanoparticles can also be considered as a reason. The samples prepared from ethanol can be affected by air moisture.

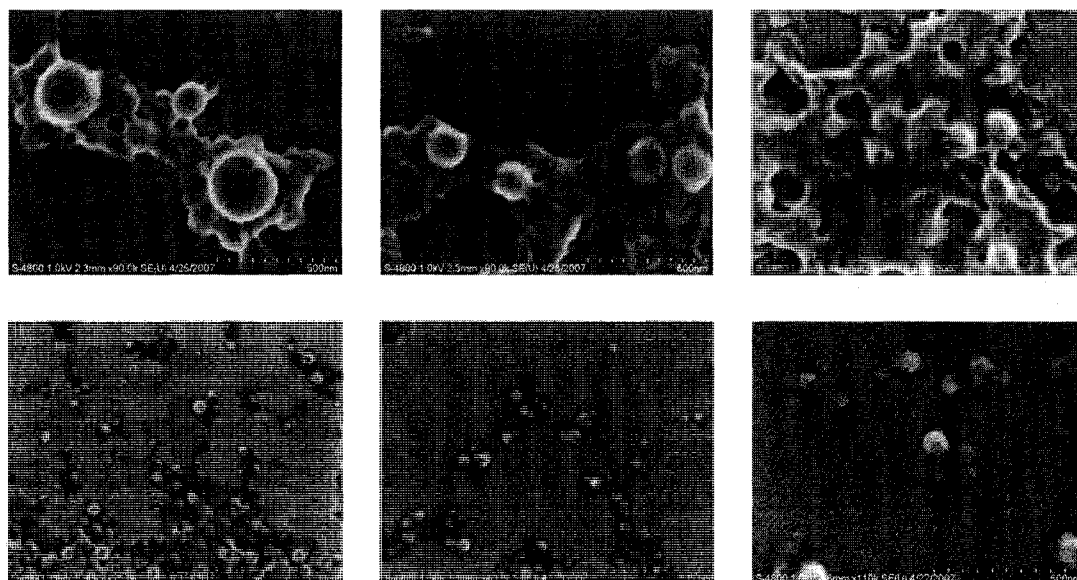


Figure 3.4: SEM images of nanoparticles obtained from experiment S-4 (Table 3.4) after washing with ethanol and before washing with water. Images were taken after sputter coating the dried sample with 2 nm thickness of Iridium.

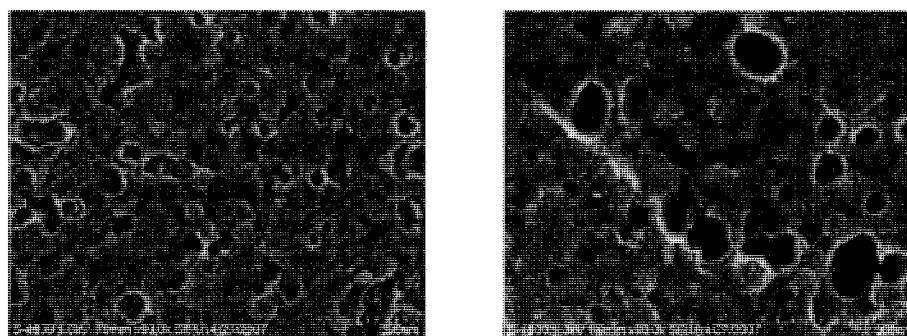


Figure 3.5: SEM images of nanoparticles obtained from experiment S-4 (Table 3.4) after washing with ethanol and water. Images were taken after sputter coating the dried sample with 2 nm thickness of Iridium.

### Preparation of Calcium Alginate Nanoparticles Using Nonaqueous Solution of $\text{CaCl}_2$

Since it was found that  $\text{CaCl}_2$  is soluble in ethanol [115], an attempt was made to avoid addition of a second water-based solution ( $\text{CaCl}_2$  solution) during nanoparticles preparation by replacing it with ethanolic solution of  $\text{CaCl}_2$ . Ethanol is mixable with isooctane and it can avoid disruption of nanoparticles.

Emulsion of 5g 3%alginic acid in 54.2 mL isooctane+1.7 g SPAN85 was added to 20 mL 10%  $\text{CaCl}_2$  in ethanol under stirring for 30 min. SPAN85 was extracted with isooctane tree times. Nanoparticles were washed with ethanol four times using centrifugation at 3000 rpm for 5 min. SEM for this sample gives wide size distribution, some particles around 1 micron, small particles less than 300 nm. Measured nanoparticle size is  $343.1\pm 4.3$  nm (in ethanol, average of 3),  $304.4\pm 9.2$  nm (in water, average of 3).

There are big (around 1 micron) particles as well as smaller (less 300 nm) particles in the sample (Figure 3.6). The images were taken at the edge of the sample, where individual, non-agglomerated particles were found.

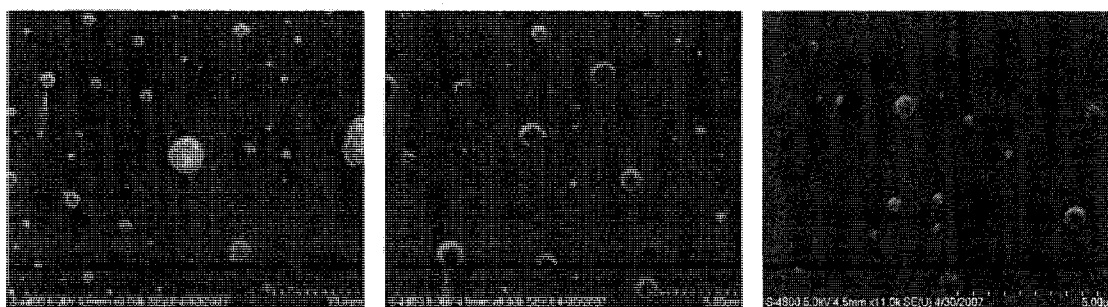


Figure 3.6: SEM images of nanoparticles obtained from Sample 8 (Table 3.1). Images were taken after sputter coating the dried sample with 2 nm thickness of Iridium.

### **Influence of Viscosity of Alginic Acid on Calcium Alginate Nanoparticles**

To investigate the influence of molecular weight of the polymer on properties of calcium alginate nanoparticles, samples of alginic acid from different sources were used. They are characterized by different viscosity, the parameter related to molecular weight of alginic acid, and also different G/M ratio. The galacturonic acid, a main component of pectin, which also can be gelled by  $\text{Ca}^{2+}$  ions, was used for comparison. All nanoparticles were prepared using separate emulsification of alginic acid and  $\text{CaCl}_2$ , followed by addition of alginic acid emulsion into  $\text{CaCl}_2$ -containing emulsion. To extract SPAN85, the modified procedure was used, which consists of addition of 500 ml DI water, 100 ml ethanol and 50 ml of isooctane to the reaction mixture in a separation funnel, followed by the second extraction of the surfactant with 50 ml of isooctane, and, finally, two washings with ethanol using centrifugation at 5000 rpm for 10 min to separate then nanoparticles. From the results presented in Table 3.5, nanoparticles prepared from alginic acid of high viscosity have relatively lower diameter as compared with those obtained using low and medium viscosity samples. While one of the latter was used, diameter of nanoparticles varied drastically from sample to sample. In spite the fact that alginic acid of low viscosity can provide big fraction of nanoparticles with a diameter smaller than 100 nm, the nanoparticles have a wider size distribution (higher polydispersity) and uneven nanoparticle surface (Figure 3.7). On the basis of the obtained results, alginic acid of high viscosity can be recommended for preparation of nanoparticles with size less than 300 nm and low polydispersity. Particles in such a

sample have rather good round shape (Figure 3.7). Polygalacturonic acid gives very nanoparticles of very small size, but their shape is uneven (Figure 3.7).

Table 3.5: Diameter for calcium alginate nanoparticles prepared from alginic acid of different viscosity by emulsification technique.

Viscosity of alginic acid/ manufacturer	Hydrodynamic diameter, nm	Half width, nm	Polydispersity
high viscosity /FMC	223.0 ± 9.9	82.9 ± 11.4	0.14 ± 0.09
	291.2 ± 10.1	98.5 ± 23.7	0.14 ± 0.04
	274.8 ± 6.0	92.0 ± 19.2	0.14 ± 0.04
low viscosity /FMC	269.1 ± 4.9	82.9 ± 14.6	0.10 ± 0.03
	400.9 ± 8.0	210.3 ± 67	0.28 ± 0.01
	381.4 ± 16.9	205.5 ± 10.9	0.29 ± 0.04
medium viscosity/Sigma	678.7 ± 15.0	366.7 ± 16.8	0.29 ± 0.05
medium viscosity/FMC	497.5 ± 20.2	241.4 ± 18.1	0.24 ± 0.02
	471.4 ± 13.1	255.9 ± 11.6	0.29 ± 0.01
Polygalacturonic acid/Sigma	257.2 ± 6.2	76.7 ± 14.7	0.11 ± 0.03
	204.8 ± 4.1	80.6 ± 8.0	0.16 ± 0.02

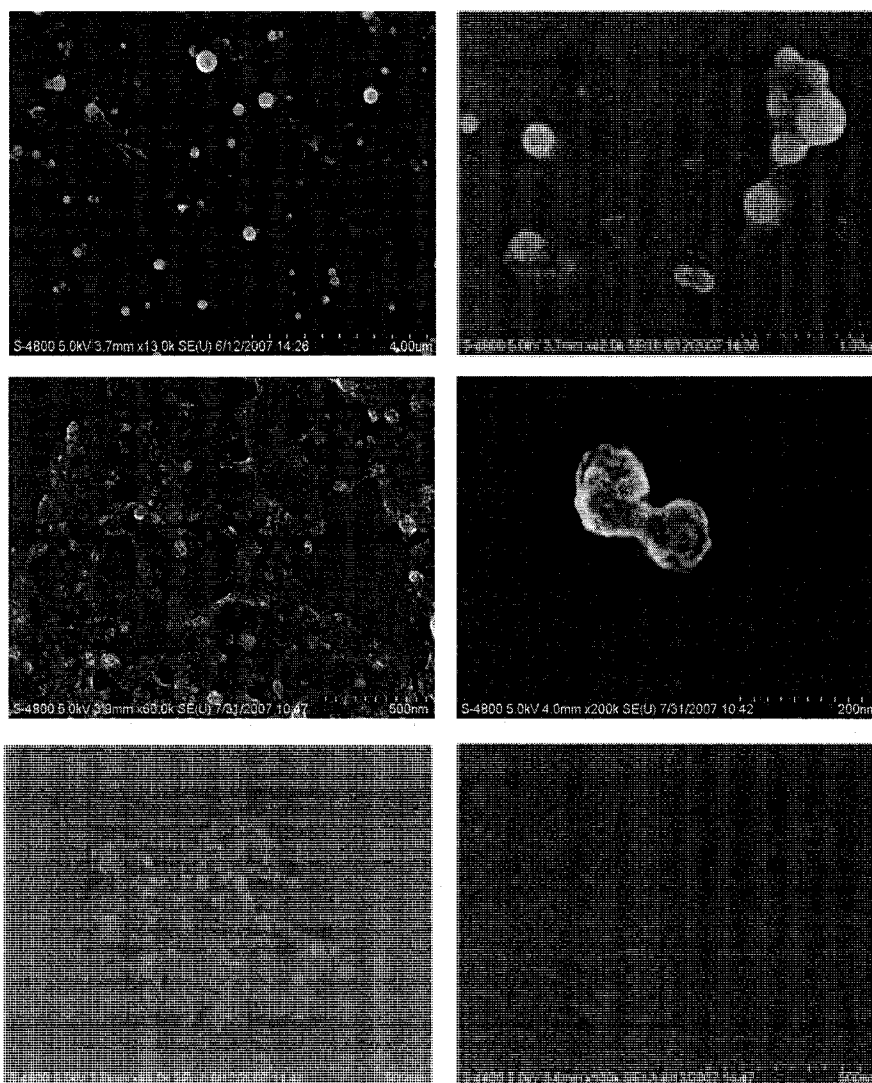


Figure 3.7: SEM images of calcium alginate nanoparticles prepared using alginate of high viscosity (upper row) and low viscosity (middle row) and using polygalacturonic acid (lower row). Images were taken after sputter coating the dried sample with 2 nm thickness of Iridium.

### **Chitosan Coating onto Calcium Alginate Nanoparticles**

It has been shown that calcium alginate particles are chemically unstable when chelators such as phosphate and citrate and nongelling cations such as sodium or magnesium ions are present [33]. To increase the stability of alginate microparticles and

to minimize the loss of encapsulated material, the microparticles are coated with polycationic polymers of poly-L-lysine [24, 34], polyvinylamine [35], and chitosan [26, 27, 36, 37].

Chitosan, a polycationic polysaccharide derived from the natural polymer chitin, forms polyelectrolyte complexes with alginate, a polyanionic polymer [38, 39]. The addition of cationic chitosan, resulting in chitosan-coated alginate microparticles, further strengthens the alginate gel structure of microparticles [37]. As prepared, calcium alginate nanoparticles have a surface charge of  $-34.12 \pm 1.23$  in water. Coating of the nanoparticles with a layer of chitosan using the Layer-by-Layer technique reverses the surface charge to  $8.58 \pm 2.70$  mV. However, the coating causes the nanoparticles to agglomerate, forming particles of bigger size (Figure 3.8).

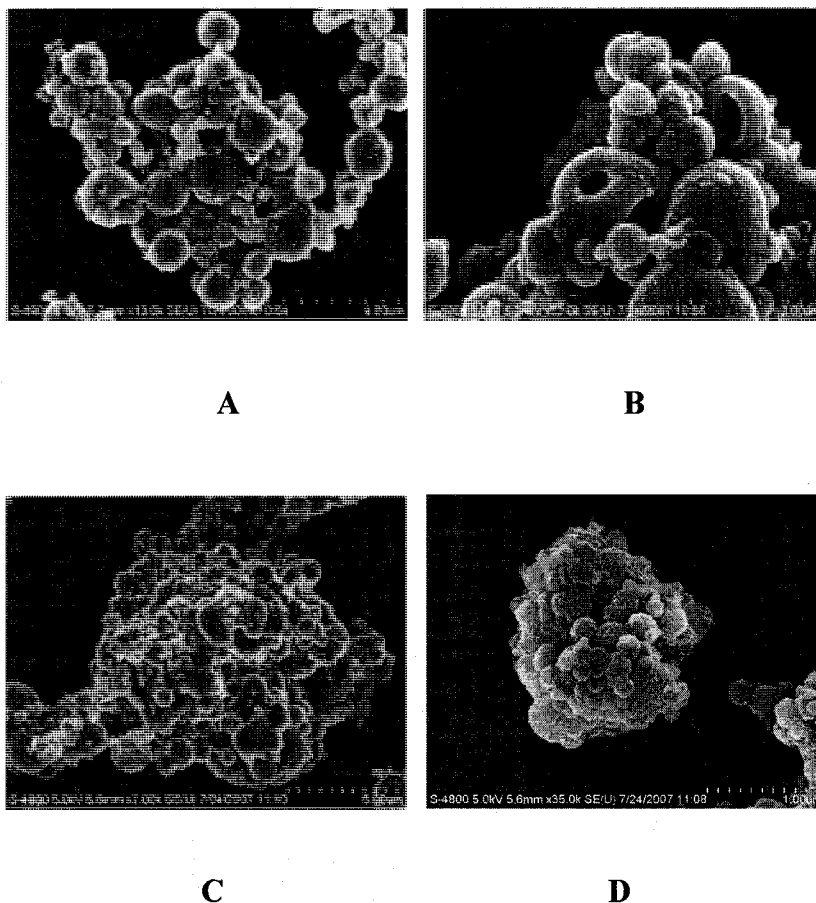


Figure 3.8: SEM images of calcium alginate nanoparticles before (A,B) and after (C,D) coating with one layer of chitosan. Images were taken after sputter coating the dried sample with 2 nm thickness of Iridium.

### **Encapsulation and Release of Curcumin**

The encapsulation of the curcumin was observed by CLSM images (Figure 3.9) and SEM microscopy (Figure 3.10). The release kinetics in comparison with the curcumin naked crystals is shown in Figure 3.11. The release kinetics study shows the enhanced dissolution profile of curcumin from chitosan alginate microspheres. The enhanced dissolution might be due to the use of a organic solvent (in this case

hexadecane) during the encapsulation process. It was clear from the CLSM images that in aqueous phase curcumin remains in a dissolved condition inside the chitosan-alginate matrix (as shown by innate fluorescence of curcumin), and in SEM images it remains as crystals in dried condition (absence of hexadecane). Due to the presence of chitosan and its nature to form aggregation (as per previous results) the formed alginate particle size was around  $566 \pm 17.5$  nm, and the surface charge of the curcumin loaded alginate particles was measured around  $-10.78 \pm 0.67$  mV. The amount of curcumin loaded was 0.01mg/ mg of microspheres (1% by mass, determined by complete dissolution of curcumin using ethanol).

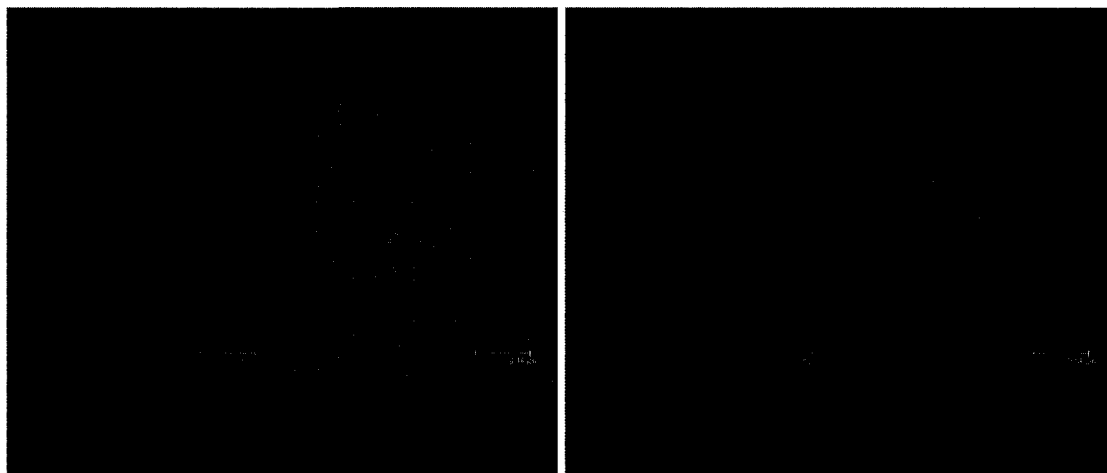


Figure 3.9: CLSM images of Curcumin loaded chitosan-alginate particles. Fluorescence was due to innate nature of curcumin.





Figure 3.10 SEM images of Curcumin loaded chitosan-alginate particles. Images were taken after sputter coating the dried sample with 2 nm thickness of Iridium.

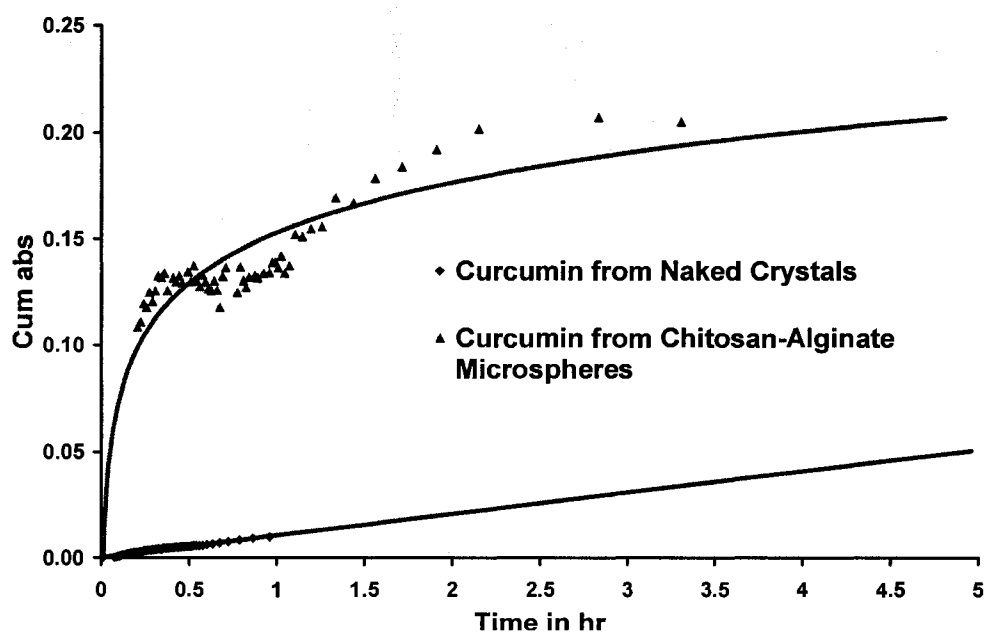


Figure 3.11: In vitro release kinetics of Curcumin in deionized water at pH 6.5.

## Conclusion

By the emulsion method Ca-alginate nanoparticles with a diameter less than 300 nm can be prepared. According to SEM the particle size is less than 200 nm. Separate emulsification of alginic acid and calcium chloride followed by mixing the emulsion and continuous stirring (see Exp-4 above) gives relatively better results than other approaches. The procedure consist of separate emulsification of 10 ml of 10% CaCl<sub>2</sub> solution in water and 5 g 3% alginic acid sodium salt in 37.5g (54.2 mL) isooctane containing 1.7 g SPAN 85 each by sonication at 90% power for 30 min. During sonication the batches were iced. Then alginic acid emulsion was added to the emulsion containing calcium chloride under vigorous mixing and stirred for 30 min.

Nanoparticle size depends on emulsion preparation parameters and the following parameters made a positive influence on making smaller size Ca-alginate nanoparticles:

- Large oil-to-water ratio for alginate emulsions gives smaller particle size.

Smaller concentration of alginate solution used for emulsion preparation also seems to decrease particle size.

- SPAN85 alone without TWEEN gives smaller particle size.

- Mixing two separate emulsions of reagents gives smaller particle size

Decrease in emulsion stability or no reduction in particle size was found for the experiments, in which

- Chloroform was used in oil phase. Stability of emulsions drastically decreases.

- AOT does not stabilize the emulsions to sufficient degree.

- Ca-AOT as a gelling agent-surfactant increases nanoparticle size.

Multiple extraction of SPAN85 with isooctane followed by washing nanoparticles with ethanol several times can remove SPAN85 from the samples almost completely.

The encapsulation of the curcumin in chitosan alginate particles resulted in bigger size particles and in vitro release kinetics study showed an enhanced dissolution in comparison to the naked curcumin crystals.

**CHAPTER 4**

**ENCAPSULATION AND SUSTAINED  
RELEASE OF POORLY SOLUBLE  
DRUGS USING NATURAL CLAY  
NANOTUBULAR TEMPLATE  
HALLOYSITE**

**Introduction**

Halloysite ( $\text{Al}_2\text{Si}_2\text{O}_5(\text{OH})_4 \cdot 2\text{H}_2\text{O}$ ) is a two-layered aluminosilicate which has a predominantly hollow tubular structure in the submicron range and is chemically similar to kaolin [48, 49]. It occurs naturally and can be mined as a raw mineral, making it economically viable. Neighboring alumina and silica layers, and their waters of hydration, create a packing disorder which causes the layers to curve into tubes. Dehydrated halloysite consists of 15 - 20 clay layers rolled into tubule walls with a layer spacing of 0.7 nm [51]. Halloysite obtained from the Atlas Mining Company was used in this work. These tubules have an external diameter of  $50 \pm 10$  nm and a lumen of ca 15 nm when completely rolled [49, 66]. The use of halloysite nanotubes offers significant advantages over other nanotubes. Because it occurs in nature, production is neither tedious nor hazardous. It is inexpensive in comparison with other nanotubes in use

(carbon nanotubes, and inorganic nanotubes made of tungsten, titanium etc). The loading procedure is simple.

Halloysite is a promising biocompatible material for encasing and sustaining the release of bioactive molecules for pharmacology and tissue scaffolds [49, 55, 56, 63, 66, 116, 117]. Although usage of halloysite for loading and slowly releasing some hydrophilic drugs has been demonstrated, its effectiveness in delivering poorly soluble drugs (which constitute the majority of therapeutics) was not studied. Herein this chapter describes the use of halloysite nanotubules for the entrapment, storage, and subsequent release of three drugs: nifedipine (anti-anginal), furosemide (anti-hypertension and diuretic) and dexamethasone (synthetic corticosteroid). The chemical formulae of these drugs are shown in Figure 4.1. To increase loading of these poor soluble drugs, we loaded them in water-alcohol solvents (0, 10, and 50 % ethanol). The effect of pH on the loading and release of dexamethasone was also studied. Halloysite is non toxic to cells, but its biodegradability is unclear; therefore, its use in medicine for sustained drug release is feasible for dermatological and dental applications.

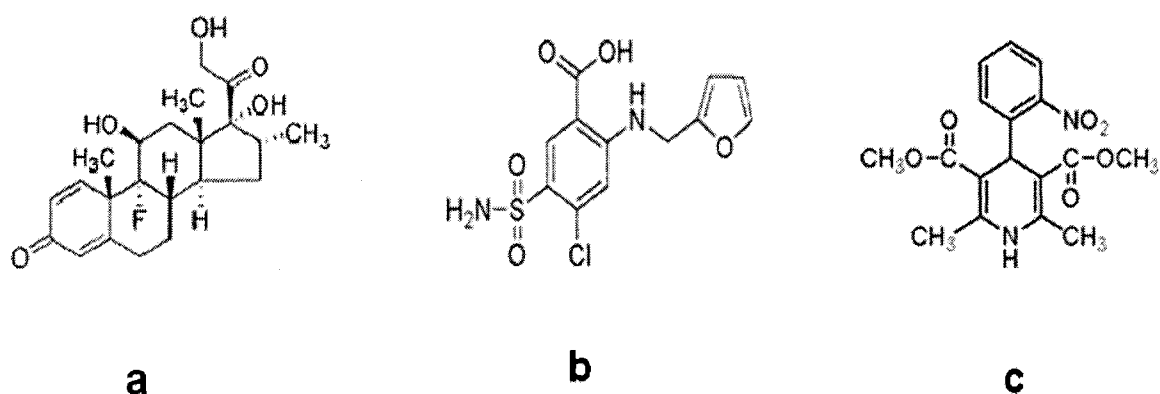


Figure 4.1: Chemical formulae of the drugs used: a-Dexamethasone (MW 392.5), b-Furosemide (MW 330.8), and c-Nifedipine (MW 346.3).

## **Materials and Methods**

Processed halloysite G was purchased from Atlas Mining Company in Utah. Furosemide, dexamethasone and nifedipine were bought from Spectrum Chemicals and Laboratory Products. The solvent ethanol was obtained from Sigma.

### **Surface Characterization**

The surface potential of the halloysite at different pH levels was determined using Zeta-potential micro-electrophoresis measurements (Zeta Plus Brookhaven Instrument).

### **Drug Loading**

Loading was performed by vacuum pulling saturated solutions of the drugs in 0, 10 and 50 % ethanol/water solvent in two steps. In the first step, pre-weighed halloysite (ca 10 mg) was soaked in saturated drug solution, vacuum pulled, and broken twice. The halloysite was extracted by centrifugation. In the second step, the removed halloysite was further soaked in saturated drug solution and the same procedure repeated. Finally, the tubules were washed using DI water and vacuum dried. All processing took 30 min exclusive of vacuum drying. In another set of experiments, the loading of a drug was performed using 10 mM PBS buffer at different pH (1.4, 7.4, and 9.4).

### **In Vitro Drug Release Kinetics**

The drug dissolution studies were performed using diffusing chambers of 1 mL capacity from PermeGear Incorporation. The released drug diffused through a 0.2 micron membrane filter to the other side of the chamber. Time-based samples were taken from the chamber for drug concentration determination by UV-Vis spectrophotometer (Agilent-8453). For monitoring Furosemide, Dexamethasone, and Nifedipine concentrations, an absorbance study was performed at 277 nm, 240 nm, and 235 nm at

22° C. The rate of release was calculated based upon assuming 90 % release during 1 hour sonication of the loaded tubules.

### **Results and Discussion**

The Zeta-potential surface charge measurements of the halloysite are shown in Figure 4.2. Zeta potentials for silica and alumina nanoparticles are also given and may represent the behavior of the outer and innermost of halloysite nanotubules respectively. The surface potential of the halloysite falls between the curves of silica and alumina, indicating the predominance of silica properties on its exterior surface as earlier indicated [50]. The input of alumina features may be due to incompletely rolled tubes or to the exposure of some inner alumina layer at the non-geometric ends of the tubes (tube surface defects).

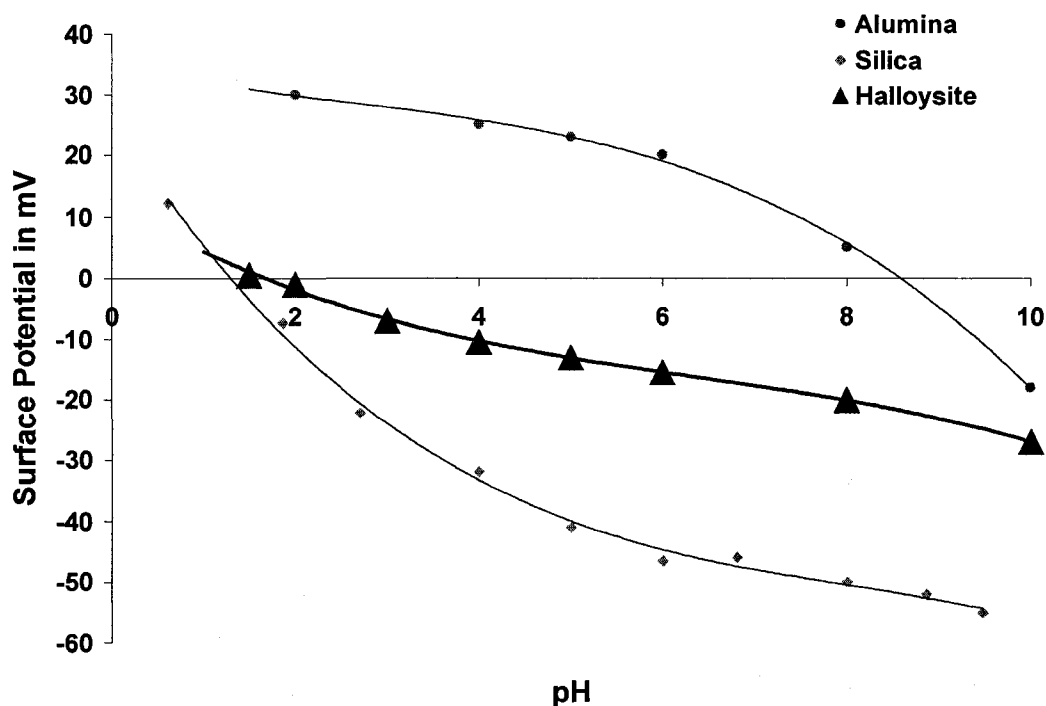


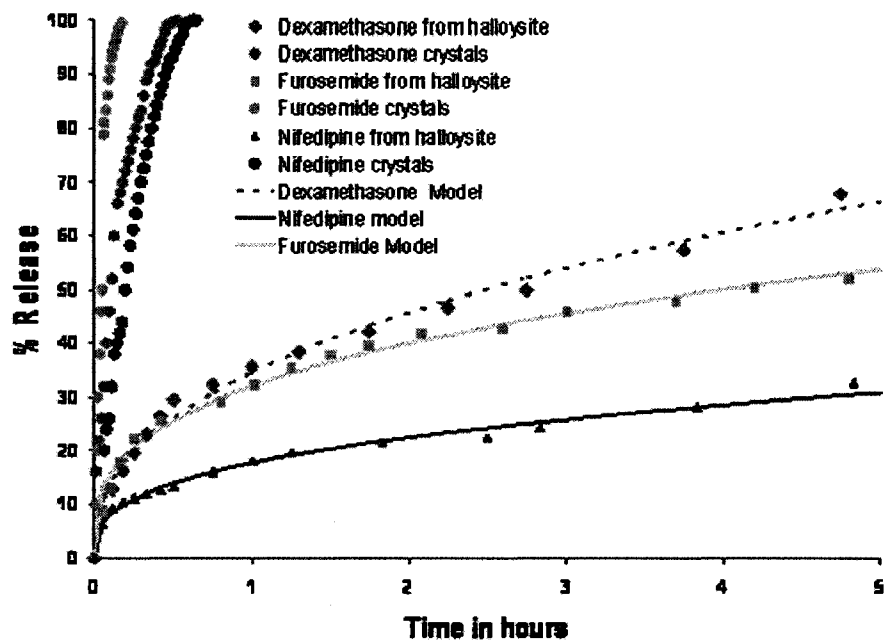
Figure 4.2: Zeta Potential results of halloysite, silica, and alumina.

Below pH 8.5, the tubule's lumen has a positively charged surface and the outer surface has a negatively charged surface. This charge difference on surface promotes the loading of negatively charged molecules (such as chosen drugs dexamethasone, nifedipine and furosemide) specifically inside the lumen and prevents their adsorption onto the negative outer surface of the tubules. The chosen drugs are poorly soluble in water; the solubility of dexamethasone in water is 0.1 mg/mL, for nifedipine it is 0.05 mg/mL, and for furosemide it is 0.1 mg/mL Hence, loading was performed from aqueous solvents containing 10 % alcohol, which provided higher solubility for the drugs. The release condition was maintained at pH 7.4 and continuous body sink conditions were maintained to simulate physiological conditions. The release profiles of the drugs from halloysite in comparison with those of the drug microcrystals are shown in Figure 4.3a.

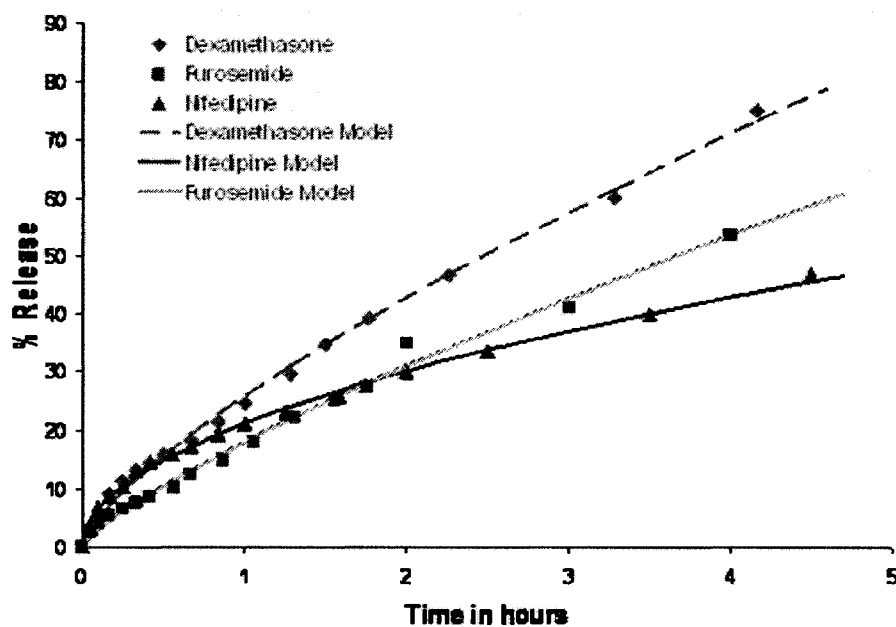


The drug release from the halloysite tubules was much longer than that from the micro-crystals. For nifedipine, it was 25 times longer from the tubules than from the crystals, and in the case of furosemide and dexamethasone it was 75 times longer. In all three release curves, an initial burst within 10 min followed by a 6-10 hour release can be observed. The initial burst may be due to release from exogenously bounded drugs on the surface of the tubes.

The next experiments were performed to optimize drug loading using saturated solutions in 0 %, and 50 % ethanol solvents. Drug loading was higher at higher alcohol to water ratios. For 0 % alcohol, 3 wt % of the drugs were loaded; for 10 % alcohol, 4 wt % were loaded; and for 50 % alcohol, 5 wt % were loaded. The release became more linear for loading from higher alcohol ratio solvent. Linear release means that the rate of release remains constant over time, which is a desirable attribute for medicine. Figure 4.3b shows that release became more linear for loading from higher alcohol ratio solvent.



a



b

Figure 4.3: Profiles of the drugs from halloysite nanotubules in water at pH 7.4: a-loading from 10 % alcohol; b- loading from 50 % ethanol / aqueous solvent.

Linear four-hour release of nicotinamide adenine dinucleotide (NAD) from halloysite was achieved by increasing the viscosity of the loading solvent. Similar linear behavior was observed for cytochalasin release through nanopores by Berg et al. [118]. The release profile from the halloysite fits the Peppas model [119] ( $M_t/M_\infty = kt^n$ , where  $M_t$  is the amount of drug released at time  $t$ ,  $M_\infty$  is the amount of drug released at infinite time,  $n$  is the exponent characteristic of the release mechanism, and  $k$  is a constant). For the cases of loading in 10% alcohol and release in water, the value of  $n$  is around 0.5 for all three drugs, indicating that the release mechanism is Fickian diffusion. In the case of loading using 50 % ethanol and release in water (Figure 4.3b), the value of  $n$  is around 0.75 for the drugs, indicating that the release mechanism is approaching zero-order kinetics (for which the value of 'n' is 1) [119]. This linear release might be due to heavier loading of the drug inside the halloysite tubules, giving us a nanopore controlling release. The absence of this mechanism in the cases of loading in 10 % alcohol and in water might be due to smaller amounts of the drug being spread along the lumen walls and not closing the tube opening. Therefore, an extended 10-20 hour drug release from 15 nm lumen diameter tubular halloysite was demonstrated. Using an alcohol drug solution for loading allowed for larger loading and linear release that was close to zero-order mechanisms. On assumption that no loading occurs between rolled layers, then maximum loading in the lumen is equal to  $r^2/(R^2-r^2)$ , which is ca 14 volume % (where  $R = 25$  nm is outer radius, and  $r = 7.5$  nm is lumen radius). The optimized experimental conditions yielded ca 5 wt % and 13 volume % ratios (taking the density of halloysite to be 2.53 g/cm<sup>3</sup>).<sup>2</sup> No drug was inserted between halloysite clay layers in the roll, as confirmed by preserved 7.2 Å packing X-ray reflection. It was indicated that it is possible to intercalate

only ethylene glycol or small ions by drying hydrated halloysite (halloysite-10 Å) in the presence of NH<sub>4</sub><sup>-</sup>, K<sup>-</sup>, Cs<sup>-</sup>, Rb<sup>-</sup>-salts [49]. For this experimental setup, thermodynamically stable dehydrated halloysite-7 Å, which does not allow intercalation, was used [51].

It is difficult to judge how much of the drugs were adsorbed on the surface of the tubes. Before each release experiment, the loaded halloysite was washed with large amounts of water for 5 min to ensure removal of material from the surface. However, it is difficult to exclude some materials that may still have been attached to the outer surface, especially in the natural gap-defect on the cylinder surface at the end of the rolled clay sheet (it is a natural pocket on the tubule surface). The typical 5 - 10 % initial release burst may be related to the dissolution of this externally attached matter. To have better washing initially, washing was done with the same solvent which was used for loading, but heavy loss of the drug in washing was observed. This result might be due to the washing of loaded drug by the high-solubility solvent. Hence, DI water was opted for, which is good at removing the loosely bound particles and causes minimum loss to the particles loaded inside the lumen.

In the pH range of 4-7, surface charge in the tubule lumen is positive and surface charge on the external surface is negative. This factor allowed for more efficient loading of halloysite with negatively charge molecules at lower pH as demonstrated in Figure 4.4a for Dexamethasone. At low pH, the loading was maximal at 5.5 wt %. At higher pH, the loading was less than 2-3 wt %. Thus, low pH facilitates to reach a loading amount close to that of the 50 % alcohol solvent. Dexamethasone release was observed in water at pH 7.4 (Figure 4.4 b). A similar release rate for different loadings, but the initial drug burst associated with quick dissolution of externally attached drug was larger for

lower pH. This might indicate that at low pH, some of loaded material can be associated with undesirable external deposition (not in the lumen). A maximum loading of 5.5 wt % at pH 1.4 when both lumen and outermost surface are positive is close to full loading capacity (ca 14 volume %). Minimal 2 wt % loading was performed at pH 9 when both halloysite lumen and Dexamethasone had the same negative charge, and it corresponds to the loading of only one third of the lumen volume.

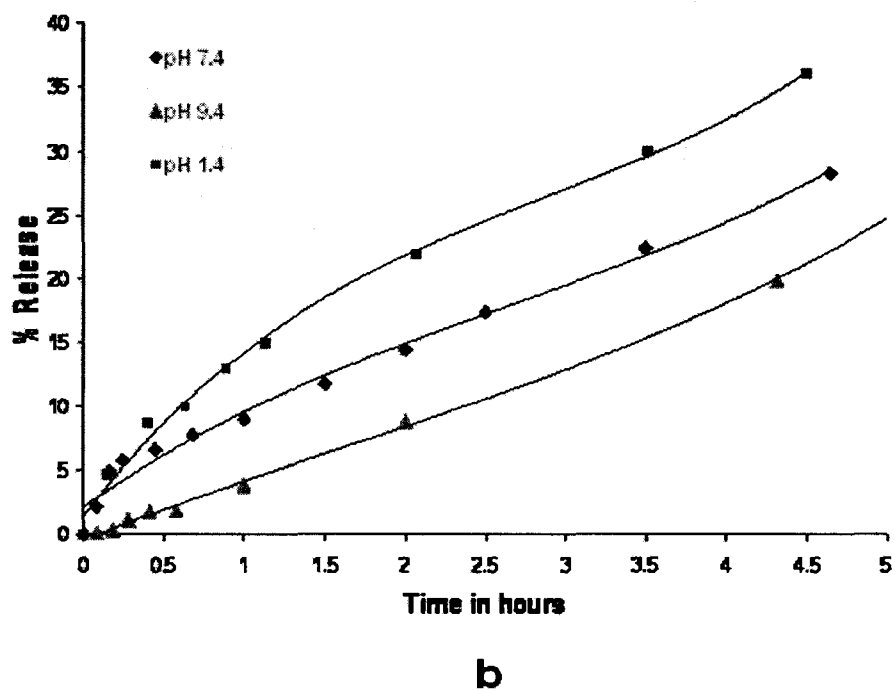
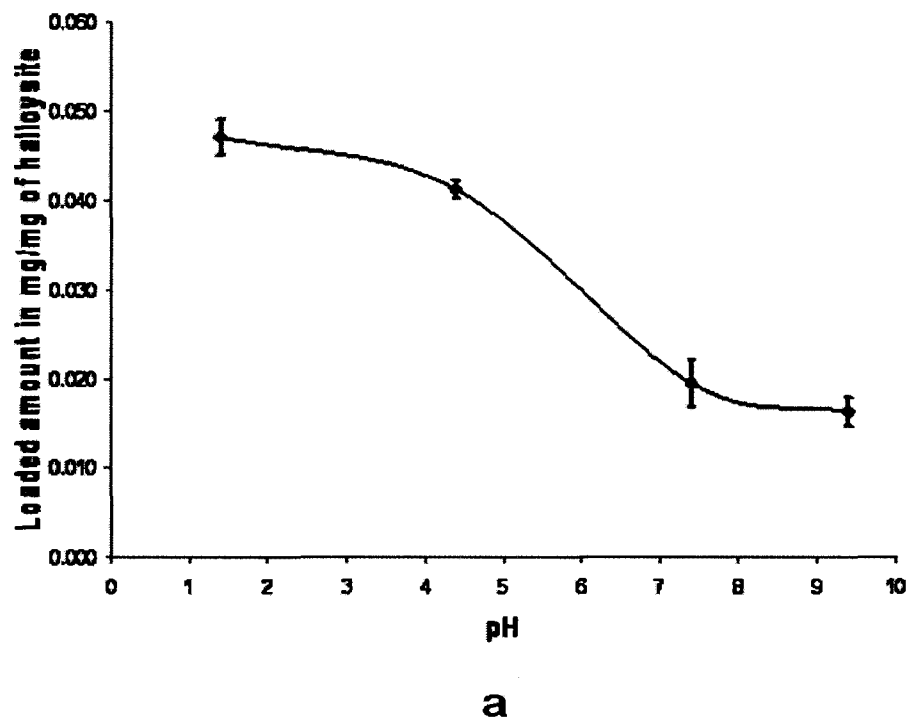


Figure 4.4: Amount of Dexamethasone loading depending on pH (a), and its initial release in water at pH 7.4 (b).

## **Conclusion**

An extended 6-10 hours drug release from 15-nm lumen diameter tubular halloysite has been demonstrated for dexamethasone, furosemide, and nifedipine. By optimizing solvents with pH and alcohol content, the highest loading of 12 volume %, which is close to the theoretical capacity of these nanotubules, was obtained. Maximal loading resulted in more linear release (close to zero-order release mechanisms for dexamethasone and furosemide).

**CHAPTER 5**

**TUNABLE CONTROLLED RELEASE OF**

**DEXAMETHASONE USING**

**LAYER-BY-LAYER**

**FORMULATED**

**HALLOYSITE**

**Introduction**

The usefulness of any drug is based not only on its effect on the disease but also on how specifically, how readily, how controllable and how prolonged its effect on the disease without having any side effects. Thus the techniques involved in the drug encapsulation and its controlled release forms one of the important processes of drug formulation. In recent years nanotechnology, through its arms of nanomedicine and biomedical nanotechnology, is revolutionizing the field of pharmaceuticals. Its applications makes use of the properties of nanoparticles as drugs or constituents of drugs as a novel design or strategies to controlled release, drug targeting, and making availability of low bioavailability drugs [120-122]. These more complex submicron or nanosized drug delivery systems are either self-assembling or involve covalent conjugation of multicomponent systems, e.g., drug, protein and polymer. The bioresponsive or biomimetic materials used to create such drug delivery systems typically



include synthetic or semi-synthetic polymers, and natural materials such as lipids, polymers and proteins. One such submicron or nanosized drug delivery system discussed in this chapter is the ceramic-based naturally available clay nanomaterial called halloysite. In spite of its huge advantage of having a high availability to cost ratio over other conventional nanotubes like carbon nanotubes, metallic nanotubes etc, halloysite has received only meager attention by the scientific community in the last 10-15 years. But even with a very little attention, in perspective halloysite has been shown as a promising material for various fields of nanotechnology application [50, 52, 64]. The inner positively charged lumen surface of halloysite nanotubes was used to fill with a large range of organic and biologically active agents including lubricants, herbicides, pest repellents, pharmaceuticals, cosmetics, food and personal products, as well as other agents that could benefit from a controlled release [49, 51, 55, 56, 123]. The combined use of charge difference in outer and inner surfaces of halloysite was recently exploited for loading benzotriazole (corrosion inhibitor) and encapsulation of the loaded halloysite by Schukin et al. [124]. In this chapter a detailed study of the halloysite as a template for LbL assembly and its utilization for the controlled delivery of the chosen drug dexamethasone is presented. The various advantages of LbL assembly like its thickness tunability in nanometer range control over permeability of the nanoshells, modification of surface property and simple process has overruled the selection of other encapsulation techniques [76-82]. Control over the drug release was studied by observing the effect of number of assembled layers and the effect of molecular weight of the assembled polymers on the release rate.

## **Materials and Methods**

Processed halloysite was obtained from Atlas Mining Corporation and used without any further treatment. Polyelectrolytes such as poly-allylamine (PAH, MW 70000 and MW 15000), poly-styrene sulfonate (PSS, MW 70000 and MW 32000), poly-ethyleneimine (PEI, MW 1100), and poly-acrylic acid (PAA, MW 5200), were purchased from Sigma Aldrich, USA. Also natural polymers such as chitosan (MW 1 million), gelatin from bovine skin, type-B (Gelatin-B, MW 70000), and silica nanoparticles (7nm and 22nm diameter) were purchased from Sigma Aldrich, USA, and used as such. The drug dexamethasone was purchased from Spectrum Chemicals and Laboratory Products, CA, USA.

### **Layer-by-Layer Assembly on Halloysite**

LbL assembly on halloysite was done by following a traditional procedure as described elsewhere [82, 84, 103]. In our case, negatively charged halloysite nanotubes were used as template with PAH, (MW 70000 and MW 15000), PEI (MW 2000), and chitosan (MW 1 million) as polycations and PSS (MW 70000 and MW 32000), PAA (MW 5100), Gelatin-B (MW 70000), and silica nanoparticles (7nm and 22nm diameter) as polyanions. Typically polycations (0.75 ml of 3 mg/ml in deionised (DI) water) and polyanions (0.75 ml of 3mg/ml in DI water) were alternatively added in to 0.75 ml of halloysite suspension in DI water (~10 mg). Then, two intermediate washings were done with DI water using centrifugation speed at 5000 rpm for 5 min at room temperature (Eppendorf 5804R Centrifuge) to remove the unadsorbed polymers before the next layer was assembled.

### **Characterization of Assembled Layers**

The assembly of layers on halloysite template was confirmed by monitoring Quartz Crystal Microbalance resonant frequency changes (QCM, USI-Systems, Japan), and observing the surface charge alternation after deposition of each layer using a Zeta Potential analyzer (Brookhaven Instruments Corporation). Assembly of silica nanoparticles was visually confirmed by taking Transmission Electron Microscope (TEM) images (ZEISS-LIBRA 120 KV).

### **Dexamethasone Loading**

The loading of halloysite with drug was achieved by following the procedure as described in earlier work [123, 49, 124] with slight modifications. In the first step the pre-weighed halloysite (around 10 mg) is mixed with 5 mg of dexamethasone and made into thick paste by adding 50  $\mu$ L of DI water and sonicated for 30 min for proper mixing, and then vacuum pulling and breaking done several times until the fizzing stopped for loading. Then finally the tubules were washed with DI water twice (centrifugation speed at 5000 rpm for 1 min at room temperature) and vacuum dried. The loading of the drug was confirmed by porosity test using mercury porosimeter (Micromeretics). Around 100mg of dry halloysite powder (loaded or unloaded) was taken, and mercury was forced through the pore volume of the sample by slowly increasing the pressure up to 30000 psia using micromeretics porosimeter equipment. At each stage of pressure the amount of mercury intruded into pores was used to evaluate the pore volume.

### **Encapsulation of Drug-Loaded Halloysite**

Encapsulation of the drug loaded halloysite was achieved by LbL assembly. The same above mentioned LbL assembly procedure was followed except for the washing speed and time modified to 8000 rpm and 1 min to avoid the loss of loaded drug.

### **In Vitro Dexamethasone Release Kinetics**

The in vitro drug dissolution studies were performed using 2ml centrifuge tube. Known amount of dry encapsulated drug in halloysite nanotubes (~10mg) was taken and suspended in 1.5ml of DI water with continuous stirring at 500 rpm. From this suspension, time-based samples (750  $\mu$ L) are collected from the supernatant of this mixture after centrifuging it at 8000 rpm for 1 min. For each sample taken, an equivalent amount of fresh DI water is added and the halloysite is resuspended. The concentration of the drug in the collected samples was determined by UV-Vis spectrophotometer (Agilent-8453). For monitoring dexamethasone the absorbance was studied at 240 nm. The total amount of drug loaded was calculated based upon complete release from the encapsulated nanotubes (till no absorbance peak was observed in spite of sonicating the final sample for an hour).

## **Results and Discussion**

First, halloysite was established as a nanotubular template for LbL assembly by adsorbing layers of PAH(MW 70000)/PSS(MW 70000), PEI(MW 2000)/PAA(MW 5100), and PEI(MW 2000)/Si nanoparticles, then later on we extended LbL assembly for the encapsulation of dexamethasone-loaded halloysite for controlled release. Figure 5.1 explains the illustration of the entire assembly process.

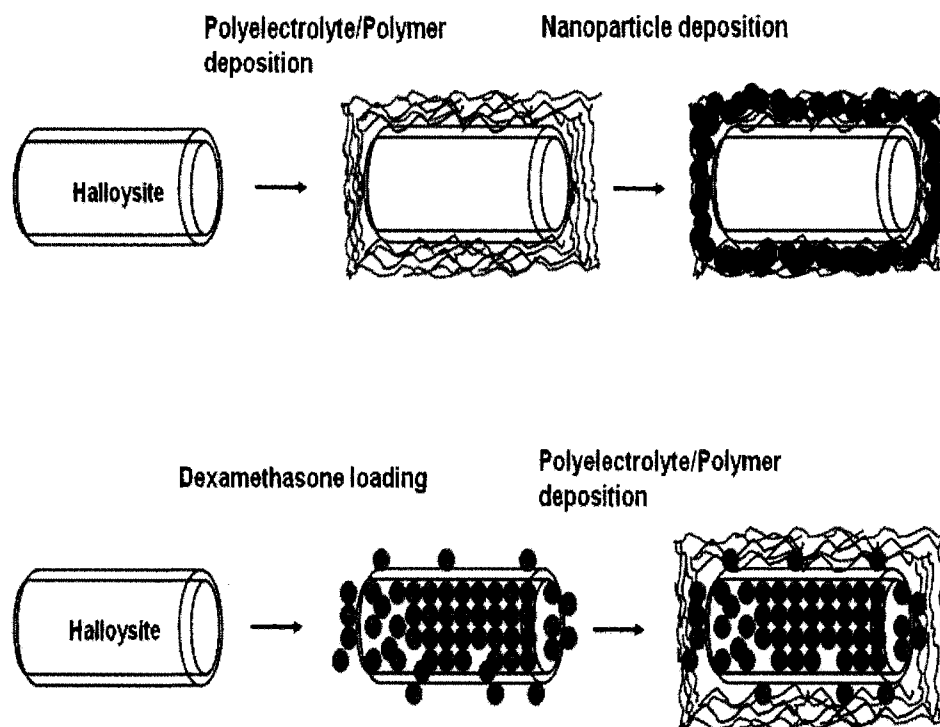


Figure 5.1: Schematic illustration of layer-by-layer assembly of polymer/nanoparticle coating on halloysite and halloysite loaded with drug.

The zeta potential surface charge alternation for each layer adsorption of PAH(MW 70000)/PSS(MW 70000) and PEI(MW 2000)/PAA(MW 5100) was shown in Figure 5.2. For Silica nanoparticle adsorption (7nm and 22nm diameter) 1.5 bilayer of PEI(MW 2000)/PAA(MW 5100) was used as a precursor layer and 2.5 bilayer of PEI(MW 2000)/PAA(MW 5100) was used as an intermediate bed layer for second layer adsorption of silica nanoparticles. The zeta potential surface charge alternation for each layer polymer and nanoparticle adsorption was shown in Figure 5.3. Complete alternation of charge was observed until the first layer of nanoparticle coating after that only reduction of positive charge was observed. This result might be due to the heavy adsorption of low molecular weight PEI (2000) over silica nanoparticle layer, followed by less adsorption of higher molecular weight PAA (5100). The growing of the thickness

of polymer/nanoparticle layer around halloysite was monitored using QCM and shown in Figure 5.4. The bilayer thickness of PEI (MW 2000)/PAA (MW 5100) is around 1-3 nm and the average thickness of 7 nm diameter silica nanoparticle layer is around 6-8 nm and of 22 nm diameter silica nanoparticle is around 14-16 nm. The adsorption of silica nanoparticles was also observed by TEM, the images are shown in Figure 5.5 for silica nanoparticles having 7 nm diameter and in Figure 5.6 for silica nanoparticles having 22 nm diameter. A uniform coating of silica nanoparticle is observed for both 1st layer and 2nd layer of nanoparticle coatings in the case of lesser diameter particles (7 nm), for higher diameter nanoparticles (22 nm) uniform coating is observed only for 2nd layer of coating.

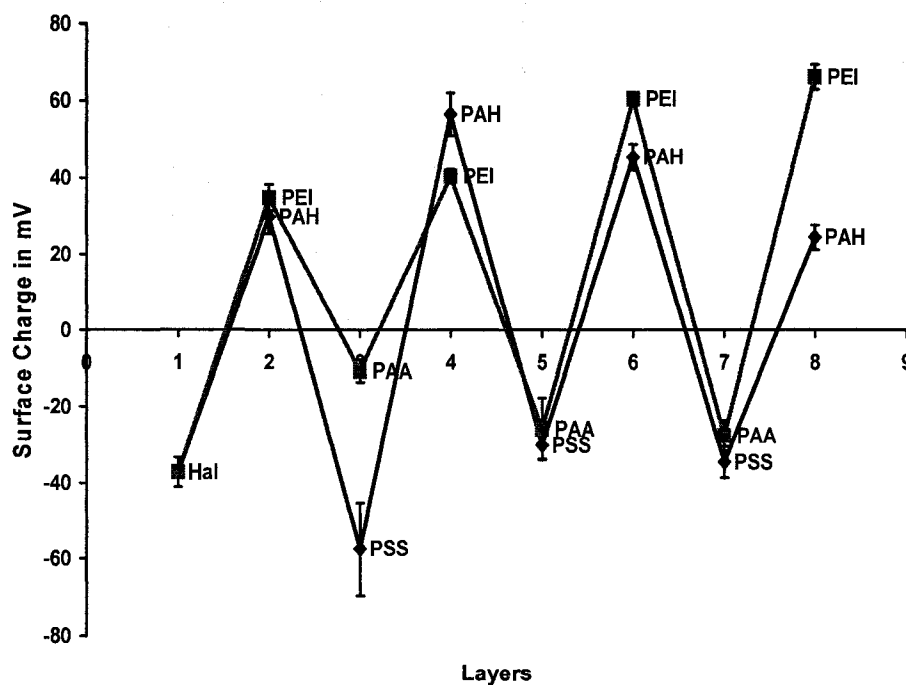


Figure 5.2: Zeta potential readings of four bilayer coating of PAH(MW 70000)/PSS(MW 70000) and PEI(MW 2000)/PAA(MW 5100) on halloysite at pH 6.5.

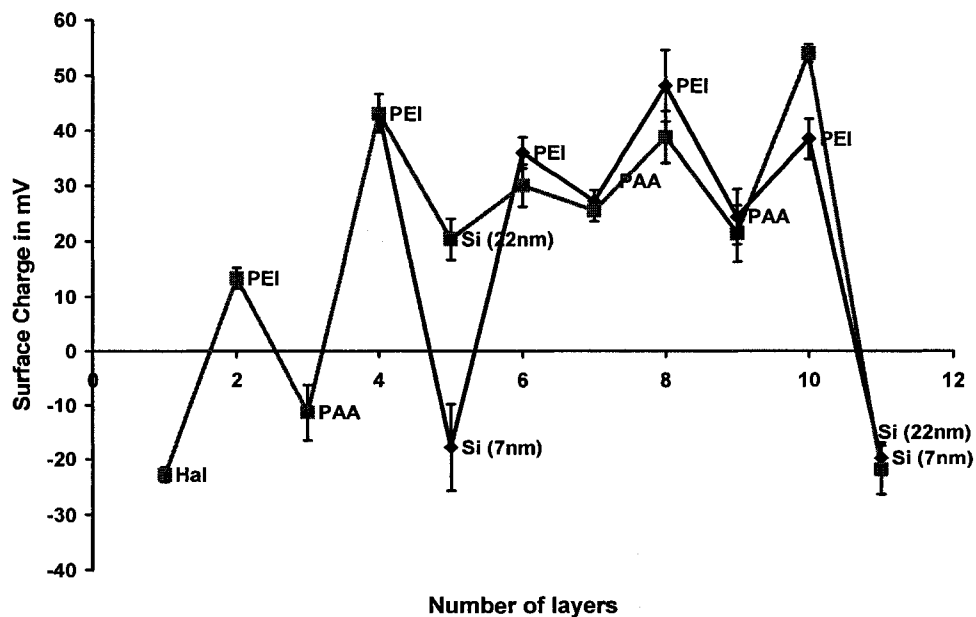


Figure 5.3: Zeta potential readings of layer-by-layer coated polymers (with PEI(MW 2000)/PAA(MW 5100)) along with silica nanoparticles (7nm and 22nm in diameter) on halloysite at pH 6.5.

To confirm qualitatively the loading of dexamethasone by the modified procedure mentioned above, the porosity of the dexamethasone-loaded halloysite nanotubes was compared with the porosity of the unloaded nanotubes using mercury porosimeter. Figure 5.7 shows the reduction in the pore volume for the dexamethasone loaded nanotubes. Quantitatively the porosity of the unloaded halloysite reduced from 67.7% to 50.5% on loading of dexamethasone.

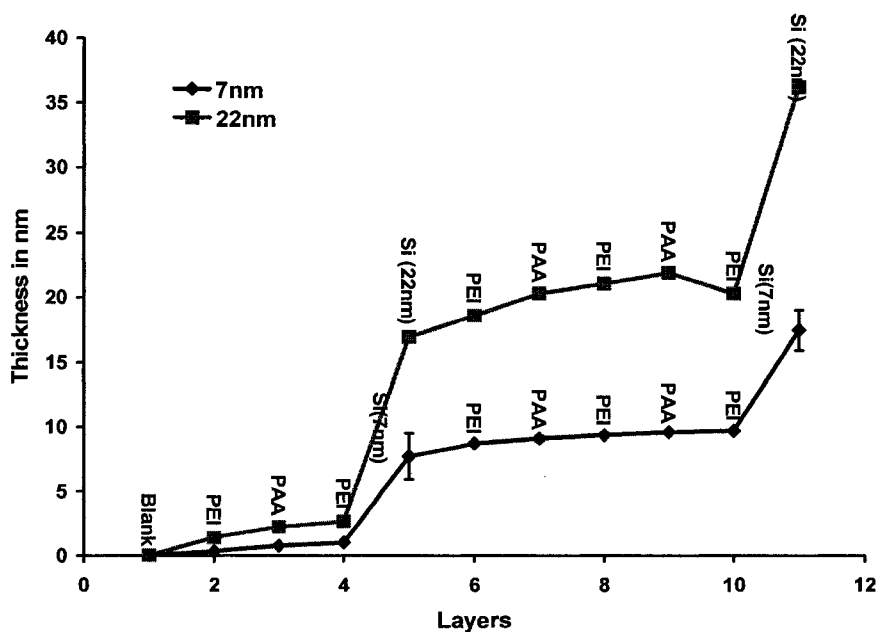
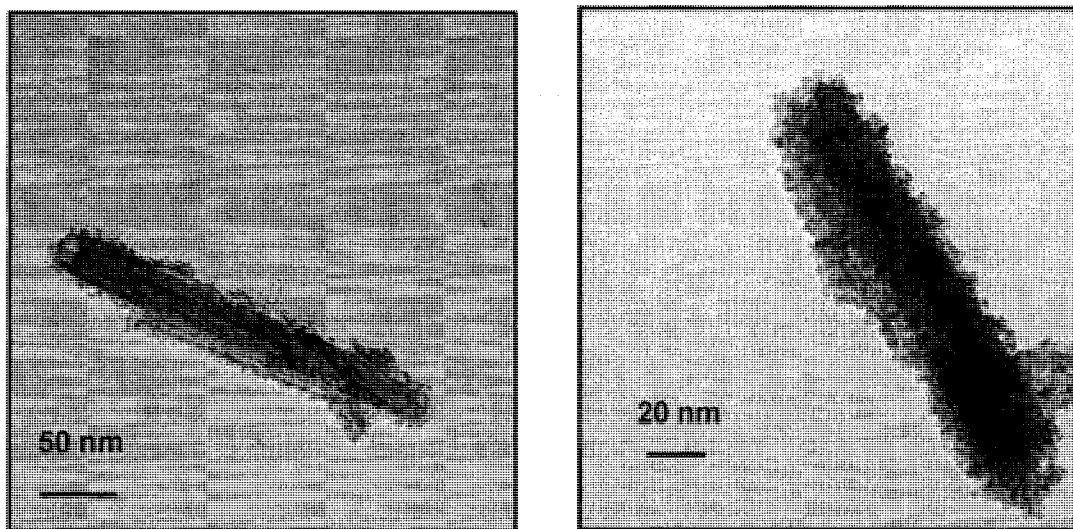


Figure 5.4: Film thickness monitoring by Quartz crystal microbalance studies for polymer (PEI(MW 2000)/PAA(MW 5100)) and nanoparticle (silica nanoparticles 7nm and 22nm in diameter) assembly.



1<sup>st</sup> layer of 7nm dia Si nanoparticle

2<sup>nd</sup> layer of 7nm dia Si nanoparticle

Figure 5.5: Transmission electron microscopy image of Si nanoparticle with diameter of 7nm assembly on halloysite.



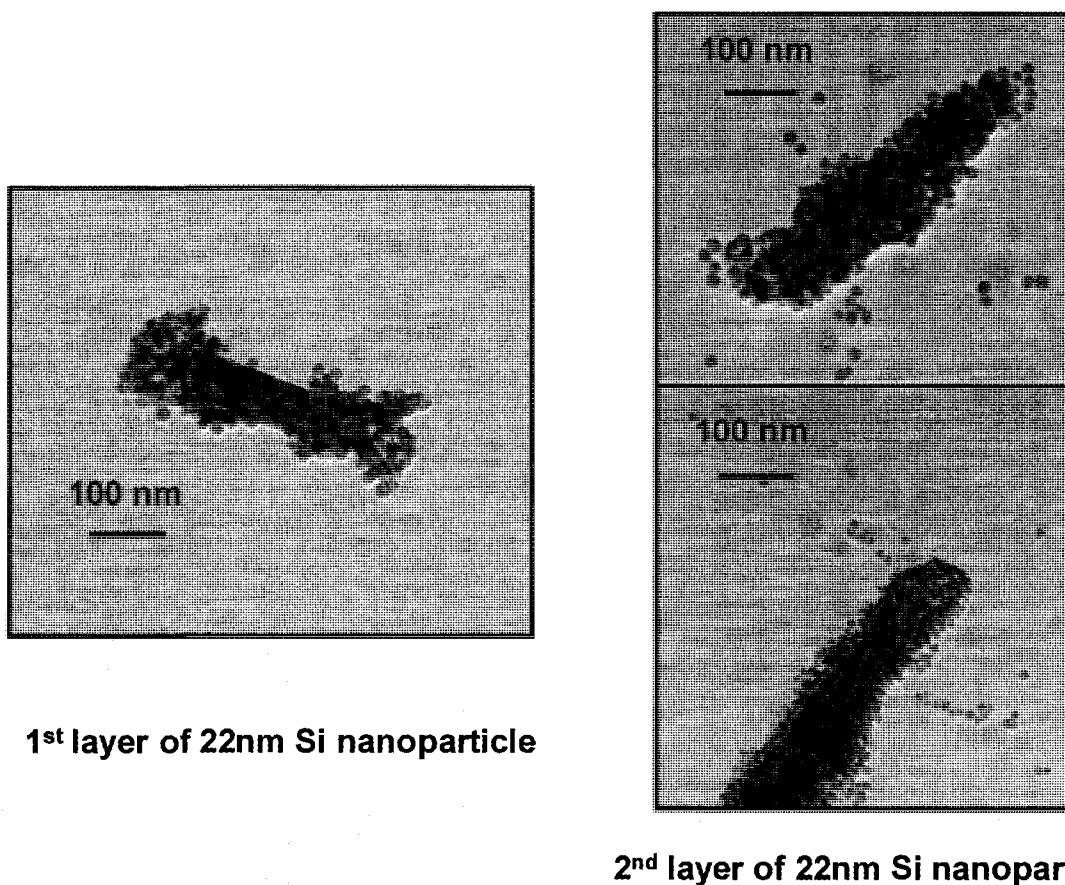


Figure 5.6: Transmission electron microscopy image of Si nanoparticle with diameter of 22nm assembly on halloysite.

Encapsulation of the dexamethasone-loaded halloysite was done using layers of PEI(MW 2000)/PAA(MW 5100) and later on extended to various polymers of different molecular weight. The effect of the number of adsorbed layers on the release rate of dexamethasone was studied using several bilayers of PEI(MW 2000)/PAA(MW 5100). Figure 5.8 shows zeta potential surface charge alternation for each layer adsorption of PEI(MW 2000)/PAA(MW 5100) on dexamethasone-loaded halloysite. The release profiles of dexamethasone from the LbL (1, 3, 6, and 9 bilayer of PEI(MW 2000)/PAA(MW 5100)) formulated composite was compared with uncoated (0 bilayer)

halloysite loaded with drug in Figure 5.9. A very marginal and decent retardation in the release rate was observed for 1 & 3 bilayer coated samples when compared with uncoated halloysite loaded with drug. Whereas in the case of 6 & 9 bilayer coated samples the release rates of dexamethasone were found to be increased, it was due to heavy loss of dexamethasone during the LbL assembly which resulted in a lesser quantity of final loaded drug, hence the faster release. Similar results were observed earlier in Chapter 2 [123]. Hence, an optimum number of bilayers were required for retardation, in our case the optimum being 3 bilayers. The decent retardation achieved for 3 bilayers might be due to low molecular weight of the compounds used for encapsulation (MW 2000 and MW 5100).

To confirm the significance of molecular weight of the assembled polymers the molecular weight effect of the adsorbed polymers on the drug release rate was studied. Three variations of the molecular weight range has been studied: low molecular weight polymers PEI(MW 2000)/PAA(MW 5100), medium molecular weight polymers PAH(MW 15000)/PSS(MW 32000), and high molecular weight polymers PAH(MW 70000)/PSS(MW 70000). The assembly of the above polymers over the dexamethasone loaded drug was studied by zeta potential measurements and shown in Figure 5.10. The release profiles of dexamethasone from three bilayer coated samples using three different molecular weight combinations of the coated polymers was compared with the release from the uncoated halloysite in Figure 5.11. From the release rate curves it was established that as the molecular weight of the coated polymer increases the retardation of the drug increases further for the same number of layers. This increase in retardation can be attributed to the mechanical and chemical stability of the formed layers to harsh

conditions which has molecular weight greater than 10000 [125]. With the shown control over the release rate of dexamethasone by LbL assembly; this clay-drug composite provides a novel formulation for controlled release of drugs.

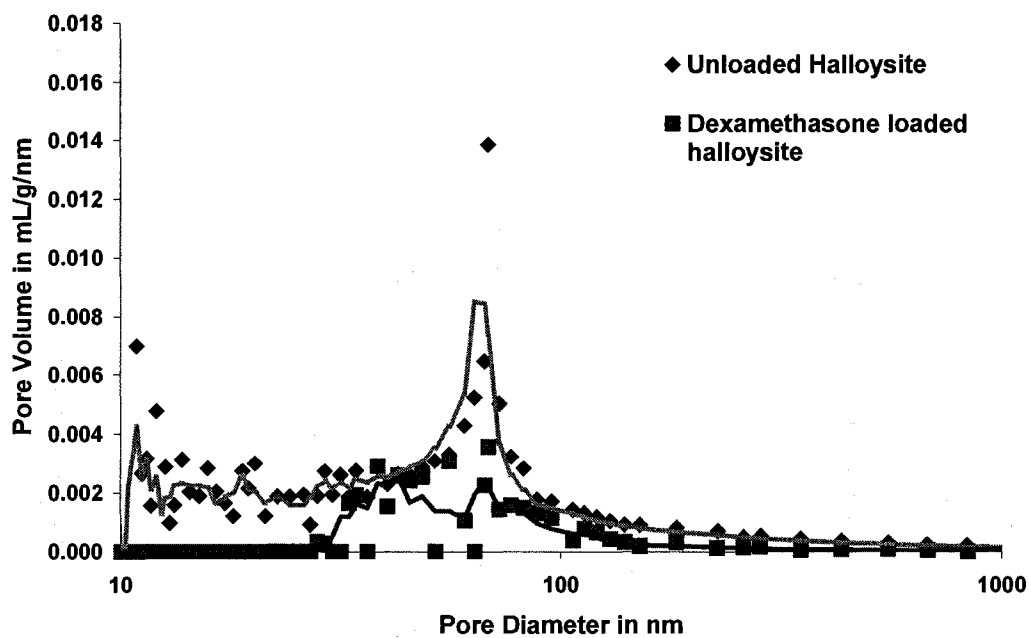


Figure 5.7: Mercury porosimeter results of dexamethasone loaded halloysite in comparison with unloaded halloysite.

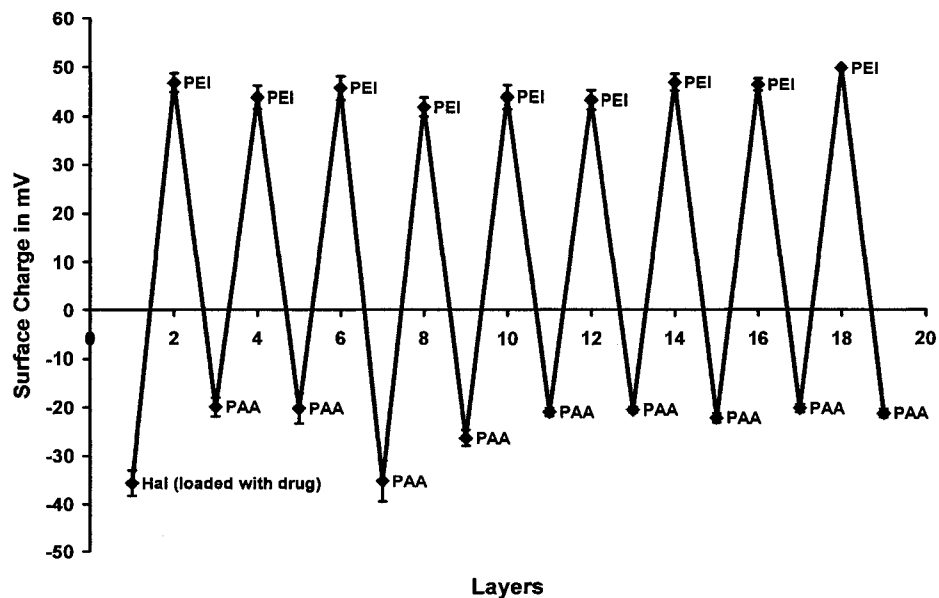


Figure 5.8: Zeta potential readings of LbL coating of (PEI(MW 2000)/PAA(MW 5100)) halloysite loaded with dexamethasone drug.

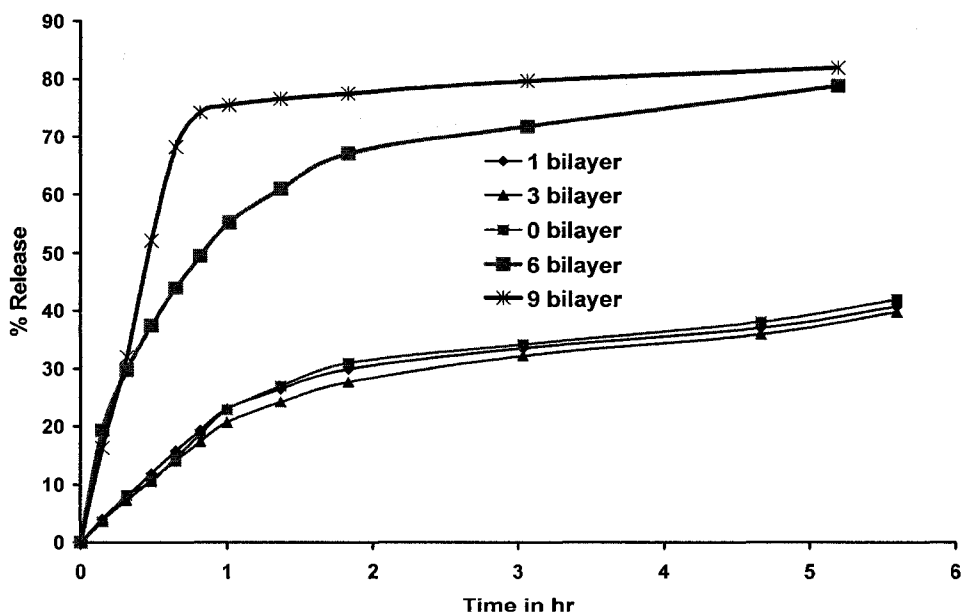


Figure 5.9: Effect of number of bilayers on the release profile of dexamethasone drug in deionised water at pH 6.5 from LbL (PEI/PAA) coated halloysite loaded with dexamethasone.

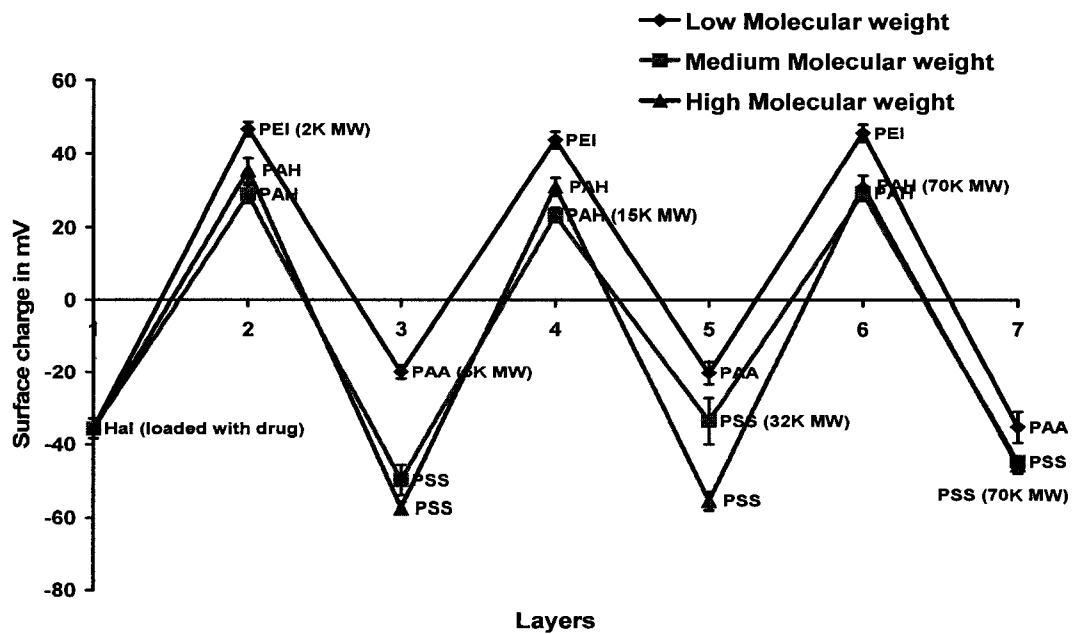


Figure 5.10: Zeta potential readings of layer-by-layer coated halloysite loaded with Dexamethasone drug.

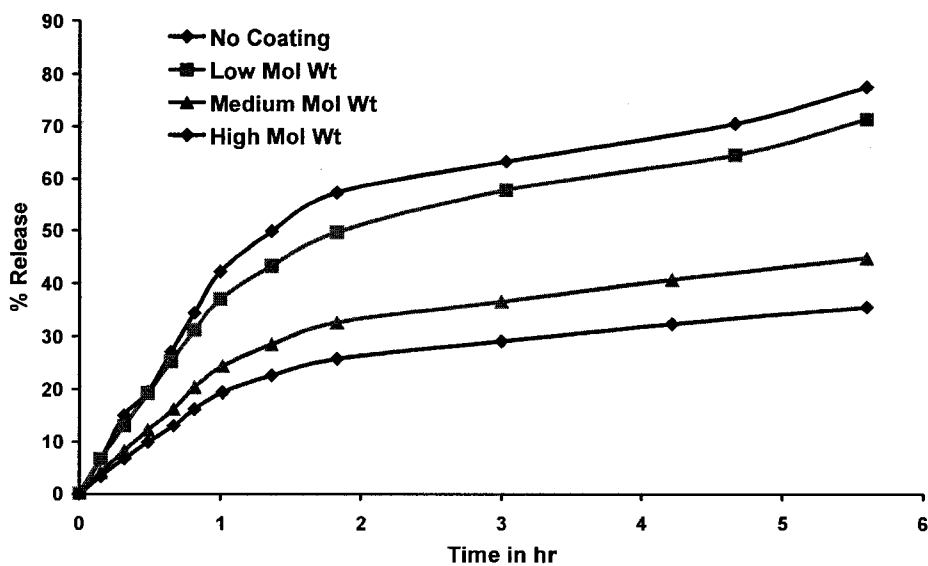


Figure 5.11: Molecular weight effect of the coated polymers on the release profile of dexamethasone drug in deionised water at pH 6.5 from LbL coated halloysite loaded with dexamethasone.

Though halloysite is biocompatible, some of the polymers used for encapsulation are not FDA approved; hence it is necessary to shift to natural polymers for the encapsulation to use this novel formulation for real life applications. To ensure that whatever has been observed with polymers is also possible with natural polymers, a very high molecular weight natural polymers chitosan (MW 1 Million) and Gelatin B (MW 70000) are chosen for LbL encapsulation by following the earlier mentioned procedure.

Figure 5.12 shows the zeta potential surface charge alternation for each layer adsorption of Chitosan (MW 1 Million) and Gelatin B (MW 70000) on dexamethasone loaded halloysite and the release rate in comparison with all other earlier methods was shown in Figure 5.13. This release rate comparably slower than the release rate of high molecular weight polymers used earlier might exist because of higher molecular weight of chitosan Hence in encapsulation, retardation and biocompatibility natural polymers are having advantage over conventional polymers used for LbL assembly in making novel drug-clay composite formulations.

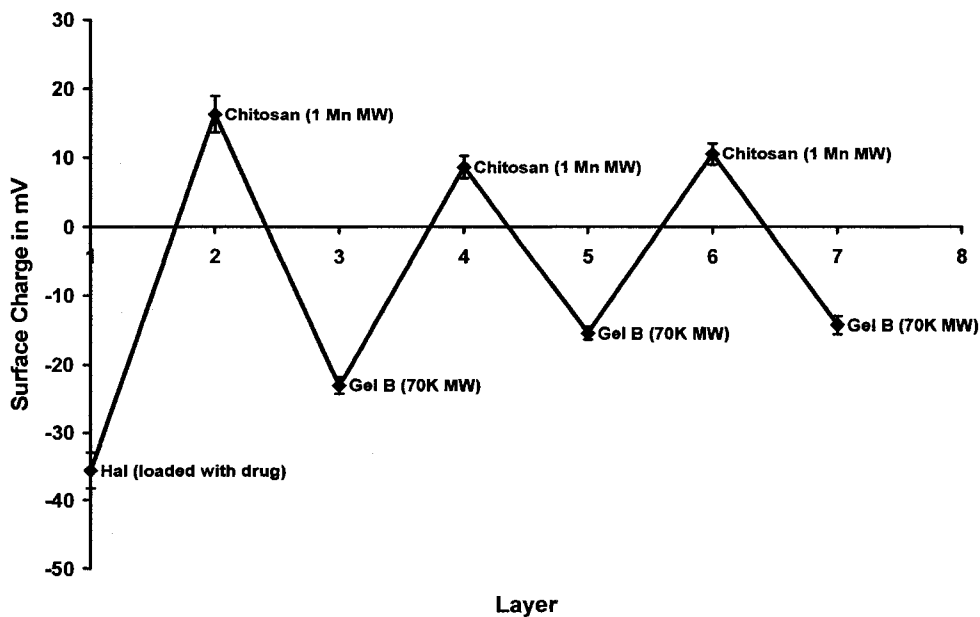


Figure 5.12: Zeta potential readings of layer-by-layer coating of very high molecular weight natural polymers (Chitosan and Gelatin B) on halloysite loaded with dexamethasone drug.

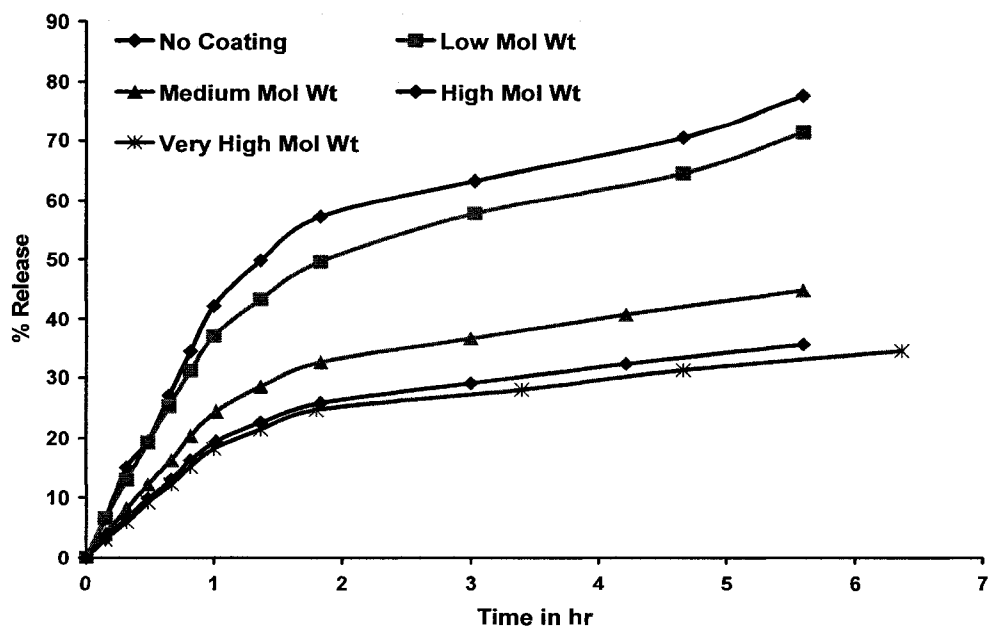


Figure 5.13: Molecular weight effect of the coated polymers on the release profile of dexamethasone drug from LbL coated halloysite loaded with dexamethasone.

## **Conclusion**

Halloysite clay was used as a nanotemplate for Layer-by-Layer assembly of polymers and silica nanoparticles. The LbL assembly of polymers was confirmed by Zeta potential & Quartz crystal microbalance. (QCM) studies and the assembly of silica nanoparticles were confirmed by TEM images. Lower diameter (7 nm) silica nanoparticles gave better uniform assembly rather than higher diameter (22 nm) silica nanoparticles. The LbL assembly was later extended to dexamethasone drug-loaded halloysite for its controlled release. The loading of drug was confirmed by reduction in porosity from 67.7% for empty tubes to 50.5% for loaded tubes using mercury porosimeter equipment. The effect of number of assembled layers and the effect of molecular weight of the assembled polymers on the release profile of the drug revealed that an optimum number of layers and high molecular weight of the assembled polymers gave a very slow sustained release. Encapsulation of the drugs inside the lumen of the halloysite coupled with LbL assembly of natural polymers provides a novel formulation for controlled release of drugs. Our future work is to further study the assembly of specific nanoparticles and polymers on the clay-drug composites for targeted and as well as switchable drug release, for example assembly of magnetic particles can help us in switchable release and assembly of antibodies can help us in drug targeting.



## **CHAPTER 6**

### **HALLOYSITE - IN VITRO CYTOTOXICITY TESTING**

#### **Introduction**

As shown in previous chapters, LbL modified halloysite-based novel drug delivery systems are one of the most economically promising systems. Biocompatibility is one of the main prerequisites for its safe use as a drug delivery system. Although the biocompatible nature of halloysite can be sensed indirectly by the studies of Kommireddy et al. [117], when he used it as a substrate for cell attachment and proliferation and by Kelly et al. [56], who used halloysite as a drug delivery system and performed in vivo studies on dogs for the treatment of periodontitis. A comprehensive study of biocompatibility of halloysite has not been done. A general guideline on the testing of biocompatibility of materials for biomedical applications is specified in the International Standard Organization (ISO) 10993. In vitro cytotoxicity testing is one of the important biological test methods for checking the biocompatibility of a material as per ISO standards. Due to the presence of silica on the outer surface, the halloysite has a negatively charged surface. This negative charge can influence the surface contact of the cells electro statically as the surface charge on the cells is also negative. To have proper understanding about the surface interaction of the halloysite with the cells, both negatively charged halloysite (raw halloysite) and as well as positively charged

halloysite, obtained by coating the halloysite with positively charged biocompatible polymers like poly-L-lysine and protamine sulphate has been used for cytotoxicity study.

## **Experiments**

### **Materials**

Processed halloysite was obtained from Atlas Mining Corporation, Utah and used without any further treatment. Polyelectrolyte's such as poly-Ethyleneimine (PEI, MW 1100), and poly-Acrylic acid (PAA, MW 5200), were purchased from Sigma Aldrich, USA. Also natural polymers such as protamine sulphate, poly-L-lysine and sodium chloride salt were purchased from Sigma Aldrich, USA, and used as such.

### **Layer-by-Layer Assembly on Halloysite**

LbL assembly on halloysite was done by following a traditional procedure as described elsewhere [82, 84, 103]. In our case negatively charged halloysite nanotubes were used as a template with PEI (MW 2000), protamine sulphate and poly-L-lysine as polycations and PAA (MW 5100) as polyanions. Typically polycations (0.75 ml of 2 mg/ml in deionised (DI) water) and polyanions (0.75 ml of 2 mg/ml in DI water) were alternatively added in to 0.75 ml of halloysite suspension in DI water (~10 mg). Then, two intermediate washing was done with DI water using centrifugation speed at 5000 rpm for 5 min at room temperature (Eppendorf 5804R Centrifuge) to remove the unadsorbed polymers before the next layer was assembled.

### **Characterization of Assembled Layers**

The assembly of layers on halloysite template was confirmed by observing the surface charge alternation after deposition of each layer using a Zeta Potential analyzer (Brookhaven Instruments Corporation).

### **Cell Culture**

Two types of cells were used for cytotoxicity testing, one is 3T3 fibroblast cells and the other is human breast cancer MCF-7 cells. Each type of cells were grown separately at 37 deg C in a humidified atmosphere (95% air and 5% CO<sub>2</sub>), DMEM (Dulbecco's Modified Eagle medium) supplemented with phenol red, 3% L-glutamine, penicillin (100 U/ml), gentamycin (100 µg/ml) and 10% foetal calf serum

### **Cytotoxicity Assay**

Briefly, each type of cells was separately seeded approx.10000/well cells into the 96-well plate (flat bottom). Halloysite (both coated and uncoated) was added separately in three different rows around 100 µg/ml of the medium. For positive control some rows were left untreated and for negative control some rows are treated with NaCl (which kills cells). After certain time of incubation, the plate was washed and reagent (CellTiter 96 from promega) was added. The resulting change of color was read on a Plate Reader at 490nm. The percentage of live cells was calculated based upon initial number of cells seeded.

## Results and Discussion

The surface modification of halloysite by LbL assembly was observed by the zeta potential surface charge measurements. Figure 6.1 shows the alternation of surface charge after each coating of polymer layers.

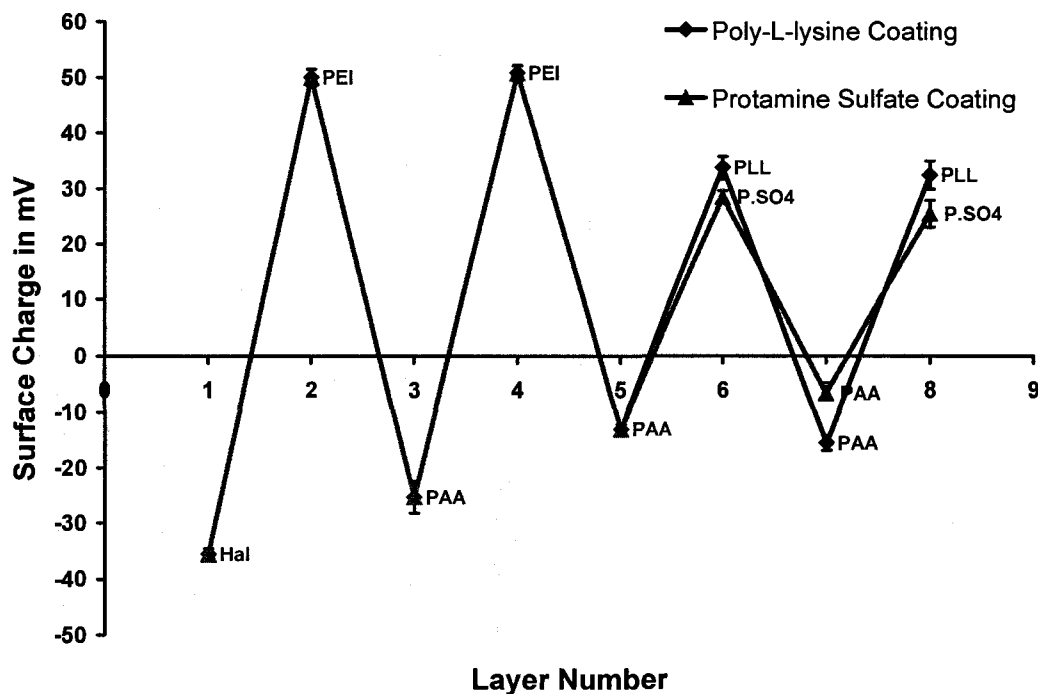
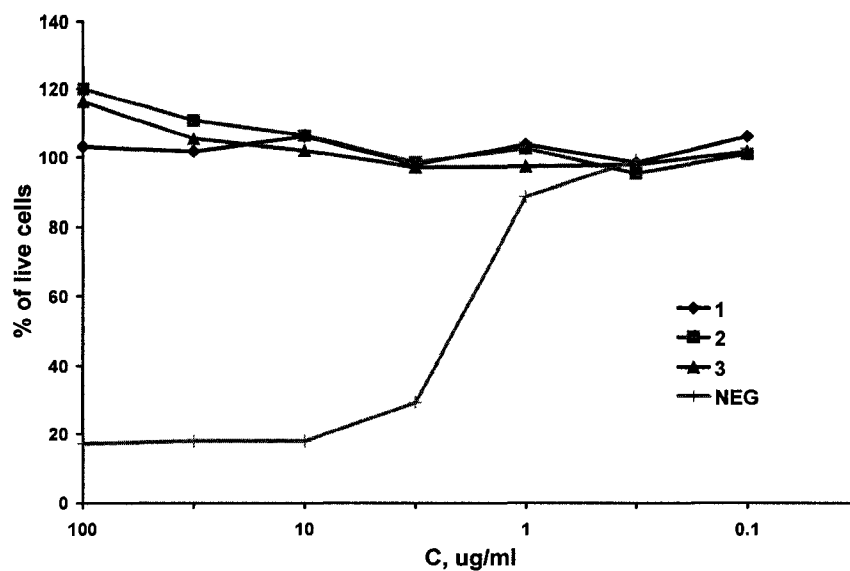
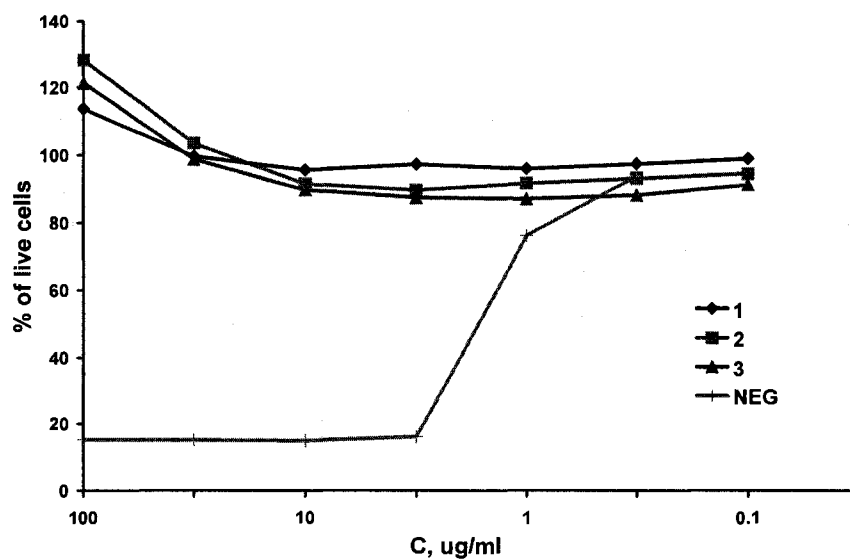


Figure 6.1: LbL coating of halloysite with natural polymers (poly-L-lysine and protamine sulphate) after coating two bilayers of PEI(MW 2000)/PAA(MW 5100) as precursors at pH 6.5.

The cytotoxicity of the charged halloysite was tested after 24 hours and 48 hours of incubation time for both types of cells, 3T3 and MCF-7 cells. The percentage of live cells as determined by celltiter-96 reagent was measured for various concentration of testing agents (raw halloysite, poly-L-lysine coated halloysite, protamine sulphate coated halloysite, sodium chloride (negative control)). The results are shown in Figure 6.2 and Figure 6.3.

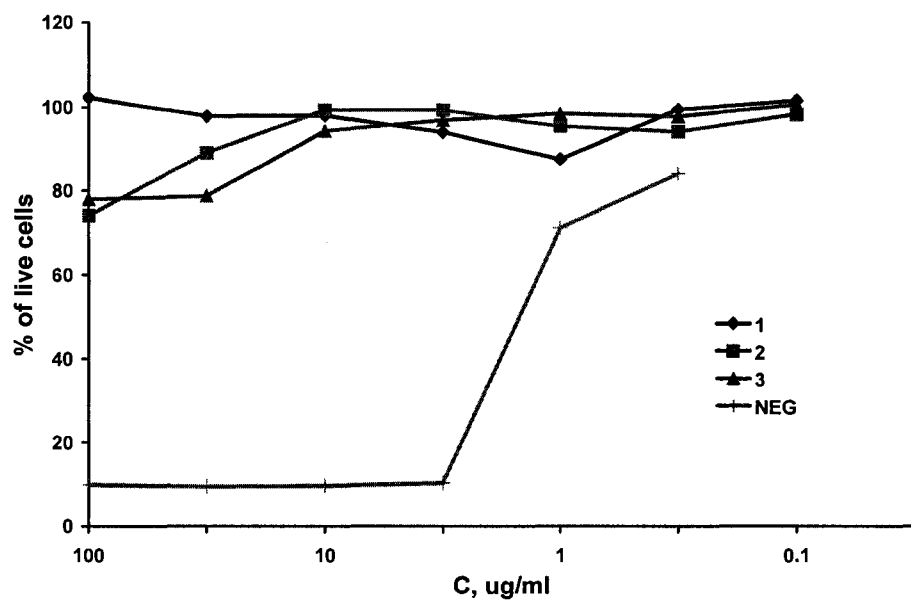


A

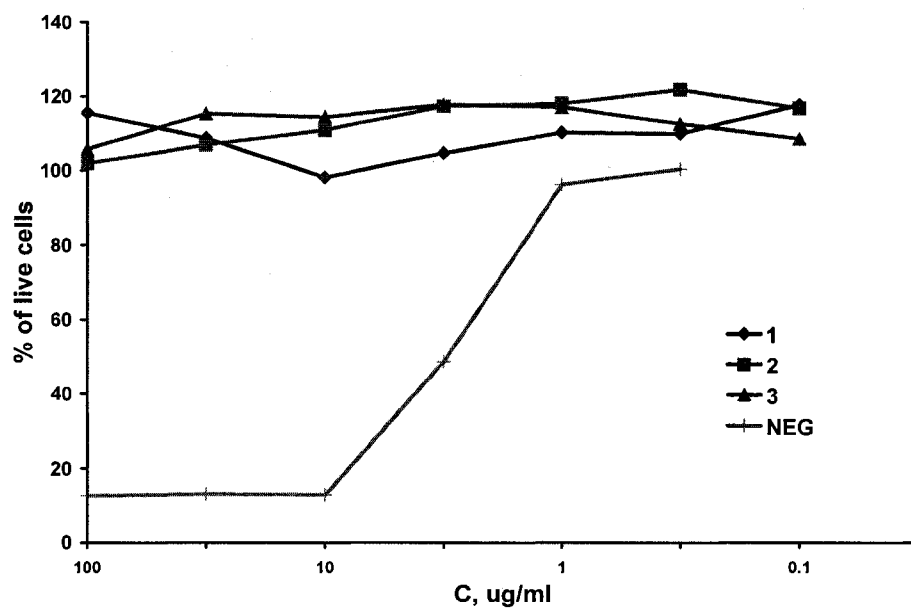


B

Figure 6.2: Viability of 3T3 cells after 24 hr (A) and after 48 hr (B) as determined by celltiter-96 reagent. The legend stands for 1. Raw halloysite, 2. poly-L-lysine coated halloysite, 3. Protamine sulphate coated halloysite, 4. Sodium chloride (negative control).



A



B

Figure 6.3: Viability of MCF-7 cells after 24 hr (A) and after 48 hr (B) as determined by celltiter-96 reagent. The legend stands for 1. Raw halloysite, 2. poly-L-lysine coated halloysite, 3. Protamine sulphate coated halloysite, 4. Sodium chloride (negative control).

From all the above plotted results it is shown that bare halloysite as well as natural polymer coated halloysite are non-toxic to the cells. Similar experiments conducted for drug (dexamethasone and furosemide) loaded halloysite also yielded similar results.

### **Conclusion**

To conclude, the summary of the cytotoxicity test results clearly indicates that halloysite is a truly biocompatible material and can be used as a component in drug delivery systems.

## **CHAPTER 7**

# **TEMPLATE SYNTHESIS OF SILVER/SILVER OXIDE NANOPARTICLES USING HALLOYSITE AS NANOREACTOR**

### **Introduction**

Metallic nanoparticles, due to their size-dependent properties and their metal-support interaction, have provided many significant features like novel quantum confined effects [126, 127]. In recent years the techniques used for synthesizing these nanoparticles on organic and inorganic templates have increased rapidly and helped us in understanding the science and the controlled engineering of these nanoparticles [128]. This chapter explains in detail about the use of halloysite as an inorganic template for synthesizing silver nanoparticles. Chapter 4, Chapter 5, Chapter 6 and some recent scientific studies on halloysite have showed it as a promising material for encasing and sustaining the release of bioactive molecules for pharmacology and tissue scaffolds [49, 63, 123]. Also silver nanoparticles as such are known to have some antimicrobial properties [129]. The very first use of halloysite as a nanoreactor was done by Shchukin et al. for synthesizing calcium carbonate [65]. The template synthesis of Silver nanoparticles on halloysite is very important not only from academic viewpoint but also from industrial viewpoint as the synthesizing method is simple, also halloysite is available in nature as huge deposits, so negligible cost, and the halloysite-silver



composite complex can be applied as thin coating to any surface. Herein, the synthesis of silver nanoparticles by loading silver acetate inside halloysite nanotubes and further reducing it by proven reducing agents like light [130], heat [131] and hydrogen gas [128] was reported. This in situ synthesis offers a novel way of fabricating surface modified clay materials, nano-rod metals, and core-shell type ceramic nanocomposites.

## **Experiments**

### **Materials**

Halloysite Clay was purchased from Atlas Mining Corporation, Utah. Silver acetate and Lysozyme (from Chicken egg white) were bought from Sigma-Aldrich, USA.

### **Silver/Silver Oxide Synthesis**

Three different methods have been used for template synthesis of silver nanoparticles. Scanning electron microscope viewing (after 2nm thickness coating with Iridium by sputter coater) and porosity test using mercury porosimeter was used to characterize the size and location of the silver nanoparticles.

### **Method 1**

About 5mg of halloysite is mixed with 10 mg of silver acetate in 1ml suspension of DI water and sonicated for 15 min. Then loading of the silver acetate is achieved by pulling and breaking vacuum (100 mm of Hg) for three times. The resultant mixture is kept on stirring at 500rpm and heated on a hot plate at 100 deg C. The mixing is continuously kept on until all the solution is completely dry (nearly 4 hrs). The resultant material is washed with DI water for five times using centrifuge @ 4500rpm for 5 min. Then the washed halloysite is heated to 300 deg C for an hour to decompose the silver acetate to silver.

## **Method 2**

The same steps as described in method 1 were followed except for the final step. After washing with DI water the washed halloysite is kept under hydrogen gas purge for 3 hrs to reduce silver acetate to silver.

## **Method 3**

About 5mg of halloysite is mixed with 5mg of silver acetate and 5mg of lysozyme in 1ml suspension of DI water and sonicated for 15 min. Then loading of the silver acetate is achieved by pulling and breaking vacuum (100 mm of Hg) for three times. The resultant material is washed with DI water for five times using centrifuge @ 4500rpm for 5 min. Then the washed halloysite is exposed to normal visible light for nearly 8hrs to decompose the silver acetate to silver catalyzed by the enzyme lysozyme.

## **Porosity Test**

For mercury porosimeter experiments around 100mg of dry halloysite powder (loaded or unloaded) was taken and mercury was forced through the pore volume of the sample by slowly increasing the pressure up to 30000 psia using micromeritics porosimeter equipment. At each stage of pressure the amount of mercury intruded into pores was used to evaluate the pore volume.

## **Results and Discussion**

The scanning electron microscope (SEM) images of unloaded halloysite are shown in Figure 7.1, the cylindrical nature of the halloysite and the empty lumen is clearly evident. Synthesis by method 1 (reduction by heat) yielded silver nanoparticles ~ 5-25 nm in diameter and predominantly on the outer surface of the halloysite (Figure 7.2). This might be due to high heating at 300 deg C which forced the loaded silver

acetate inside the lumen of halloysite to come out and deposit on the surface. There is a clear separation among the nanoparticles present on the surface, no aggregation observed. Similar observation was also made by Fu et al. when they deposited Palladium nanoparticles [132].



Figure 7.1: SEM images of unloaded empty halloysite. Images were taken after sputter coating the dried sample with 2 nm thickness of Iridium.

Synthesis by method 2 (reduction by hydrogen gas) yielded silver nanoparticles around 5-10 nm and predominantly as a clumps on the outer surface of the halloysite (Figure 7.3). No coating or the presence of silver at the opening ends is observed.

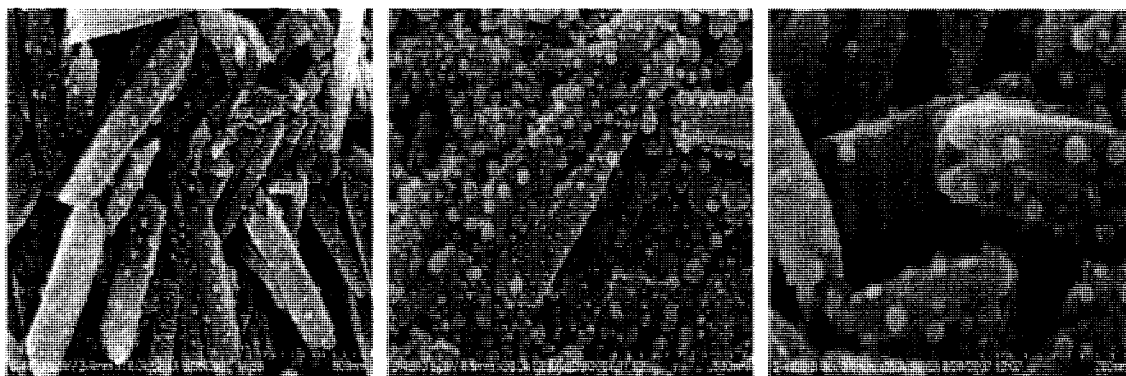


Figure 7.2: SEM images of silver nanoparticles prepared by reducing silver acetate by heat. Images were taken after sputter coating the dried sample with 2 nm thickness of Iridium.

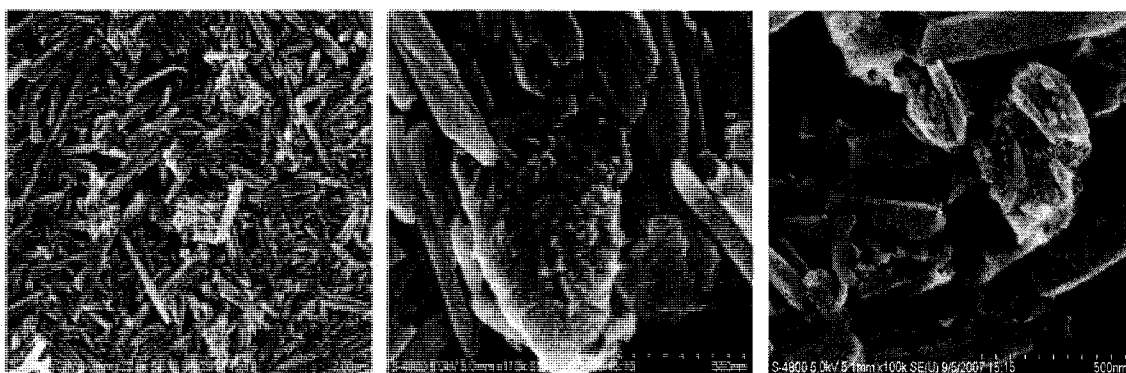


Figure 7.3: SEM images of silver nanoparticles prepared by reducing silver acetate by hydrogen gas. Images were taken after sputter coating the dried sample with 2 nm thickness of Iridium.

Synthesis by method 3 (reduction by light) yielded plugged halloysite nanotubes (Figure 7.4). No presence of silver nanoparticles on the surface of the halloysite observed. On comparing Figure 7.1 and Figure 7.4 the plugging is visually confirmed, but In order to confirm qualitatively, the porosity of the silver loaded halloysite nanotubes was compared with the porosity of the unloaded nanotubes using mercury porosimeter. Figure 7.5 shows the reduction in the pore volume for the silver loaded

nanotubes. Quantitatively the porosity of the unloaded halloysite reduced from 67% to 47% on synthesis of silver by this method.



Figure 7.4: SEM images of silver nanoparticles prepared by reducing silver acetate by normal light in the presence of lysozyme. Images were taken after sputter coating the dried sample with 2 nm thickness of Iridium.

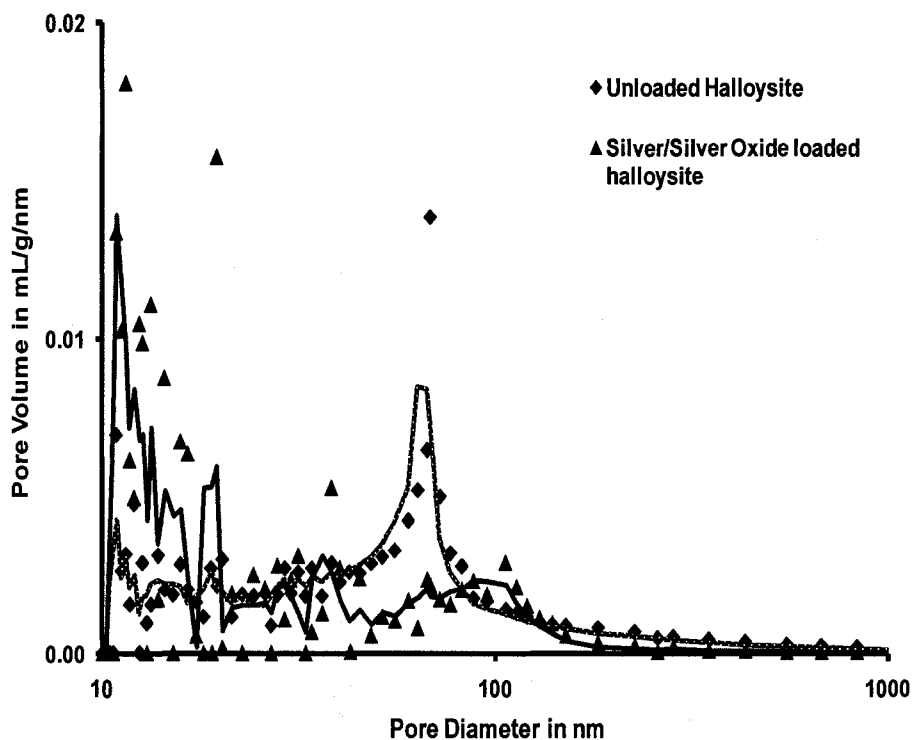


Figure 7.5: Porosimeter results of halloysite loaded with silver prepared by reducing silver acetate by normal light in the presence of lysozyme.

### Conclusion

The reduction of silver acetate, by proven reducing agents like light, heat and hydrogen gas, have consistently yielded silver nanoparticles of the range of 5-50nm in the macro environment, in a nanoconfinement using the halloysite nanotubules the results are completely different. Each method gave different sizes of silver nanoparticles and at different locations on halloysite tubules. Only the lysozyme-catalyzed reduction of silver acetate in the presence of normal visible light showed the presence of silver material inside the lumen; the other methods showed silver particle presence on the surface of halloysite tubes. Since things in the nanoworld are happening complete differently, our presumption of the nanoparticle formed to be silver needs to be confirmed by X-ray

diffraction studies, as there is a probability of the particles being silver oxide also. Hence our forward plan is to confirm those particles are silver and later on to show some application based on the location of silver nanoparticles. For example silver inside the lumen of halloysite can be used to study the kinetics of the antimicrobial activity of silver and silver nanoparticles on the outside surface of the halloysite can be used in the field of photonics, electronics etc.

## CHAPTER 8

### CONCLUSIONS AND FUTURE WORK

#### Conclusions

In this dissertation, two geometrically different shape templates are nanoengineered for controlled delivery of bioactive compounds. The first template used was a spherical alginate particle made from alginic acid, a biopolymer (polysaccharide) derived from brown seaweed, and the second was clay nanotubular template, available in nature deposits known as halloysite.

This dissertation introduces the procedure and optimizes the process of alginate nanoparticle synthesis by emulsification technique. Alginate nanoparticles of approximately 300 nm in diameter can be prepared. Curcumin, a potential anti-inflammatory and anti-cancer drug, was used to encapsulate inside the alginate nanoparticle in the presence of chitosan to enhance its release.

Halloysite drug loading was optimized by varying pH and alcohol / water ratio in the solvent with a maximum drug loading of 12 volume %. The LbL assembly was used to nanoengineer the extended release of dexamethasone. The study of the effect of the number of assembled layers and the effect of molecular weight of the assembled polymers on the release profile of the drug revealed that a high molecular weight of the assembled polymers and an optimum number of layers gave a very slow sustained release. Encapsulation of the drugs, positive results of the cytotoxicity studies of the



halloysite, and other biomedical applications of halloysite shown by using halloysite as a nanoreactor for synthesizing silver nanoparticles shows that halloysite as a prospective biomaterial for novel formulation of controlled release of drugs.

### **Future Work**

Several things can be done in the future to further build upon the obtained results.

Further studies need to be done to advance this development such as:

- Use of other types of drugs and proteins for encapsulation and sustained release using alginate nanoparticle matrix;
- Application of LbL assembly using various polymers on the drug-loaded alginate nanoparticles as an additional step of control for drug diffusion;
- Elaboration of the drug-loading study of halloysite for application in wound healing and cosmetics and extension of loading and release to other class of compounds like protein, corrosion inhibitors, etc.
- Analysis of the reaction at the tube openings between releasing polycations and polyanions in the bulk solution for the formation of stoppers at the tube ends, which helps in achieving tunable controlled release of active ingredients. For example, magnetic stoppers can help us in making magnetic actuated release.
- Loading tubules with nanoparticles (gold, silica) with diameter corresponding to the lumen diameter. Location of these nanoparticles in the tubes with the help of TEM. Using this approach to reach slow and controllable drug release. Comparison results with release for untreated tubules.
- Forming decorative mixture of nanotubules (Carbon nanotube & Halloysite) for novel applications.

- Modeling and simulation studies for understanding the drug release kinetics from halloysite.

## REFERENCES

1. Couvreur, P.; Dubernet, C.; Puisieux, F., Controlled Drug Delivery with Nanoparticles: Current Possibilities and Future Trends. *European Journal of Pharmaceutics and Biopharmaceutics* **1995**, 41, 2-13.
2. Reis, C. P.; Neufeld, R. J.; Ribeiro, A. J.; Veiga, F., Nanoencapsulation I. Methods for Preparation of Drug-Loaded Polymeric Nanoparticles. *Nanomedicine: Nanotechnology, Biology and Medicine* **2006**, 2, 8-21.
3. Colombo, P., Encyclopedia of Controlled Drug Delivery, ed. E. Mathiowitz. *Mucosal Drug Delivery* **1999**, New York: John Wiley & Sons, Inc.
4. Narayani, R., Polymeric Delivery Systems in Biotechnology: A Mini Review. *Trends in Biomaterials and Artificial Organs* **2007**, 21, (1), 14-19.
5. Jayanth, P.; Zhong Z. W.; Prabha, S.; Sahoo, S.K; Labhasetwar, V., Rapid Endo-lysosomal Escape of poly(DL-lactide-Co-glycolide) nanoparticles : Implications for Drug and Gene Delivery *Journal of the Federation of American Societies for Experimental Biology* **1995**, 16, 1217-1226.
6. Aoyama, T.; Yamamoto, S.; Kanematsu, A.; Ogawa, O.; Tabata, Y., Local Delivery of Matrix Metallo Proteinase Gene Prevents the Onset of Renal Sclerosis in Streptozoin Induced Diabetic Mice, *Tissue Engineering* **2003**, 9, 1289-1299.
7. Gabizon, A.; Goren, D.; Cohen, R.; Barenholz, Y., Development of Liposomal Anthracyclines: from Basics to Clinical applications. *Journal of Controlled Release* **1998**, 53, 275-279.
8. Aliabadi, H. M.; Lavasanifar, A., Hirsch, L. R.; Jackson, J. B.; Lee, A.; Halas, N. J.; West, J. L., Polymeric micelles for drug delivery. *Expert Opinion on Drug Delivery* **2006**, 3, 139-162.
9. Nishiyama, N.; Kataoka, K., Current state, Achievements, and Future Prospects of Polymeric Micelles as Nanocarriers for Drug and Gene Delivery . *Pharmacology and Therapeutics* **2006**, 112, 630-648.
10. Geng, Y.; Dalhaimer, P.; Cai, S.; Tsai, R.; Tewari, M; Minko, T.; Discher, D. E., Shape Effects of Filaments Versus Spherical Particles in Flow and Drug Delivery. *Nature Nanotechnology* **2007**, 2, 249-255.

11. Al-Tahami, K.; Singh, J., Smart Polymer Based Delivery System for Peptides and Proteins. *Recent Patent on Drug Delivery & Formulation* **2007**, 1, (1), 65-71.
12. Ravi Kumar, M. N. V., Nano and Microparticles as Controlled Drug Delivery Devices. *Journal of Pharmacy and Pharmaceutical Science* **2000**, 3, (2), 234-258.
13. Sheridan, M. H.; Shea, L. D.; Peters, M. C.; Mooney, D. J., Bioadsorbable Polymer Scaffolds for Tissue Engineering Capable of Sustained Growth Factor Delivery. *Journal of Controlled Release* **2000**, 64, 91-102.
14. Chang, S. C. N.; Rowley, J. A.; Tobias, G.; Genes, N. G.; Roy, A. K.; Mooney, D. J.; Vacanti, C. A.; and Bonassar, L. J., Injection Molding of Chondrocyte/Alginate Constructs in the Shape of Facial Implants. *Journal of Biomedical Materials Research* **2001**, 55, 503-511.
15. Draget, K. I.; Smidsrod, O.; Skjak-Braek, G., *Alginates from algae*. In *Biopolymers*. ed. E. Vandamme, S. De Baets, A. Steinbüchel., Wiley-VCH Verlag GmbH. 215-244.
16. Takka, S.; Acarturk, F., Calcium Alginate Microparticles for Oral Administration : I: Effect of Sodium Alginate type on Drug Release and Drug Entrapment Efficiency. *Journal of Microencapsulation* **1999**, 16, (3), 275-290.
17. Morch, Y. A.; Donati, I.; Strand, B. L.; Skjak-Braek, G., Effect of Ca<sup>2+</sup>, Ba<sup>2+</sup>, and Sr<sup>2+</sup> on Alginate Microbeads. *Biomacromolecules* **2006**, 7, 1471-1480.
18. Brayner, R.; Vaulay, M. J.; Fievet, F.; Coradin, T., Alginate-Mediated Growth of Co, Ni, and CoNi Nanoparticles: Influence of Biopolymer Structure. *Chemistry of Materials* **2007**, 19, (5), 1190-1198.
19. Lamelas, C.; Avaltroni, F.; Benedetti, M.; Wilkinson, K. J.; Slaveykova, V. I., Quantifying Pb and Cd Complexation by Alginates and the Role of Metal Binding on Macromolecular Aggregation. *Biomacromolecules* **2006**, 6, (5), 2756-2764.
20. Baruck, L.; Machluf, M., Alginate-Chitosan Complex Coacervation for Cell Encapsulation: Effect on Mechanical Properties and on Long-term Viability. *Biopolymer* **2006**, 82, (6), 570-579.
21. Wong, T. W.; Chan, L. W.; Kho, S. B.; Heng, P. W. S., Aging and Microwave Effects on Alginate/Chitosan Matrices. *Journal of Controlled Release* **2005**, 104, (3), 461-475.
22. Filipovic-Grcic, J.; Maysinger, D.; Zoic, B.; Jalsenjak, I., Macromolecular prodrugs. IV. Alginate-Chitosan Microspheres of PHEA-L-dopa Adduct. *International Journal of Pharmaceutics* **1995**, 116, (1), 39-44.

23. Tay, L. F.; Khoh, L. K.; Loh, C. S.; Khor, E., Alginate-chitosan coacervation in production of artificial seeds. *Biotechnology and Bioengineering* **1993**, 42, (4), 449-454.
24. Douglas, K. L.; Tabrizian, M. J., New Approach to the Preparation of Alginate-Chitosan Nanoparticles as Gene Carriers - Part I: Effect of Experimental Parameters on Particle Formation. *Journal of Biomaterial Science and Polymer Edition* **2005**, 16, (1), 43-56.
25. Sarmento, S.; Ribeiro, A.; Veiga, F.; Sampaio, P.; Neufeld, R.; Ferreira, D., Alginate-Chitosan Nanoparticles are Effective for Oral Insulin Delivery. *Pharmaceutical Research* **2007**, 24, 2198-2206.
26. Abe, M.; Tanaka, K.; Nakayama, A.; Kondo, T.; Tsuchiya, K.; Tantayakom, V.; Ohkubo, T.; Sakai, H., Preparation of Nanocapsules with Alginate/Polylysine Complex Wall. *Journal of Oleo Science* **2006**, 55, (12), 615-621.
27. Lin, H. R.; Sung, K. C.; Vong, W. J., In Situ Gelling of Alginate/Pluronic Solutions for Ophthalmic Delivery of Pilocarpine. *Biomacromolecules* **2004**, 5, (6), 2358-2365.
28. Cathell, M. D.; Shauer, C. L., Structurally Colored Thin Films of Ca<sup>2+</sup>-cross-linked Alginate. *Biomacromolecules* **2007**, 8, (1), 33-41.
29. Qurat-ul-Ain.; Sharma, S; Khuller, G. K.; Garg, S. K., Alginate-based Oral Drug Delivery System for Tuberculosis: Pharmacokinetics and Therapeutic Effect. *Journal of Antimicrobial Chemotherapy* **2003**, 51, 931-938.
30. Qi, H.; Hu, P.; Xu, J.; Wang, A., Encapsulation of Drug Reservoirs in Fibers by Emulsion Electrospinning: Morphology Characterization and Preliminary Release Experiment. *Biomacromolecules* **2006**, 7, (8), 2327-2330.
31. Liu, Z. M.; Becker, T.; Neufeld, R. J., Spherical Alginate Granules Formulated for Quick-Release Active Subtilisin. *Biotechnology Progress* **2005**, 21 (2), 568-574.
32. Pinto, R. C.; Ribeiro, A. J.; Neufeld, R. J.; Veiga, F., Alginate Microparticles as Novel Carrier for Oral Insulin Delivery. *Biotechnology and Bioengineering* **2007**, 96, (5), 977-989.
33. Zhu, H.; Srivastava, R.; McShane, M. J., Spontaneous Loading of Positively Charged Macrocapsules into Alginate-Templated Polyelectrolyte Multilayer Microcapsules. *Biomacromolecules* **2005**, 6, (4), 2221-2228.
34. Zhu, H.; Srivastava, R.; Brown, J. Q.; McShane, M. J., Combined Physical and Chemical Immobilization of Glucose Oxidase in Alginate Microspheres Improves Stability of Encapsulation and Activity. *Bioconjugate Chemistry* **2005**, 16, (6), 1451-1458.

35. Brown, J. Q.; Srivastava, R.; McShane, M. J.; Encapsulation of Glucose Oxidase and an Oxygen-Quenched Fluorophore in Polyelectrolyte-Coated Calcium Alginate Microspheres as Optical Glucose Sensor Systems. *Biosensors and Bioelectronics* **2004**, 21, 212-216.
36. Zahoor, A.; Sharma, S.; Khuller, G. K., Inhalable Alginate Nanoparticles as Antitubercular Drug Carriers against Experimental Tuberculosis. *International Journal of Antimicrobial Agents* **2005**, 26, (4), 298-303.
37. Quong, D.; Neufeld, R. J.; Skjak-Braek, G.; Poncelet, D., External versus Internal Source of Calcium during the Gelation of Alginate Beads for DNA Encapsulation. *Biotechnology and Bioengineering* **1998**, 57, (4), 438-446.
38. Chan, L.W.; Lee, H.Y.; Heng, P. N. S., Production of Alginate Microspheres by Internal Gelation using an Emulsification Method. *International Journal of Pharmaceutics* **2002**, 242, (1), 259-262.
39. Johansen, A.; Flink, J. M., A New Principle for Immobilized Yeast Reactors Based on Internal Gelation of Alginate. *Biotechnology Letters* **1986**, 8, (2), 121-126.
40. Seifert, D. B.; Phillips, J. A., Porous Alginate-Poly(ethylene glycol) Entrapment System for the cultivation of Mammalian cells. *Biotechnology Progress* **1997**, 13, (5), 569-576.
41. Ho, J.; Neufeld, R., Retention and release of low molecular weight DNA from alginate beads. *S.T.P. Pharma Sciences* **2001**, 11, 109-115.
42. Gu, F.; Amsden, B.; Neufeld, R., Sustained Delivery of Vascular Endothelial Growth Factor with Alginate Beads. *Journal of Controlled Release* **2004**, 96, 463-472.
43. Murata, Y.; Nakada, K.; Miyamoto, E.; Kawashima, S.; Seo, S.H., Influence of Erosion of Calcium-Induced Alginate Gel Matrix on the Release of Brilliant Blue. *Journal of Controlled Release* **1993**, 23, 21-26.
44. Kikuchi, A.; Kawabuchi, M.; Sugihara, M.; Sakurai, Y.; Okano, T., Pulsed Dextran Release from Calcium-Alginate Gel Beads. *Journal of Controlled Release* **1997**, 47, 21-29.
45. Chretien, C.; Boudy, V.; Allain, P.; Chaumeil, J. C., Indomethacin Release from Ion-Exchange Microspheres: Impregnation with Alginate Reduces Release Rate. *Journal of Controlled Release* **2004**, 96, 369-378.
46. Kwok, K. K.; Groves, M. J.; Burgess, D. J., Production of 5-15  $\mu\text{m}$  Diameter Alginate-polylysine Microcapsules by an Air Atomization Technique. *Pharmaceutical Research* **1991**, 8, 341 - 344.

47. Chretien, C.; Chaumeil, J. C., Release of a Macromolecular Drug from Alginate-Impregnated Microspheres. *International Journal of Pharmaceutics* **2005**, 304, 18-28.
48. Bates, T.; Hildebrand, F.; Swineford, A., Morphology and Structure of Endellite and Halloysite. *American Mineralogist* **1950**, 35, 463-484.
49. Price, R.; Gaber, B.; Lvov, Y., In-vitro Release Characteristics of Tetracycline HCl, Khellin and Nicotinamide adenine dinucleotide from Halloysite; A Cylindrical Mineral. *Journal of Microencapsulation* **2001**, 18, 713-722.
50. Tari, G.; Bobos, I.; Gomes, C. S. F.; Ferreira, J. M. F., Modification of Surface Charge Properties during Kaolinite to Halloysite – 7A Transformation. *Journal Colloids and Interface Science* **1999**, 210, 360-366.
51. Joussein, E.; Petit, S.; Churchman, J.; Theng, B.; Righi, D.; Delvaux, B., Halloysite Clay Minerals – A Review. *Clay minerals* **2005**, 40, 383-426.
52. Lu, Z.; Eadula, S.; Zheng, Z.; Xu, K.; Grozdits, G.; Lvov, Y., Layer – by – layer Nanoparticle Coatings on Lignocellulose Wood Microfibers. *Colloids and Surfaces A: Physicochemical and Engineering Aspects* **2007**, 292, 56-62.
53. Baral, S.; Brandow, S.; Gaber, B., Electroless Metalization of Halloysite, a Hollow Cylindrical 1:1 Aluminosilicate of Submicron Diameter. *Chemistry of Materials* **1993**, 5, 1227-1232.
54. Wilson, I. R., Kaolin and Halloysite deposits of China. *Clay minerals* **2004**, 39, 1-15.
55. Levis, S. R.; Deasy, P. B., Characterization of Halloysite for use as a Microtubular Drug Delivery System. *International Journal of Pharmaceutics* **2002**, 243, 125-134.
56. Kelly, H. M.; Deasy, P. B.; Zaika, E.; Claffey, N., Formulation and Preliminary in vivo Dog Studies of a Novel Drug Delivery System for the Treatment of Periodontitis. *International Journal of Pharmaceutics* **2004**, 274, 167-183.
57. Bougeard, D.; Smirnov, K. S.; Geidel, E., Vibrational Spectra and Structure of Kaolinite: A Computer Simulation Study. *Journal of Physical Chemistry B* **2000**, 104, 9210-9217.
58. Carr, R. M.; Chaikum, N.; Patterson, N., Intercalation of Salts in Halloysite. *Clay and Clay minerals* **1978**, 26, 144-152.
59. Hiller, S.; Ryan, P. C., Identification of Halloysite (7A) by Ethylene Glycol Salvation: the ‘MacEvan effect’. *Clay minerals* **2002**, 37, 487-496.

60. Joussein, E.; Petit, S.; Delvaux, B., Behavior of Halloysite clay under Formamide Treatment. *Applied Clay Science* **2007**, 35, 17-24.
61. Batchelor, G. K., *An Introduction to Fluid Dynamics*. **2000**, Cambridge University Press.
62. Antill, S. J., Halloysite: A Low-Cost Alternative Nanotube. *Australian Journal of Chemistry*, **2003**, 56, 723.
63. Levis, S. R.; Deasy, P. B., Use of Coated Microtubular Halloysite for the Sustained Release of Diltiazem Hydrochloride and Propranolol Hydrochloride. *International Journal of Pharmaceutics* **2003**, 253, 145-157.
64. Kutsuna, S.; Ibusuki, T.; Takeuchi, K., Heterogenous Photoreaction of Tetrachloroethene – Air Mixture on Halloysite Particles. *Environmental Science and Technology* **2000**, 34, 2484-2489.
65. Schukin, D. G.; Sukhorukov, G. B.; Price, R. R.; Lvov, Y. M., Halloysite Nanotubes as Biomimetic Nanoreactors. *Small* **2005**, 1, 510 – 513.
66. Lvov, Y.; Price, R.; Gaber, G.; Ichinose, I., Thin film nanofabrication via layer-by-layer adsorption of tubule halloysite, spherical silica, proteins and polycations. *Colloids and Surfaces A: Physicochemical and Engineering Aspects* **2002**, 198, 375-382.
67. Reis, C. P.; Neufeld, R. J.; Ribeiro, A. J.; Veiga, F., Nanoencapsulation I. Methods for preparation of drug-loaded polymeric nanoparticles. *Nanomedicine: Nanotechnology, Biology, and Medicine* **2006**, 2, 8-21.
68. Maier, S. A.; Kik, P. G.; Atwater, H. A.; Meltzer, S.; Harel, E.; Koel, B. E.; Requicha, A. A. G., Local Detection of Electromagnetic Energy Transport Below the Diffraction Limit in Metal Nanoparticle Plasmon Waveguides. *Nature Materials* **2003**, 2, 229-232.
69. Sershen, S. R.; Westcott, S. L.; Halas, N. J.; West, J. L., Temperature-Sensitive Polymer-Nanoshell Composites for Photothermally Modulated Drug Delivery. *Journal of Biomedical Materials Research* **2000**, 51, (3), 293-298.
70. Mie, G., Beiträge zur Optik Trüber Medien, Speziell Kolloidaler Metallösungen. *Annalen der Physik* **1908**, 330, (3), 377-445.
71. Kreibig, U.; Vollmer, M., *Optical Properties of Metal Clusters*. Springer: 1995; p 552.
72. Oldenburg, S. J.; Averitt, R. D.; Westcott, S. L.; Halas, N. J., *Chemistry Physical Letters* **1995**, 288, 243-247.



73. Prodan, E.; Lee, A.; Nordlander, P., The Effect of a Dielectric Core and Embedding Medium on the Polarizability of Metallic Nanoshells. *Chemical Physics Letters* **2002**, 360, (3-4), 325-332.
74. Hirsch, L. R.; Jackson, J. B.; Lee, A.; Halas, N. J.; West, J. L., A Whole Blood Immunoassay Using Gold Nanoshells. *Analytical Chemistry* **2003**, 75, (10), 2377-2381.
75. Ai, H.; Jones, S. A.; Lvov, Y. M., Biomedical Applications of Electrostatic Layer-by-Layer Nano-Assembly of Polymers, Enzymes and Nanoparticles. *Cell Biochemistry and Biophysics* **2003**, 39, (1), 23-43.
76. Lvov, Y.; Decher, G.; Möhwald, H., Assembly, Structural Characterization, and Thermal Behavior of Layer-by-Layer Deposited Ultrathin Films of Poly(vinyl sulfate) and Poly(allylamine). *Langmuir* **1993**, 9, (2), 481-486.
77. Decher, G., Fuzzy Nanoassemblies: Toward Layered Polymeric Multicomposites. *Science* **1997**, 277, (5330), 1232-1237.
78. Lvov, Y.; Ariga, K.; Ichinose, I.; Kunitake, T., Assembly of Multicomponent Protein Films by Means of Electrostatic Layer-by-Layer Adsorption. *Journal of the American Chemical Society* **1995**, 117, (22), 6117-6123.
79. Lvov, Y. M.; Caruso, F., Biocolloids with Ordered Urease Multilayer Shells as Enzymatic Reactors. *Analytical Chemistry* **2001**, 73, (17), 4212-4217.
80. Tieke, J. B.; van Ackern, F.; Krasemann, L.; Toutianoush, A., Ultrathin Self-Assembled Polyelectrolyte Multilayer Membranes. *European Physical Journal E* **2001**, 5, (1), 29-39.
81. Iler, R. K., Multilayers of Colloidal Particles. *Journal of Colloidal Science* **1966**, 21, (6), 569-594.
82. Ai, H.; Jones, S. A.; de Villiers, M. M.; Lvov, Y. M., Nano-Encapsulation of Furosemide Microcrystals for Controlled Drug Release. *Journal of Controlled Release* **2003**, 86, (1), 59-68.
83. Sukhorukov, G. B.; Donath, E.; Davis, S.; Lichtenfeld, H.; Caruso, F.; Popov, V. I.; Möhwald, H., Stepwise Polyelectrolyte Assembly on Particle Surfaces: A Novel Approach to Colloid Design. *Polymers for Advanced Technologies* **1998**, 9, (10-11), 759-767.
84. Antipov, A. A.; Sukhorukov, G. B.; Donath, E.; Möhwald, H., Sustained Release Properties of Polyelectrolyte Multilayer Capsules. *Journal of Physical Chemistry B* **2001**, 105, (12), 2281-2284.

85. Suzuki, I.; Ishizaki, T.; Ihoue, H.; Anzai, J.-i., Modification of Polyelectrolyte Layered Assembly Using an Active Ester of Azobenzene Carboxylate. *Macromolecules* **2002**, 35, (16), 6470-6474.
86. Yoo, D.; Shiratori, S. S.; Rubner, M. F., Controlling Bilayer Composition and Surface Wettability of Sequentially Adsorbed Multilayers of Weak Polyelectrolytes. *Macromolecules* **1998**, 31, (13), 4309-4318.
87. Schlenoff, J. B.; Dubas, S. T., Mechanism of Polyelectrolyte Multilayer Growth: Charge Overcompensation and Distribution. *Macromolecules* **2001**, 34, (3), 592-598.
88. Harris, J. J.; Stair, J. L.; Bruening, M. L., Layered Polyelectrolyte Films as Selective, Ultrathin Barriers for Anion Transport. *Chemistry Materials* **2000**, 12, (7), 1941-1946.
89. Lvov, Y. M.; Lu, Z.; Schenkman, J. B.; Zu, X.; Rusling, J. F., Direct Electrochemistry of Myoglobin and Cytochrome P450<sub>cam</sub> in Alternate Layer-by-Layer Films with DNA and Other Polyions. *Journal of the American Chemical Society* **1998**, 120, (17), 4073-4080.
90. Donath, E.; Sukhorukov, G. B.; Caruso, F.; Davis, S. A.; Möhwald, H., Novel Hollow Polymer Shells by Colloid-Templated Assembly of Polyelectrolytes. *Angewandte Chemie - International Edition* **1998**, 37, (16), 2201-2205.
91. Antipov, A. A.; Sukhorukov, G. B.; Fedutik, Y. A.; Hartmann, J.; Giersig, M.; Möhwald, H., Fabrication of a Novel Type of Metallized Colloids and Hollow Capsules. *Langmuir* **2002**, 18, (17), 6687-6693.
92. Dähne, L.; Leporatti, S.; Donath, E.; Möhwald, H., Fabrication of Micro Reaction Cages with Tailored Properties. *Journal of the American Chemical Society* **2001**, 123, (23), 5431-5436.
93. Ai, H.; Fang, M.; Jones, S. A.; Lvov, Y. M., Electrostatic Layer-by-Layer Microtemplates: Platelets. *Biomacromolecules* **2002**, 3, (3), 560-564.
94. Sukhorukov, G., *Novel Methods to Study Interfacial Layers*. Elsevier Science: 2001; p 536.
95. Ibarz, G.; Dähne, L.; Donath, E.; Möhwald, H., Smart Micro- and Nanocontainers for Storage, Transport, and Release. *Advanced Materials* **2001**, 13, (17), 1324-1327.
96. Mendelsohn, J. D.; Barrett, C. J.; Chan, V. V.; Pal, A. J.; Mayes, A. M.; Rubner, M. F., Fabrication of Microporous Thin Films from Polyelectrolyte Multilayers. *Langmuir* **2000**, 16, (11), 5017-5023.

97. Antipov, A. A.; Sukhorukov, G. B.; Leporatti, S.; Radtchenko, I. L.; Donath, E.; Möhwald, H., Polyelectrolyte Multilayer Capsule Permeability Control. *Colloids and Surfaces A: Physicochemical and Engineering Aspects* **2002**, 198-200, 535-541.
98. Tiourina, O. P.; Antipov, A. A.; Sukhorukov, G. B.; Larionova, N. I.; Lvov, Y.; Möhwald, H., Entrapment of  $\alpha$ -Chymotrypsin into Hollow Polyelectrolyte Microcapsules. *Macromolecular Bioscience* **2001**, 1, (5), 209-214.
99. Lvov, Y.; Antipov, A. A.; Mamedov, A.; Möhwald, H.; Sukhorukov, G. B., Urease Encapsulation in Nanoorganized Microshells. *Nano Letters* **2001**, 1, (3), 125-128.
100. Radtchenko, I. L.; Sukhorukov, G. B.; Möhwald, H., A Novel Method for Encapsulation of Poorly Water-Soluble Drugs: Precipitation in Polyelectrolyte Multilayer Shells. *International Journal of Pharmaceutics* **2002**, 242, (1-2), 219-223.
101. Sukhorukov, G. B.; Antipov, A. A.; Voigt, A.; Donath, E.; Möhwald, H., pH-Controlled Macromolecule Encapsulation in and Release from Polyelectrolyte Multilayer Nanocapsules. *Macromolecular Rapid Communications* **2001**, 22, (1), 44-46.
102. Antipov, A. A.; Sukhorukov, G. B.; Möhwald, H., Influence of the Ionic Strength on the Polyelectrolyte Multilayers' Permeability. *Langmuir* **2003**, 19, (6), 2444-2448.
103. Sukhorukov, G. B.; Donath, E.; Moya, E.; Susha, S.; Voigt, A.; Hartmann, A.; Möhwald, H., Microencapsulation by Means of Step-Wise Adsorption of Polyelectrolytes. *Journal of Microencapsulation* **2000**, 17, (2), 177-185.
104. Antipov, A. A.; Sukhorukov, G. B., Polyelectrolyte Multilayer Capsules as Vehicles with Tunable Permeability. *Advances in Colloid and Interface Science* **2004**, 111, (1-2), 49-61.
105. Ghan, R.; Shutava, T.; Patel, A.; John, V. T.; Lvov, Y., Enzyme-Catalyzed Polymerization of Phenols within Polyelectrolyte Microcapsules. *Macromolecules* **2004**, 37, (12), 4519-4524.
106. Shutava, T.; Zheng, Z.; John, V.; Lvov, Y., Microcapsule Modification with Peroxidase-Catalyzed Phenol Polymerization. *Biomacromolecules* **2004**, 5, (3), 914-921.
107. Sano, M.; Lvov, Y. M.; Kunitake, T., Formation of Ultrathin Polymer Layers on Solid Substrates by Means of Polymerization-Induced Epitaxy and Alternate Adsorption. *Annual Review of Materials Science* **1996**, 26, 153-187.

108. Lvov, Y. M.; Ariga, K.; Kunitake, T., Layer-by-Layer Assembly of Alternate Protein/Polyion Ultrathin Films. *Chemistry Letters* **1994**, 23, (12), 2323-2326.
109. Shutava, T.; Prouty, M. D.; Kommireddy, D.; Lvov, Y. M., pH Responsive Decomposable Layer-by-Layer Nanofilms and Capsules on the Basis of Tannic Acid. *Macromolecules* **2005**, 38, (7), 2850-2858.
110. Pargaonkar, N.; Lvov, Y. M.; Li, N.; Steenekamp, J. H.; de Villiers, M. M., Controlled Release of Dexamethazone from Microcapsules Produced by Polyelectrolyte Layer-by-Layer Nanoassembly. *Pharmaceutical Research* **2005**, 22, (5), 826-835.
111. Lvov, Y. M.; Ariga, K.; Onda, M.; Ichinose, I.; Kunitake, T., A Careful Examination of the Adsorption Step in the Alternate Layer-by-Layer Assembly of Linear Polyanion and Polycation. *Colloids and Surfaces A: Physicochemical and Engineering Aspects* **1999**, 146, (1-3), 337-346.
112. Lvov, Y.; Munge, B.; Giraldo, O.; Ichinose, I.; Suib, S. L.; Rusling, J. F., Films of Manganese Oxide Nanoparticles with Polycations or Myoglobin from Alternate-Layer Adsorption. *Langmuir* **2000**, 16, (23), 8850-8857.
113. Onda, M.; Lvov, Y. M.; Ariga, K.; Kunitake, T., Sequential Reaction and Product-Separation on Molecular Films of Glucoamylose and Glucose Oxidase Assembled on an Ultrafilter. *Journal of Fermentation and Bioengineering* **1996**, 82, (5), 502-506.
114. Hoogeveen, N. G.; Stuart, M. A. C.; Fler, G. J.; Böhmer, M. R., Formation and Stability of Multilayers of Polyelectrolytes. *Langmuir* **1996**, 12, (15), 3675-3681.
115. Santiago, I.; Pereyra, C.; Ariza, M. R.; de la Ossa E. M., Ethanol + 2-Methyl-1-butanol + Calcium Chloride System: Vapor-Liquid Equilibrium Data and Correlation Using the NRTL Electrolyte Model. *Journal of Chemical and Engineering Data* **2007**, 52, 458.
116. Lvov, Y. M., *Handbook of Surface and Interfaces of Materials: Nanostructured Materials*. Ed H. Nalwa, Chapter 4, Academic Press, New York, **2001**, 170-189.
117. Kommireddy, D. S.; Ichinose, I.; Lvov, Y. M.; Mills, D. K., Nanoparticle Multilayers: Surface Modification for Cell Attachment and Growth. *Journal of Biomedical Nanotechnology* **2005**, 1, (4), 286-290.
118. Berg, C. M.; Zhai, L.; Cohen, R. E.; Rubner, M. F., Controlled Drug Release from Porous Polyelectrolyte Multilayers. *Biomacromolecules* **2006**, 7, 357-364.
119. Peppas, N. A., Analysis of Fickian and non-Fickian Drug Release from Polymers. *Pharmaceutica Acta Helveticae* **1985**, 60, 110-111.

120. Roy, I.; Ohulchanskyy, T. Y.; Pudavar, H. E.; Bergey, E. A.; Oseroff, A. R.; Morgan, J.; Dougherty, T. J.; Prasad, P. N., Ceramic-Based Nanoparticles Entrapping Water-Insoluble Photosensitizing Anticancer Drugs: A Novel Drug-Carrier System for Photodynamic Therapy. *Journal of American Chemical Society* **2003**, *125*, 7860-7865.
121. Brigger, I.; Dubernet, C.; Couvreur, P., Nanoparticles in Cancer Therapy and Diagnosis. *Advanced Drug Delivery Reviews* **2002**, *54*, 631-651.
122. Crommelin, D. J.; Storm, G.; Jiskoot, W.; Stenekes, R.; Mastrobattista, E.; Hennink, W. E., Nanotechnological Approaches for the Delivery of Macromolecules. *Journal of Controlled Release* **2003**, *87*, 81-88.
123. Veerabadran, N. G.; Price, R. R.; Lvov, Y. M., Clay Nanotubes for Encapsulation and Sustained Release. *NANO* **2007**, *2*, (2), 115-120.
124. Shchukin, D.; Mohwald, H., Surface-Engineered Nanocontainers for Entrapment of Corrosion Inhibitors. *Advanced Functional Materials* **2007**, *17*, 1451-1458.
125. Okubo, T.; Suda, M., Alternate Sign Reversal in the  $\zeta$  Potential and Synchronous Expansion and Contraction in the Absorbed Multi-Layers of Poly(4-vinyl-*N-n*-butylpyridinium bromide) Cations and Poly(styrene sulfonate) Anions on Colloidal Silica Spheres. *Colloid Polymer Science* **1999**, *277*, (9), 813-817.
126. Jena, P.; Khanna, S. N.; Rao, B. K., Role of Interface on the Properties of Cluster Assemblies. *Journal of Cluster Science* **2001**, *12*, 443-456.
127. Alivisatos, A.P., Semiconductor Clusters, Nanocrystals, and Quantum Dots. *Science* **1996**, *271*, 933-937.
128. Joly, S.; Kane, R.; Radzilowski, L.; Wang, T.; Wu, A.; Cohen, R. E.; Thomas, E. L.; Rubner, M. F., Multilayer Nanoreactors for Metallic and Semiconducting Particles. *Langmuir* **2000**, *16*, 1354-1359.
129. Morones, J. R.; Elechiguerra, J. L.; Camacho, A.; Holt, K.; Kouri, J. B.; Ramirez, J. T.; Yacaman, M. J., The bactericidal effect of silver nanoparticles. *Nanotechnology* **2005**, *16*, 2346-2353.
130. Eby, D. M.; Luckarift, H. R.; Johnson, G. R. AIChe National meeting Salt lake city, Utah. *Topical 8 - Bionanotechnology* **2007**, 637.
131. Kalenczuk, R. J.; Borowiak-Palen, E.; Ruemmelli, M. H.; Gemming, T.; Pichler, T., Synthesis and Characterization of Silver Filled Single-Wall Carbon nanotubes. *Reviews on Advance Materials Science* **2006**, *12*, 78-83.
132. Fu, Y.; Zhang, L.; Zheng, J., In-Situ Deposition of Pd Nanoparticles on Tubular Halloysite Template for Initiation of Metallization. *Journal of Nanoscience and Nanotechnology* **2005**, *5*, (4), 558-574.

## VITA

Nalinkanth Ghone Veerabadran received his Bachelors of Technology degree in Chemical engineering from Coimbatore Institute of Technology (affiliated to Bharathiyar University) in 2000. In his first year of the course, an international conference on biomedical engineering – INCONBME '96 was held; it allured him to the challenges offered by the human body for engineering community. During his undergraduate work he took some special interests in germane subjects like transport phenomena, reaction engineering and process modeling. After graduating with his Bachelors degree, his quest for practical experience ended with Reliance Industries limited, the largest private sector company in India. His assignments over there helped him to understand the difficulties faced during scaling up of pilot plant, the significance of time management and the amount of proactive care to be taken whenever we do an activity for the first time.

Having gained the necessary engineering fundamentals and its application in a chemical industry, Mr. Veerabadran was confident that similar practice is possible in the field of biomedical engineering. He resigned his professional career in chemical industry and enrolled himself in the biomedical engineering PhD program at Louisiana Tech University. His graduate research work was focused on nanoengineering templates for controlled delivery of bioactive agents under Dr Yuri M. Lvov. He has also pursued student research participation program at United States Air Force Research Laboratory (USAFRL), which is administered by Oak ridge institute of science and education

(ORISE). Nalinkanth Ghone Veerabadran, along with his colleagues, successfully transformed one of his research topics, layer-by-layer self-assembly on pulp fibers, into a small company, Better Paper Technologies, LLC. This company was placed second in a university sponsored business plan competition.

Mr. Veerabadran has had many publications and attended many conferences throughout his graduate studies. His publications and other works are listed here.

### **Peer-Reviewed Journals**

**Nalinkanth G. Veerabadran**, Ronald R. Price, Yuri M. Lvov, “Layer by Layer formulated clay composites for controlled release of drugs”, manuscript in preparation, **2008**.

Shantanu S. Balkundi, **Nalinkanth G. Veerabadran**, Yuri M. Lvov, G. Johnson, M. Eby, “Microbial Spore encapsulation by Layer by layer assembly”, manuscript in preparation, **2008**.

**Nalinkanth G. Veerabadran**, Poorna L. Goli, Skylar S. Stewart-Clark, Yuri M. Lvov, David K. Mills, “Nanoencapsulation of Stem Cells within Polyelectrolyte Multilayer Shell”, *Journal of Macromolecular Bioscience*, 7(7), July **2007**, 877-882.

**Nalinkanth G. Veerabadran**, Ronald R. Price, Yuri M. Lvov, “Clay Nanotubes for Encapsulation and Sustained Release of Drugs”, *NANO*, 2(2), April **2007**, 115-120

### **Conference Proceedings**

**Nalinkanth G. Veerabadran**, Ronald R. Price, Yuri M. Lvov, “Tubule Clay Nanoreactor for Template Synthesis of Silver Nanoparticles”, submitted to 236th ACS National meeting, PA, *Polymeric Materials: Science & Engineering division*, August **2008**.

Shantanu S. Balkundi, **Nalinkanth G. Veerabadran**, Glenn Johnson, M. Eby, Yuri M. Lvov, “Nanoshells on Microbial Spores through polyelectrolyte LbL assembly”, submitted to 236th ACS National meeting, PA, *Polymeric Materials: Science & Engineering division*, August **2008**.

### Conference Talks

**Nalinkanth G. Veerabadrán**, Elshad A. Abdullayev, Shantanu S. Balkundi, Ronald R. Price, Yuri M. Lvov, "Tunable Controlled Release of Active Agents from Tubular Nano Clay", *International Union of Materials Research Societies- 10th International Conference on Advanced Materials (IUMRS-ICAM)*, Bangalore, India, Oct 2007.

### Conference Posters

Shantanu S. Balkundi, **Nalinkanth G. Veerabadrán**, Yuri M. Lvov, Glenn Johnson, Matthew Eby, "Nanoorganised Polyelectrolyte Shells on Microbial Spores", *HSEMB - 25<sup>th</sup> annual meeting*, Houston, TX, 7<sup>th</sup>-8<sup>th</sup> Feb 2008.

Elshad A. Abdullayev, **Nalinkanth G. Veerabadrán**, Yuri M. Lvov, Dmitry Fix, Dmitry Shchukin, "Anticorrosion Coatings for Metals using Nanotubular Clay Composite", *The Waterborne Symposium - 35th Annual international symposium on advances in sustainable coating technologies*, New Orleans, LA, 30th Jan- 1st Feb 2008.

Yuri M. Lvov, **Nalinkanth G. Veerabadrán**, Shantanu Balkundi, "Biomimetic Nanoassembly for Protein and Drug Encapsulation", *ACS Conference: Macromolecules for a Safe, Sustainable and Healthy World*, 2nd Strategic Polymer Symposium, New York, NY, 10th-13th June 2007.

Aadel A. Darrat, **Nalinkanth G. Veerabadrán**, Shantanu S. Balkundi, Yuri M. Lvov, "Nanoengineered halloysite tubules for controlled release of drugs and proteins", *233rd ACS National meeting*, Chicago, IL, 25th-29th March 2007.

**Nalinkanth G. Veerabadrán**, Yuri M. Lvov, "Clay Nanotubes for Encapsulation and Sustained Release of Bioactive Agents", *Seventh Louisiana Materials and Emerging Technologies Conference*, Baton Rouge, LA, 23rd – 24th October 2006.

**Nalinkanth G. Veerabadrán**, Shantanu S. Balkundi, Yuri M. Lvov, "Halloysite Clay as Tubular Nanotemplate for Layer-by-Layer Assembly", *The 62nd Southwest regional meeting of ACS*, Houston, TX, 19th-22nd October 2006.

**Nalinkanth G. Veerabadrán**, Yuri M. Lvov, "Halloysite - Prospective Drug Delivery Template", *Second Annual Biomedical Engineering Research Day*, Louisiana tech University, Ruston, LA, 5th May 2006.

**Nalinkanth G. Veerabadrán**, Yuri M. Lvov, "Clay Nanotubules for Drug Encapsulation and Sustained Release", *Fostering collaborations with Bioresearch day*, Shreveport, LA, 1st May 2006.



- Nalinkanth G. Veerabadran**, Shashikanth M. Sriram, Dinesh S. Kommireddy, Yuri M. Lvov, David K. Mills, "Stem Cell Encapsulation Using Layer by Layer Technique," *11th Annual meeting - Institute of Biological Engineering*, Tucson, AZ, 10th - 12th March **2006**.
- M. Prouty, Z. Lu, **Nalinkanth G. Veerabadran**, G. Krishna, A. Yaroslavov, C. Kumar, C. Leuschner, Y. Lvov, "Drug Nanoencapsulation and Controlled Release", *Sixth Louisiana Materials and Emerging Technologies Conference*, Ruston, LA, 12th – 13th December **2005**.
- Nalinkanth G. Veerabadran**, Krishna Gopal, Yuri Lvov, "A Novel Nanotubular Template for Delivering Bioactive Agents - Halloysite", *The 61st Southwest and the 57th South east Joint regional ACS conference*, Memphis, TN, 1st – 4th November **2005**.
- Sandeep R. Eadula, **Nalinkanth G. Veerabadran**, Yuri Lvov, "Micro encapsulation of Dexamethasone by Electrostatic Layer by Layer Assembly for a Two Phase differential release". *The 61st Southwest and the 57th South east Joint regional ACS conference*, Memphis, TN, 1st – 4th November **2005**.
- Nalinkanth G. Veerabadran**, Yuri M. Lvov, "Nanotubular Drug Delivery using Novel Biomaterial - Halloysite", *First Annual Biomedical Engineering Research Day*, Louisiana tech University, Ruston, LA, 5th May **2005**.